E-TEAM

European Masters in Advanced Textile Engineering

Characterisation of UD-Braids

Charlotte Eisenhauer

Supervisor: Dipl. Ing. Vera Hanisch
(RWTH Aachen University)
Dr. Peter Middendorf
(EADS Deutschland GmbH)
Ing. Björn Van Den Broucke
(EADS Deutschland GmbH)

Academic year: 2005-2006

E-TEAM

European Masters in Advanced Textile Engineering

Characterisation of UD-Braids

Charlotte Eisenhauer

Supervisor: **Dipl. Ing. Vera Hanisch**
(RWTH Aachen University)
Dr. Peter Middendorf
(EADS Deutschland GmbH)
Ing. Björn Van Den Broucke
(EADS Deutschland GmbH)

Academic year: 2005-2006

Preface

This Master's Thesis was developed at EADS Germany at the Cooperate Research Centre CRC in the department LG-CT (Composite Technologies) in cooperation with the institute ITA at the RWTH Aachen University.

In regard to the work for my Master's Thesis at EADS, I would like to thank Dr. Middendorf, team leader at EADS Germany, CRC, for supervising me and giving me helpful advices. A big thank you also goes to Björn Van Den Broucke, PhD-student at EADS in cooperation with the University of Leuven, for his support during my whole work at EADS. Both supported me with assistant ideas and suggestions.
Further thanks go to Mr. Geßler and Mr. Maidl for their advice.
I would like to thank all the helping hands in the working labs of EADS Corporate Research Centre, in particular Mr. Scheid, Mr. Wittmann and Mr. Karger for their practical support.
At the RWTH Aachen University, I want to thank Ms. Hanisch for taking over the supervision of my Master's Thesis and supporting me during my work at the ITA. Additionally, I give my thanks to Prof. Gries for giving me the opportunity to realize my Master's Thesis and to execute a part of the topic at his institute.

Summary

This thesis in the framework of my Master studies “Master of Advanced Textile Engineering” investigated the geometrical and mechanical characterisation of UD (unidirectional)–braids.

The experimental part started with the production, stacking and infiltration of the UD-braid.
The mechanical characterisation of the UD-braid and rovings out of the UD-braid were mainly tested to investigate the change in tensile strength due to the braiding process.
The geometrical characteristics of the dry and the infiltrated UD-braid were determined by a top-view scan of the textile and by cross-section analysis of the laminate. These characteristics provided the data needed to build a WiseTex model with which textile architecture, in-plane deformations and stress-strain behaviour of a textile can be predicted and simulated. A further step would be the conversion of the WiseTex model into an FE model with the software tool FETex.
The Ladevèze damage model was used to represent the mechanical behaviour of a laminate, produced on the basis of UD-braided fabrics as reinforcement material, which was used as input for simulations of composite structures. The Ladevèze parameters obtained are based upon experimental test data from tensile, cyclic tensile and compressive tests on various lay-ups of the material produced according to the Ladevèze testing program.
For registration of strain during the experimental mechanical tests of the various laminates, two different methods were used: 1) the standard method with strain gauges attached to the specimens and 2) a method with a strain mapping system known as the Aramis system. As a final result of the comparison of these two methods, the Aramis system was used for calculation of the final mechanical properties and the Ladevèze damage model parameters.
Based on the geometrical and mechanical characterisation a finite element model will be build using the software tools of MSC.

Keywords: UD-braid, textile geometry, WiseTex, laminate, Ladevèze damage model, mechanical characterisation, strain mapping

Table of Content

Abbreviations and Symbols

CCD camera	Charge-coupled device
CFRP(s)	Carbon fibre reinforced plastic(s)
CLT	Classical Laminate Theory
CRC	Corporate Research Centre
DIN	Deutsches Institut für Normung (German Institute for Standards)
DMS	Dehnmessstreifen (stripe for strain measurement)
D.O.S.	Direct Oriented Structures
DTP	Data Transfer Protocol
EADS-G	European Aeronautic Defence and Space Germany
EN	European norm
FEA	Finite Element Analysis
FEB	Fehlerecho, Blende B (defect echo, diaphragm B)
FEM	Finite Element Model
HEB	Hilfsreflektorecho, Blende B (auxiliary reflection echo, diaphragm B)
HTS	High technology system
INSA Lyon	Institut National des Sciences Appliquées de Lyon
	(National Institute of Applied Sciences
ISO	International Organization for Standardization
ITA Aachen	Institut für Textiltechnik Aachen (Institute for Textile Technology)
ITOOL	Integrated Tool for Simulation of Textile Composites
LAP	Laminate Analysis Program
LZB	Laufzeitechto, Blende B (delay echo, diaphragm B)
PA	Polyamide
PE	Polyethylene
PEEK	Polyetheretherketone
PET	Polyethyleterephtalate
PP	Polypropylene
PTFE	Polytetraflorethylen
REA	Rückwandecho, Blende A (rear panel echo, diaphragm A)
RFI	Resin Film Infusion
RTM	Resin Transfer Moulding
SISPRA	Sistemas y Procesos Avanzados (Advanced Systems and Processes)
UD	Unidirectional
VAP	Vacuum Assisted Process
VARI	Vacuum Assisted Resin Injection
VARTM	Vacuum-Assisted Resin Transfer Moulding

1. Positioning into overall project and objectives of the thesis

This paper is a part of the frame work of the Integrated Tool for Simulation of Textile Composites, the ITOOL Project. The partners are EADS-G and EADS CRC France, Alenia Aeronautica S.p.A., Cranfield University, Dassault Aviation, the German Aerospace Centre, the ESI Group, University of Stuttgart, University of Aachen, University of Leuven, INSA University of Lyon, SISPRA and the University of Zaragoza.

The objectives of the ITOOL project are the technical approach of simulation. The whole process line of a composite part is simulated as a virtual manufacturing chain including “preform manufacturing, draping and impregnation process”, as well as the application of external load onto the finished part, a textile preformed composite part. Investigated technologies are textile performing including advanced engineering textiles, weaving, stitching and braiding. Gathering this knowledge an “adequate integrated simulation tool” for these textile technologies is developed.

Figure 1.1 gives an overview of the described cycle. [32]

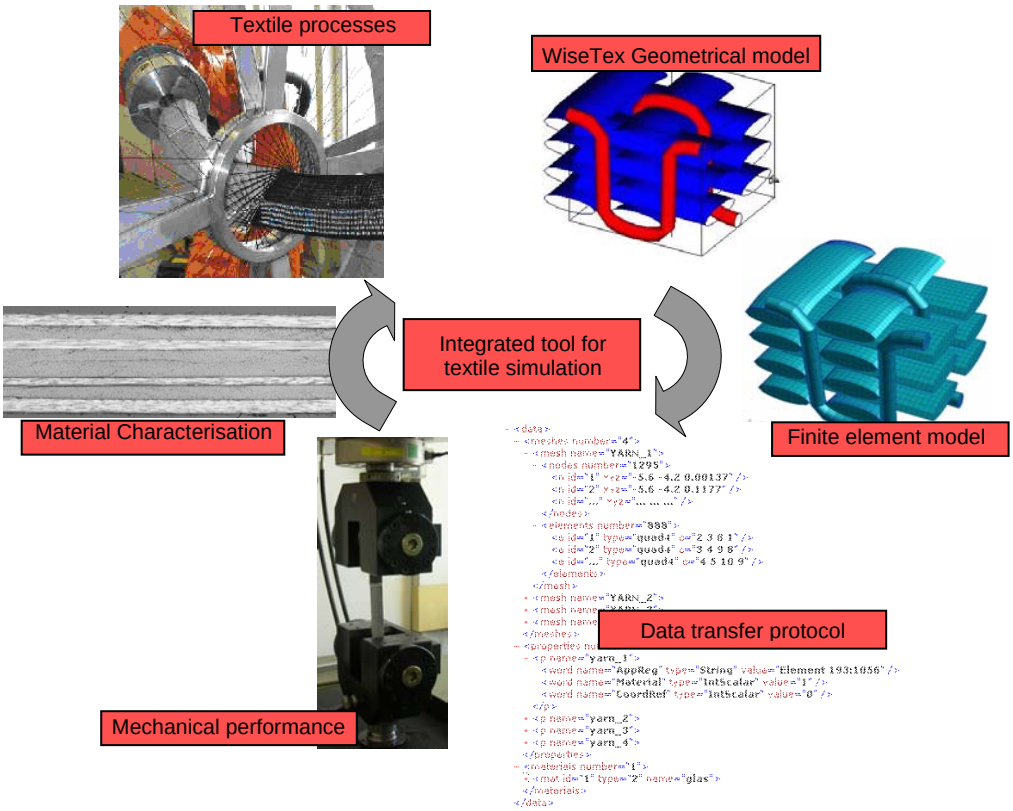

Figure 1.1: Application: ITOOL

To describe the behaviour of an elementary pattern several mechanical specifications of the material must be taken into account. The yarn’s mechanical behaviour is directly associated and linked with the constitution of the yarns and fibres.

To predict macroscopic structural deformation, stress and failure of textile-reinforced structures a precise model considering the elastic properties of the material and the behaviour after failure is

necessary. The damage mechanism of composite materials is based on the Ladevèze–model. With the Ladevèze-model the properties of a material are obtained on microscopic scale. These properties are incorporated into a model on a meso-scale and then into a macro-scale as shown in figure 1.2.

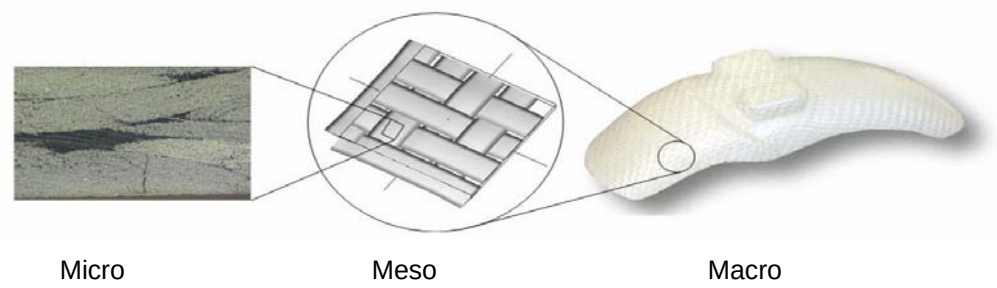

Figure 1.2: Micro-, meso- and macro-model

For simulation the commercial available products of MSC software will be used. Their non-linear solver MSC.Marc is used for calculation whereas the pre and post processors MSC.Patran and MAX.Mentat are used.
One example of the final application of the ITOOL project is the EADS-G validation example, the convex curve fuselage shell of an airplane, shown in figure 1.3.

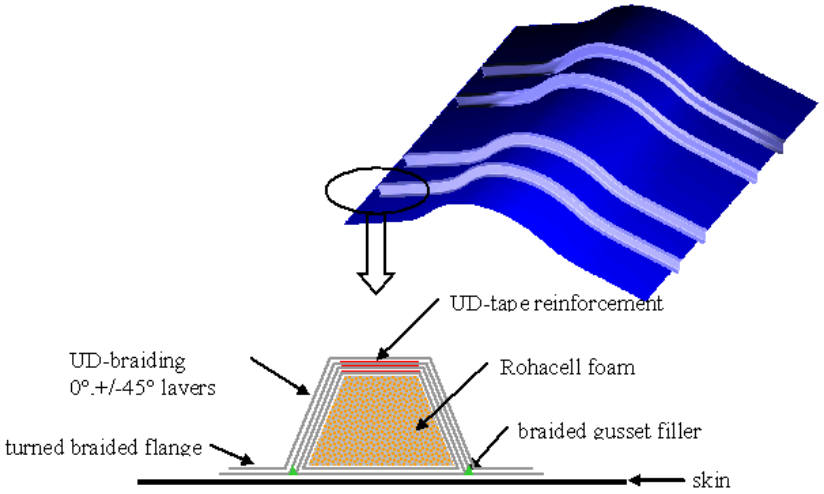

Figure 1.3: EADS-G validation example: convex curve fuselage shell

This Master's Thesis presents the theoretical background, i.e. Classical Laminate Theory, the Ladevèze damage model, the state of the art of braiding, the material used to produce a composite part and various lamination techniques. The introduction to these topics, described in chapter 3, is the basis for experimental analysis.
The main part of this thesis addresses the characterisation of a unidirectional (UD)-braided textile in four interconnected attempts: the geometrical and mechanical characterisation of the dry UD-braid and the geometrical and mechanical characterisation of a laminate produced from the UD-braid.

A key role in the studies of mechanical and geometrical properties of the textile is played by the influences of the manufacturing process, as well as the impregnation process. The braiding and lamination processes and the material used for the production of the test material are discussed in chapters 4 and 5.

The methods of the geometrical characterisation of both the dry UD-braid and the laminates and the corresponding results are presented in chapters 7 and 8. These results are fed into the WiseTex model, a simulation tool for textile structures, which is described in chapter 9.

Another aspect of describing a textile material is the mechanical characterisation. The results of the tests on the dry UD-braid are presented in chapter 6. The tests for the mechanical characterisation of the laminates, produced out of several plies of the UD-braid, are performed according to the Ladevèze experimental test series. From this the modified Ladevèze parameters are obtained. The results of these tests on the laminates are described in chapter 10.

All tests are carried out at the institute ITA at the RWTH Aachen University and at EADS CRC Germany.

The tasks described in this thesis are compiled at flow diagram in figure 1.4.

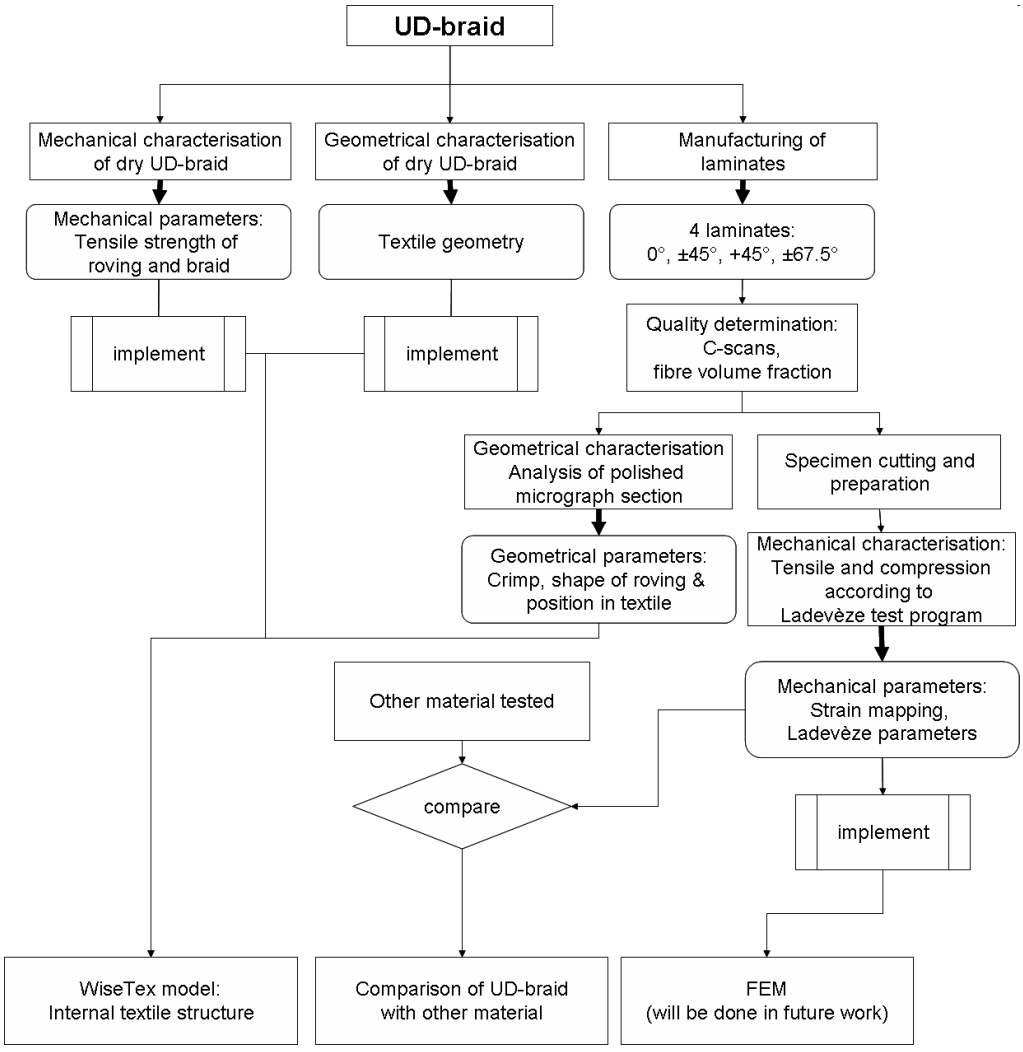

Figure 1.4: Tasks of the thesis

2. Introduction: Composites in general

Composites are solid materials composed of two or more elements. Combined they offer specific properties required to realize new constructive solutions for end-use. They are composed of a matrix and a reinforcement. The matrix can be a polymeric, duroplastic or thermoplastic resin, metal, ceramic, carbon matrix or concrete. The reinforcement is either on a natural fibre basis (wool, cotton, linen etc.), carbon, ceramic or glass fibres, or a synthetic fibre basis (PE, PA, PET, PEEK, aramid etc.). They are used in the form of whiskers, loose fibres or a textile structure, e.g., warp or weft knitted, woven, non-woven or braided fabrics. It is also common to mix fibres as a hybrid structure, e.g., carbon and Kevlar, to combine different properties in one composite structure. The most common types of fibres are high performance fibres with extraordinary mechanical properties.

The proportion of the reinforcement material to the matrix can vary, according to its desired tailor-made properties. As visible in figure 2.1, the textile reinforcement possesses high stress at low strain providing the composite structure with a high tensile strength. The matrix is responsible for the protection of the reinforcement, the cohesion of the fibres and transmission of the stresses onto the fibrous material. The resulting tensile strength of the composite lies therefore in between the mechanical properties of the two different components.

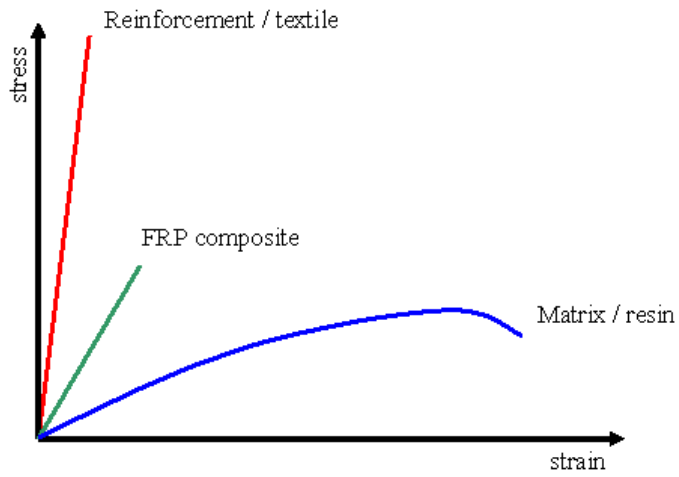

Figure 2.1: Schematic stress-strain behaviour

In addition to the fibre volume fraction and the type of fibre and matrix, the fibre orientation and the crimp ratio of the fibres play an important role in determining the mechanical properties of the composite. [12]

Fibre-reinforced plastics (FRPs) are replacing the metal structures in their application more and more. FRPs do not have the problem of corrosion and they stand out due to low weight, dimensional stability, impact strength and chemical resistance. The combination of high modulus, high strength and relatively low weight makes fibre-reinforced plastics competitive, especially in the high technology sector. The realization of the many possibilities of variations and optimal

adaptability and flexibility give FRPs the prerequisites to be used in many applications. Their main application fields are mechanical engineering, civil engineering, transportation, electric engineering, aerospace, medical equipment and sports goods. Each application makes use of various specific properties of the composite.

Contrary to all the interesting advantages of FRPs, their biggest disadvantage is the vulnerability to impact damage. Additional causes for the failure of a composite part are debonding, i.e. the failure of the bond between the fibre and the matrix at the interface, and delamination, i.e. the separation of individual plies in the composite.

Recent aerospace applications have required the use of composites, which combine high elastic stiffness, strength, UV resistance and dimensional stability at high temperature and at minimum weight. This need is met by fibre reinforced dimensionally stable composites. For the development of structural components for the aerospace industry, the main issue is weight reduction to reach economic, ecological and competitive advantage. New solutions are therefore found in fibre reinforced plastics (FRP) used at a portion of approximately 25%, for example, in the A 380.

Expectations are that by 2010 all passenger airplanes will be constructed with a share of 50% of the entire fuselage and wing structures made out of FRC. [13]

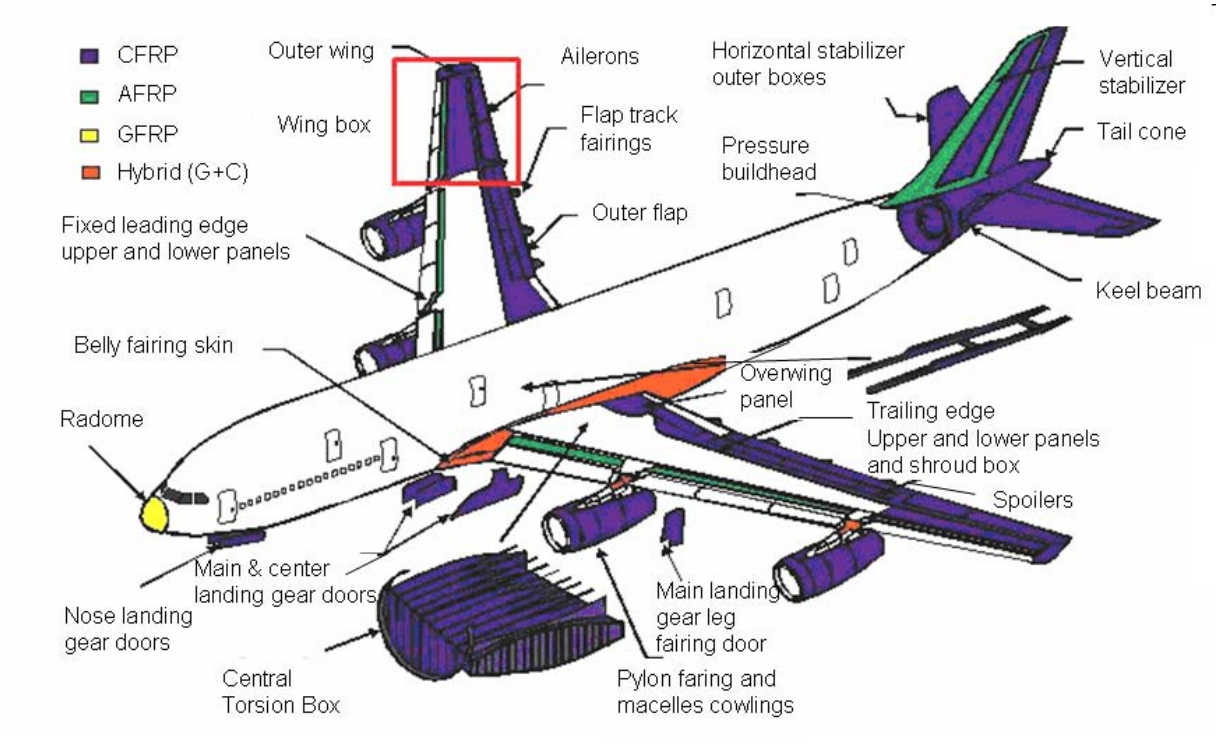

Figure 2.2: A 380 Composite Components (source: [29])

3. Theoretical background

In this chapter the theoretical background of the basic principles of composites, and specifically of laminates is described. The issues of composite mechanics as a basis for composite construction will be addressed. Additionally, Classical Laminate Theory (CLT) will be briefly described, as this theory is used for the evaluation of tensile tests in general. In this thesis, the LAP (Laminate Analysis Program), based on Classical Laminate Theory, is used to predict the expected stiffness of the laminate. Moreover, general damage criteria are described, providing a background for the Ladevèze damage model. This Ladevèze model, a special model for damage, is used in this thesis for the analysis of the tensile tests and is therefore also described in this chapter.

3.1. Composites and mechanics

In the introduction to chapter 2, composites were described on the more general level. In this section the mechanical properties resulting form the complex material architecture is described.
On a micro-mechanical level (level of several micro-meter), composites can be treated as orthotropic material. The stress-strain state is considered as shown in figure 3.1, with stresses σ and strains ε.

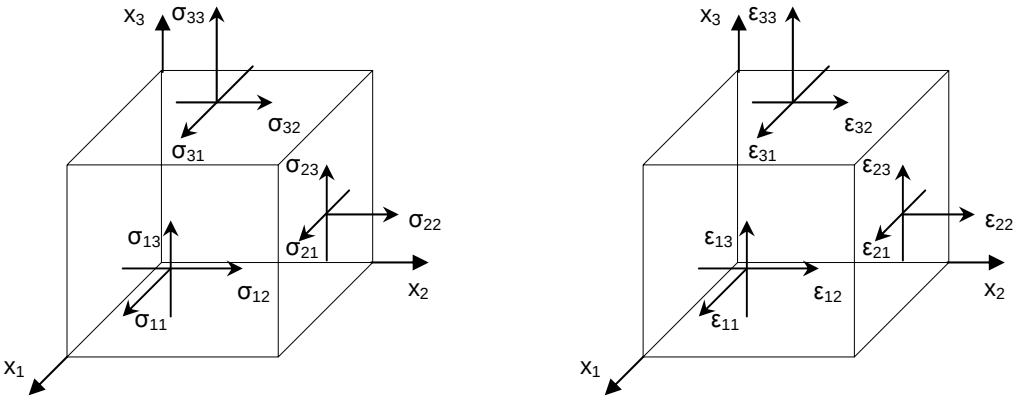

Figure 3.1: Stresses and strains acting on an elementary unit cell

The coordinate system in an elementary UD material cell is considered in the three dimensions x_1, x_2 and x_3. Figure 3.1 shows the various stresses and strains acting on an elementary UD material cell. The stress state acting on the elementary UD material cell is in mechanics described with 6 components: three normal components σ_{11}, σ_{22} and σ_{33} and three shear components σ_{12} (=σ_{21}), σ_{23} (=σ_{32}) and σ_{31} (=σ_{13}). Positive normal stress represents tension, whereas negative normal stress represents compression. The stress states are usually described as 9 vectors in mechanics, whereby only 6 are different. [3, p.21]

For strains a similar approach is applied. The stresses and strains are related to each other with the material law:

$$\sigma_\alpha = C_{\alpha\beta}\varepsilon_\beta \qquad (1)$$

3.2. Introduction to Classical Laminate Theory

In general, composite materials are inhomogeneous materials showing orthotropic or anisotropic properties depending on the state and position of the reinforcement material imparted in the matrix. If the reinforcement fibres lie parallel only in one direction, e.g. the x_1-direction, the composite material is called orthotropic. Looking at the FRP three-dimensionally, the properties for the x_1- and x_2-axis are then different, whereas in the x_2- and x_3-direction the properties are the same.

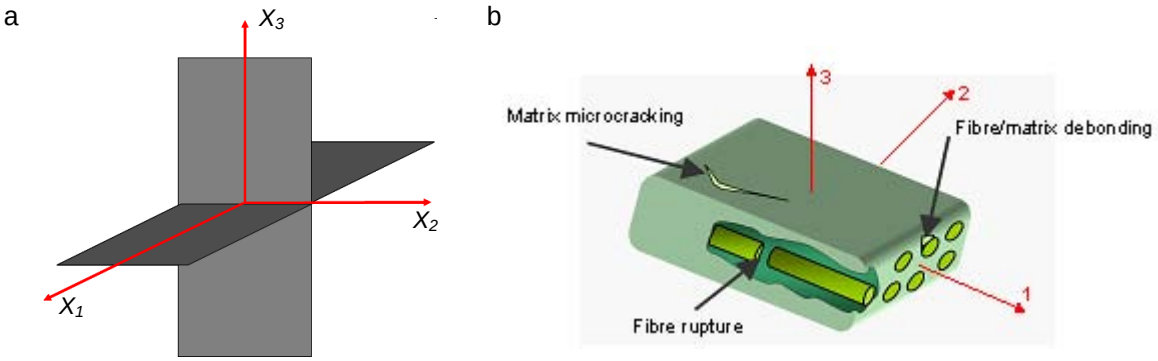

Figure 3.2: a: Orthotropic material performance, symmetric planes ($x_1 - x_2$) and ($x_2 - x_3$) [3, p.36]
b: Definition of orthotropy according to Ladevèze [25]
1: first axis in fibre direction
2: second axis: perpendicular to first axis, within the plane
3: normal to plane of unidirectional composite ply

Composites can also show more complex behaviour. This is true for laminates with a different stacking sequence using for example woven fabrics, braids or knits. In this case it is spoken of as anisotropy.

Classical Laminate Theory (CLT) is a technique which is used to calculate the rigidity of shells and the tensions in a planar laminate consisting of several laminas. The basis for the laminate theory is the distinction between lamina, a single ply, and laminate, several layers / plies in a composite and their stresses and strains. In CLT, laminates are built up of UD-plies or quasi-UD-plies. For example non-crimp fabrics or UD-braids used in this thesis can be considered as quasi-UD. Simple constructive elements of composites can be modelled and calculated with the help of hypotheses of shell and membrane theory, i.e. the model of Euler-Bernoulli and Love-Kirchhoff. [6], [7]
Laminates are composed of single plies with at least a number of $n \geq 2$ layers, idealised as a planar plate. The individual UD plies are stacked on top of each other. Each layer can have a varying direction, arranged under an angle θ compared to the reference direction.

For classical laminate theory several prerequisites are necessary:

- Ideally linear elasticity law of the individual ply
- Constant laminate thickness
- No deformation
- Validity of the assumption of Bernoulli (planar cross-section and shear inelasticity in the direction of thickness)
- Perfect bonding between the plies
- Laminate position in x, y- plane
- Macroscopic homogenous and orthotropically elastic individual plies
- Small thickness: the length and width of the laminate bigger than ten times that of the thickness

3.2.1. Material law of single UD-ply

The UD-ply can be observed on the micro-mechanical level and the macro-mechanical level. On the micro-mechanical level, the matrix and the fibrous reinforcement of the UD-ply are regarded as independent. Different material properties are assigned to the matrix and the fibres. Therefore, they inhibit different stresses and strains. On the macro-level, the UD-ply is looked at as a whole. Considering then orthotropic properties for the ply, the UD-ply is assumed to be homogenous. This assumption is used in the following part.

For the calculation of a laminate, the stiffness matrix $[Q_{ij}]$ of each UD-ply has to be determined. If the laminate inhibits orthotropic behaviour, i.e. is the stacking symmetrical, then, from the material law equation:

$$\{\varepsilon\} = [C]\{\sigma\} \text{ (with the elasticity matrix } [C_{ij}]\text{)} \quad (2)$$

and

$$[Q] = [C]^{-1} \quad (3)$$

the following can be deviated:

$$\{\sigma\} = [Q]\{\varepsilon\} \qquad (4)$$

whereby:

$$[Q_{ij}] = \begin{bmatrix} Q_{11} & Q_{12} & 0 \\ Q_{12} & Q_{22} & 0 \\ 0 & 0 & Q_{12} \end{bmatrix} = \begin{bmatrix} \frac{E_1}{1-\nu_{12}^2 \frac{E_2}{E_1}} & \frac{\nu_{12} E_2}{1-\nu_{12}^2 \frac{E_2}{E_1}} & 0 \\ \frac{\nu_{12} E_2}{1-\nu_{12}^2 \frac{E_2}{E_1}} & \frac{E_2}{1-\nu_{12}^2 \frac{E_2}{E_1}} & 0 \\ 0 & 0 & G_{12} \end{bmatrix} \qquad (5)$$

with the elasticity constants:

$E_1 = E_L$	E-modulus in the fibre direction, Young's modulus
$E_2 = E_T$	E-modulus transverse to the fibre direction
$\nu_{12} = \nu_{LT}$	Poisson's ratio at torsion in the fibre direction
$G_{12} = G_{LT}$	Ply shear modulus in the plane

With the transformed stiffness matrix a plate with an angle of fibres other than 0 ° is calculated. The stiffness matrix of a UD-ply can be written as follows, with the help of a coordinate transformation:

$$[\overline{Q}] = [T_\sigma] \; [Q] \; [T_\sigma]^T \qquad (6)$$

This results from rotating $\{\varepsilon\}$ and $\{\sigma\}$ with an angel θ to obtain the transformed stiffness matrix $[\overline{Q}]$.

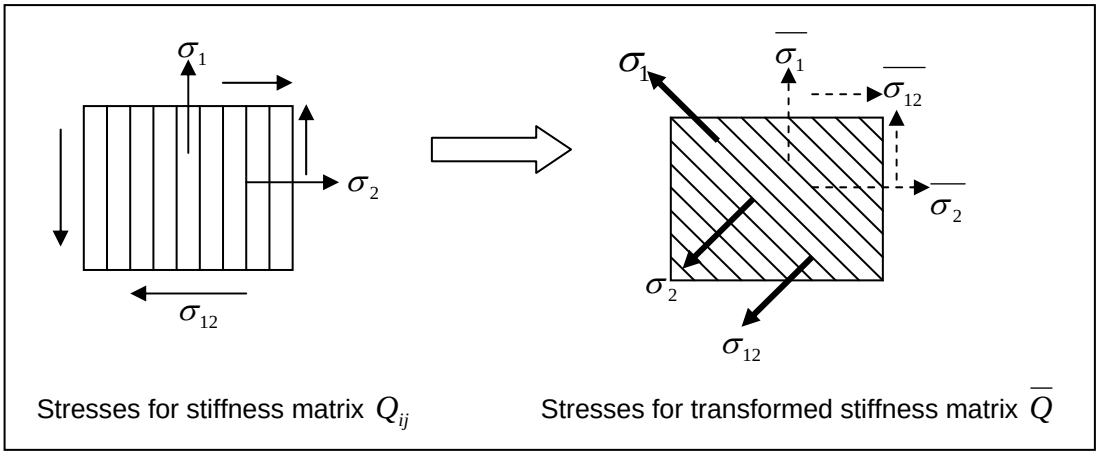

Figure 3.3: Comparison of stresses used for Q_{ij} and $\overline{Q}$

The same is valid for strains.

3.2.2. Combining UD-plies to laminate

To determine the properties of the whole laminate, the individual UD-plies have to be integrated into the stacking. For that purpose, the angel of the UD-plies, the ply thickness, the ply sequence and the fibre volume fraction have to be defined.

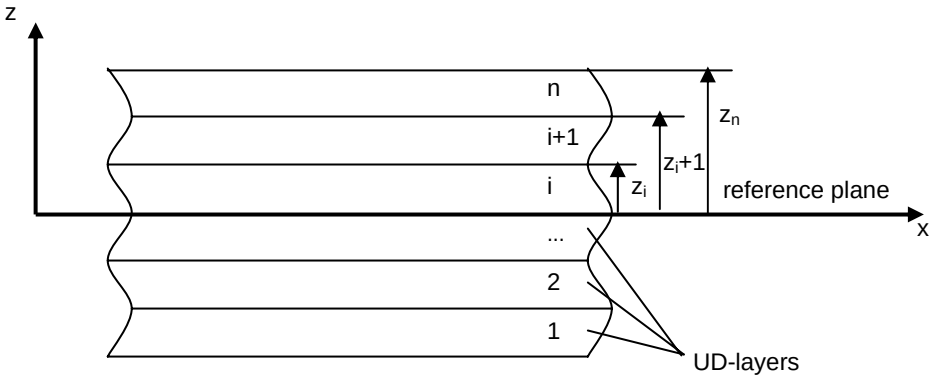

Figure 3.4: Schematic stacking of a laminate

Combining, the stiffness matrices of each single ply, the matrices [*A*], [*B*] and [*D*] for the whole laminate are obtained.

The laminate-strain-stiffness matrix [*A*] combines in-plane stresses and strains in. This matrix is used for non-balanced laminates. It is calculated from:

$$[A] = \sum_{i=1}^{n} \left[\overline{Q}\right]_i \left(z_i - z_{i-1}\right) \qquad (7)$$

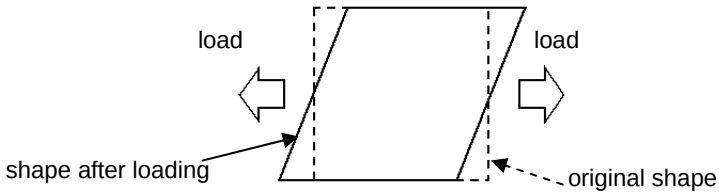

Figure 3.5: Loading of a laminate in plane direction of the laminate [36]

The coupling-stiffness matrix [*B*] describes the interrelationship of the in-plane stresses with bending behaviour as well as bending moments with in-plane stains. This means that tension and bending are coupled. Matrix [*B*] is used for asymmetrically stacked laminates.

$$[B] = \sum_{i=1}^{n} \left[\overline{Q}\right]_i \frac{\left(z_i^2 - z_{i-1}^2\right)}{2} \qquad (8)$$

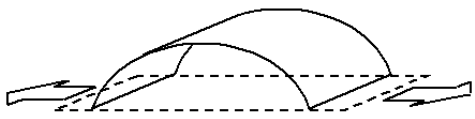

Figure 3.6: Combination of strains and coupling of moments [36]

The bending stiffness matrix [*D*] combines the bending moments with bending behaviour.

$$[D] = \sum_{i=1}^{n} [\bar{Q}]_i \frac{\left(z_i^3 - z_{i-1}^3\right)}{3} \qquad (9)$$

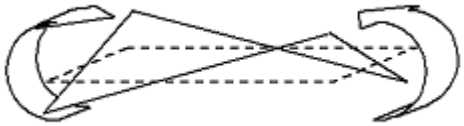

Figure 3.7: Combination of bending and coupling of moments [36]

On the basis of [*A*], [*B*] and [*D*] the fundamental relationship between the strain {ε_0} and the bending {k_0} of the centre plane of the laminate and the generated intersection forces {*N*} and the intersection momentum {*M*} are posted:

$$\begin{Bmatrix} \{N\} \\ \{M\} \end{Bmatrix} = \begin{bmatrix} [A] & [B] \\ [B] & [D] \end{bmatrix} \begin{Bmatrix} \{\varepsilon_0\} \\ \{k_0\} \end{Bmatrix} \qquad (10)$$

The engineering constants obtained from the stiffness matrix can be, in combination with shell or volume elements, directly used in the finite element method. As a result, the global behaviour of a laminate can be simulated.

3.3. Damage in composites

Damage in composites begins at the microscopic level; this means in the µm-range of the fibre diameter. This process of damage and breakage is described with the help of micro mechanical models.

Directly after the production of the composite, very small breaks exist. These cracks are due to the different thermal expansion coefficients of the matrix and the fibres. Due to their different thermal expansion coefficient, the matrix contracts more than the reinforcement, i.e. the fibres, resulting in tension during and after the curing process. At first loading of the composite part additional micro damage appears.

At higher and repeated loads, these micro cracks aggregate and lead to a larger damage zone. The single plies are mostly divided in the direction of the thickness. This so called matrix cracking causes fibre / matrix debonding, making the composite vulnerable, especially at cyclic load.

Laminate can be built out of several UD-layers with different fibre orientation. When exposed to load, the stresses and strains are different in the individual layers. Therefore, it is necessary to analyse each ply according to its stresses and strains to determine the failure criteria for each ply of the laminate.

From experiments it was shown that different damage modes exist. They can be distinguished as:

- Matrix cracking, where micro-cracks occur between the fibres and damage proceeds through the matrix
- Fibre rupture, where the filaments or fibres break or buckle
- Delamination, only in the case of laminates [5]

Transversal nominal loading in ply plane σ_2 and shear loading τ_{12} causes matrix cracking shown in figure 3.8.

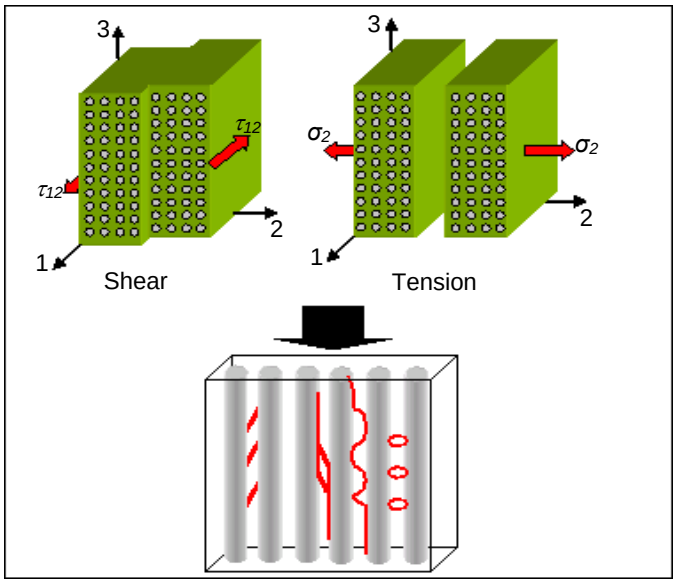

Figure 3.8: Scheme of matrix cracking

Another cause for damage is the disconnection of the single plies, called delamination. This type of damage is caused by stresses perpendicular to the interfaces of the plies or shear stresses σ_{13} and σ_{12} (figure 3.9).

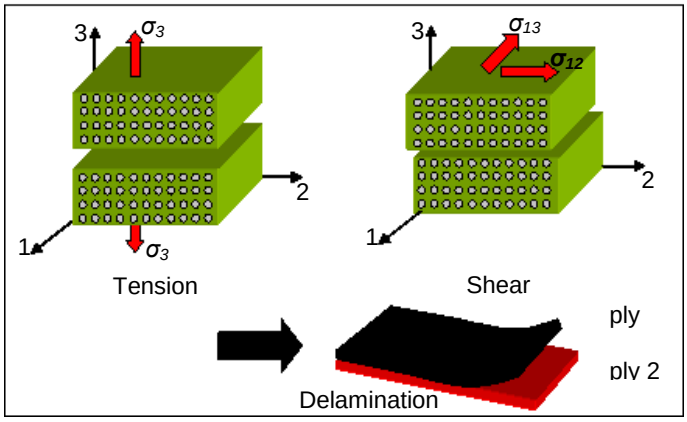

Figure 3.9: Scheme of delamination

The third type of damage is fibre rupture caused by loading in the fibre direction. Tensile stresses in the fibre direction result in sudden fibre rupture, whereas compressive loads lead to so called micro-buckling of the fibre (figure 3.10).

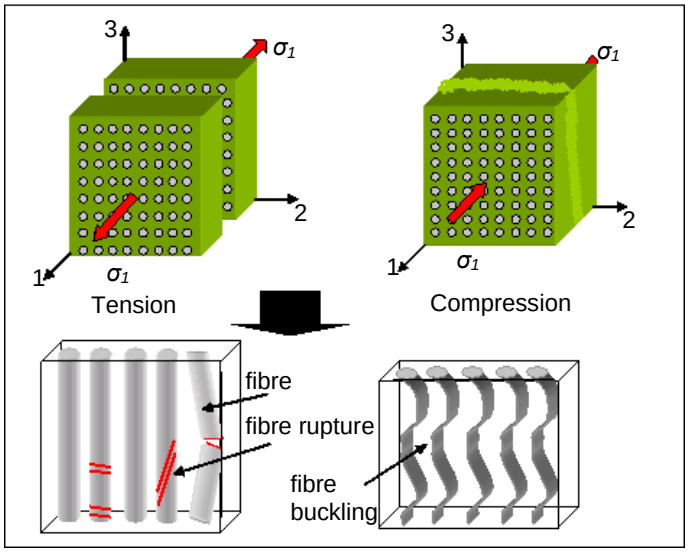

Figure 3.10: Scheme of fibre rupture

A failure of a single ply does not inevitably lead to a complete failure of the laminate, as not all plies are stressed till their limit-bearing capacity. If one ply fails, the other plies have to carry the load. At a matrix cracking, for example, the fibres can carry the load till their limit, shown in figure 3.11.

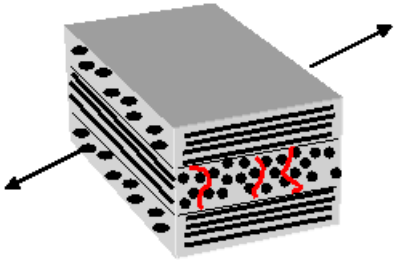

Figure 3.11: Matrix cracking

3.4. Ladevèze damage model

The Ladevèze model describes the behaviour of a unidirectional (UD) continuous fibre reinforced composite material. In the composite part the UD-ply is understood to be homogeneous, i.e. there is no differentiation between the two phases (the fibres and the matrix). Therefore, the description of the composite ply is based on the homogenous continuum mechanism. The original Ladevèze model is described in detail in [25].

In this model three laminate damage models are incorporated. Ladevèze assigns the damages to experimentally observed phenomena, illustrated in figure 3.2 b:

- Matrix micro-cracking, which appears under a transverse tensile loading
- Fibre-matrix debonding, which is generally due to a shear loading
- Fibre rupture under tensile load in fibre direction

Misalignments or microbuckling appears under compressive loads. In the model, fibre failure under tensile and compressive load is considered, as both show different phenomena.

3.4.1. Model parameters

In the following chapters a set of material constants are used. These constants characterise the modified Ladevèze model. Therefore, the constants are defined in this section.
As previously defined, the notation for the coordinate system is:

1 fibre direction
2 transverse direction
3 thickness direction of the composite ply

Elastic constants

E_1^t	$[MPa]$	Tensile ply Young's modulus in fibre direction (1)
E_1^{0t}	$[MPa]$	Initial elastic modulus of the UD-ply in fibre direction, tension
E_1^c	$[MPa]$	Compressive ply Young's modulus in fibre direction
E_1^{0c}	$[MPa]$	Initial elastic modulus of the UD-ply in fibre direction, compression
E_2^0	$[MPa]$	Initial elastic modulus of the UD-ply in transverse direction
E_1^γ	$[MPa]$	Non-linear compressive Young's modulus
G_{12}^0	$[MPa]$	Initial value of ply shear modulus of the UD-ply in ply plane direction
G_{23}^0	$[MPa]$	Initial ply shear modulus of the UD-ply
υ_{12}^0	$[-]$	Initial Poisson's ratio in ply plane direction

Matrix damage constants

Y_c	$\left[\sqrt{MPa}\right]$	Critical shear damage limit value
Y_0	$\left[\sqrt{MPa}\right]$	Initial shear damage threshold value
Y_R	$\left[\sqrt{MPa}\right]$	Elementary shear damage fracture limit
Y_c^2	$\left[\sqrt{MPa}\right]$	Critical transverse damage limit value

Y_0^2	$\left[\sqrt{MPa}\right]$	Initial transverse damage threshold value
Y_S^2	$\left[\sqrt{MPa}\right]$	Brittle transverse damage limit for fibre / matrix interface
$d_{\max}$	$[-]$	Maximum allowed value of the scalar damage variable *d* and *d´* ($d_{\max} \leq 1.0$)

Fibre tensile damage-related constants

ε_i^{ft}	$[-]$	Initial threshold level of elongation at tension in fibre direction
ε_u^{ft}	$[-]$	Ultimate threshold level of elongation at tension in fibre direction
d^{ft}	$[-]$	Tensile damage in fibre direction (fibre damage)
d_u^{ft}	$[-]$	Ultimate value of damage at tensile load in fibre direction

Fibre compressive damage-related constants

ε_i^{fc}	$[-]$	Initial threshold level of elongation at compression in fibre direction
ε_u^{fc}	$[-]$	Ultimate threshold level of elongation at compression in fibre direction
d^{fc}	$[-]$	Compressive damage in fibre direction (fibre damage)
d_u^{fc}	$[-]$	Ultimate value of damage at compressive load in fibre direction
γ	$\left[MPa^{-1}\right]$	Non-linear compressive modulus factor, correction factor

Plastic constants

$a^2 = A^2$ $[-]$	Coupling factor between shear tension and transversal elongation

3.4.2. Elastic material law

The constitutive relationship according to the modified Ladevèze model is expressed as follows:

$$\begin{Bmatrix} \varepsilon_{11}^e \\ \varepsilon_{22}^e \\ 2\varepsilon_{12}^e \end{Bmatrix} = \begin{bmatrix} \frac{1}{E_1} & -\frac{\upsilon_{12}^0}{E_1} & 0 \\ -\frac{\upsilon_{12}^0}{E_1} & \frac{1}{E_2} & 0 \\ 0 & 0 & \frac{1}{G_{12}} \end{bmatrix} \begin{Bmatrix} \sigma 11 \\ \sigma 22 \\ \sigma_{12} \end{Bmatrix} \quad (11)$$

where

in fibre direction (1-direction): tension

$$E_1^t = E_1^{0t}\left(1 - d^{ft}\right) \qquad \text{if } \varepsilon_{11} \geq \varepsilon_i^{ft}$$

$$d^{ft} = \begin{cases} 0 & \text{if } \varepsilon_{11} \leq \varepsilon_i^{ft} \\ d_u^{ft}\,\dfrac{\varepsilon_{11} - \varepsilon_i^{ft}}{\varepsilon_u^{ft} - \varepsilon_i^{fc}} & \text{if } \varepsilon_i^{ft} < \varepsilon_{11} \leq \varepsilon_u^{ft} \\ 1 - \left(1 - d_u^{ft}\right)\dfrac{\varepsilon_u^{ft}}{\varepsilon_{11}} & \text{if } \varepsilon_u^{ft} < \varepsilon_{11} \end{cases}$$

in fibre direction (1-direction): compression

$$E_1^c = E_1^{\gamma}(1 - d^{fc}) \qquad \text{if } \varepsilon_{11} \leq 0$$

$$E_1^{\gamma} = E_1^{0c} / \left(1 - \gamma E_1^{0c}\left|\varepsilon_{11}\right|\right)$$

$$d^{fc} = \begin{cases} 0 & \text{if } \left|\varepsilon_{11}\right| \leq \varepsilon_i^{fc} \\ d_u^{fc}\,\dfrac{\varepsilon_{11} - \varepsilon_i^{fc}}{\varepsilon_u^{fc} - \varepsilon_i^{fc}} & \text{if } \varepsilon_i^{fc} < \left|\varepsilon_{11}\right| \leq \varepsilon_u^{fc} \\ 1 - \left(1 - d_u^{fc}\right)\dfrac{\varepsilon_u^{fc}}{\varepsilon_{11}} & \text{if } \varepsilon_u^{ft} < \left|\varepsilon_{11}\right| \end{cases}$$

in transverse direction (2-direction):

if $\varepsilon_{22} \geq 0$; modulus for tension load $E_2 = E_2^0\left(1 - d_2\right)$

else $E_2 = E_2^0$

with $d_2 =$ matrix transverse damage in $E_2 = E_2^0\left(1 - d_2\right)$

for shear:

$$G_{12} = G_{12}^0\left(1 - d_{12}\right)$$

with $d_{12} =$ matrix shear damage in $G_{12} = G_{12}^0\left(1 - d_{12}\right)$

3.4.3. Damage behaviour of the UD-ply

Based upon experiments, the damage of a UD-ply can be divided into several partial damage categories:

- Elastic matrix damaging behaviour
- Fibre tensile damage

Therefore, a differentiation between the behaviour of the fibre and the matrix has to be made. The UD-ply is regarded as heterogeneous.

Elastic matrix damaging behaviour

The matrix related damage is described by the scalar variables d_{12} and d_2. The variables are assigned to the following experimentally observed phenomena:

d_{12}: describes the damage, which results from the debonding of fibres and matrix in the UD-ply. The parameter d_{12} is related to ply shear.

d_2: describes the damage due to micro-cracking of the matrix parallel to the fibre direction related to transverse modulus. The parameter d_2 is applied for transverse modulus.
Additionally, there is a differentiation between tensile and compressive transverse responses. Under tensile load, micro-cracks grow; while under compressive load already existing micro-cracks close.

According to the damage parameters d_{12} and d_2, the damage functions Z_d and Z_d^2 are as follows with E_D as the elastic strain energy:

For shear damage:
$$Z_d = \frac{\partial E_D}{\partial d} = \frac{1}{2}\frac{\sigma_{12}^2 + \sigma_{13}^2}{G_{12}^0\left(1-d_{12}\right)^2} \qquad (12)$$

For transverse damage:
$$Z_d^2 = \frac{\partial E_D}{\partial d'} = \frac{1}{2}\frac{\left\langle \sigma_{22}^2 \right\rangle_+}{E_2^0\left(1-d_2\right)^2} \qquad (13)$$

$$\left\langle \sigma_{22}^2 \right\rangle = \sigma_{22}^2 \text{ if } \sigma_{22}^2 > 0, \text{ else } = 0$$

The damage functions, also identified as the associated forces, describe the rate of energy release and the progress of the cracks over time. The damage evolution over time is described with thefollowing functions:

For shear damage:
$$Y_{12}(t) = Sup_{\tau \le t}\sqrt{Z_d(\tau) + bZ_2^d(\tau)} \qquad (14)$$

For transverse damage:
$$Y_2(t) = Sup_{\tau \le t}\sqrt{Z_2^d(\tau)} \qquad (15)$$

Derived from the damage functions, the damage parameters can be calculated according to:

For shear damage:
$$d_{12} = \begin{cases} \dfrac{\left\langle Y_{12}(t) - Y_{12}^{0} \right\rangle_{+}}{Y_{12}^{c}} & \text{if } d_{12} > d_{\max},\ Y_{12}(t) < Y_{12}^{S} \text{ and } Y_{12}(t) < Y_{12}^{R} \\ d_{\max} & \text{otherwise} \end{cases}$$

For transverse damage:
$$d_{2} = \begin{cases} \dfrac{\left\langle Y_{12}(t) - Y_{2}^{0} \right\rangle_{+}}{Y_{2}^{c}} & \text{if } d_{2} < d_{\max},\ Y_{2}(t) < Y_{s}^{2} \text{ and } Y(t) < Y_{R} \\ d_{\max} & \text{otherwise} \end{cases}$$

A linear approach can be recognized when solving the equation for the damage parameters according to the damage function $Y(t)$:

For shear damage: $$Y_{12}(t) = Y_{12}^{c} d_{12} + Y_{12}^{0} \qquad (16)$$

For transverse damage: $$Y_{2}(t) = Y_{2}^{c} d_{2} + Y_{2}^{0} \qquad (17)$$

Fibre damage

Due to the dominating properties of the fibres, the UD-ply shows a brittle elastic behaviour under tensile load. Therefore, the linear elastic material law can be applied until the appearance of damage. In comparison, under compressive load directly a non-linear behaviour of the UD-ply is observed. One reason could be due to fibre misalignment or the fibre buckling at micro level.

The fibre damage behaviour under tensile and compressive load is illustrated in figure 3.12, with a stress-strain and a damage-strain diagram.

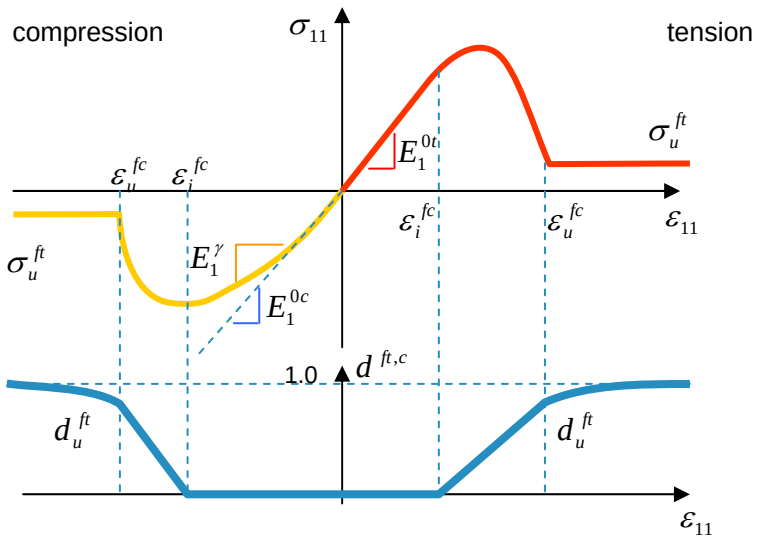

Figure 3.12: Tension and compression damage in fibre direction

Fibre tensile damage

According to the material law, no damage to the fibre appears when tensile load is applied to the fibre when $\varepsilon_{11} < \varepsilon_i^{ft}$. The parameter ε_i^{ft} is here the threshold value of the elongation where the first fibre damage under tensile load arises. From that point on, the value of the fibre damage d^{ft} rises linearly between $\varepsilon_i^{ft} \le \varepsilon_{11} < \varepsilon_u^{ft}$. ε_u^{ft} represents the maximum (ultimate) value of elongation where damage takes place. At that point the maximum (ultimate) damage of the material is reached, from where on the fibre tensile damage grows asymptotically towards $d^{ft} = 1.0$, the maximum value of fibre damage. During this approach towards the value 1.0, due to the tensile load, a complete failure of the material is caused.

According to such a material behaviour, the longitudinal damage under tensile load can be summarised for the following criteria:

- Sub-critical: $E_1 = E_1^{0t}$ if $\varepsilon_{11} < \varepsilon_i^{ft}$
- Critical: $E_1 = E_1^{0t}\left(1 - d^{ft}\right);\ d^{ft} = d_u^{ft}\,\dfrac{\varepsilon_{11} - \varepsilon_i^{ft}}{\varepsilon_u^{ft} - \varepsilon_i^{ft}}$ if $\varepsilon_i^{ft} \le \varepsilon_{11} < \varepsilon_u^{ft}$
- Post-critical: $E_1 = E_1^{0t}\left(1 - d^{ft}\right);\ d^{ft} = 1 - \left(1 - d_u^{ft}\right)\dfrac{\varepsilon_{11}}{\varepsilon_u^{ft}}$ if $\varepsilon_u^{ft} \le \varepsilon_{11} < \infty$

Non-linear fibre compressive behaviour

The behaviour of the fibre under compressive load is different from the fibre properties under tensile load. The non-linear compressive behaviour can be explained by fibre misalignment and fibre buckling. The phenomena of non-linearity and a resultant decrease of the E-modulus of the undamaged material is described by using the corrective factor γ:

$$E_1^{\gamma} = \frac{E_1^{0c}}{1 + \gamma \cdot E_1^{0c}\left|\varepsilon_{11}\right|} \qquad (18)$$

Fibre compressive damage

The fibre compressive damage is similar to the fibre tensile damage. However, due to the non-linear behaviour of the material under compressive load, the initial E-modulus is a function of the actual elongation ε_{11}. As a result, the fibre compressive behaviour can be categorized according to the following criteria:

- Sub-critical: $E_1^c = E_1^{\gamma}$ if $\left|\varepsilon_{11}\right| < \varepsilon_i^{fc}$
- Critical: $E_1^c = E_1^{\gamma}\left(1 - d^{fc}\right);\ d^{fc} = d_u^{fc}\,\dfrac{\left|\varepsilon_{11}\right| - \varepsilon_i^{fc}}{\varepsilon_u^{fc} - \varepsilon_i^{fc}}$ if $\varepsilon_i^{fc} \le \left|\varepsilon_{11}\right| \le \varepsilon_u^{fc}$
- Post-critical: $E_1^c = E_1^{\gamma}\left(1 - d^{fc}\right);\ d^{fc} = 1 - \left(1 - d_u^{fc}\right)\dfrac{\left|\varepsilon_{11}\right|}{\varepsilon_u^{fc}}$ if $\varepsilon_u^{fc} \le \left|\varepsilon_{11}\right| < \infty$

The parameter d^{fc} describes the fibre damage under compressive load with the maximum (ultimate) value of damage d_u^{fc}. The parameters ε_i^{fc} and ε_u^{fc} are the initial and the ultimate elongation for the damage value, defined according to figure 3.12.

Transformation between global frame and local frame

After the performance of the tests, the obtained parameters have to be transformed from the global frame (*L*, *T*) to the local frame (*1*, *2*) by transformation between the Test Piece Frame (Global Frame) and the Ply Frame (Local Frame).

The transformation matrix for the stresses with fibre angle *θ*:

$$\begin{Bmatrix}\sigma_{11}\\ \sigma_{22}\\ \sigma_{12}\end{Bmatrix}=\begin{bmatrix}\cos^2\theta & \sin^2\theta & 2\cos\theta\sin\theta\\ \sin^2\theta & \cos^2\theta & -2\cos\theta\sin\theta\\ -\cos\theta\sin\theta & \cos\theta\sin\theta & \cos^2\theta-\sin^2\theta\end{bmatrix}\begin{Bmatrix}\sigma_L\\ \sigma_T\\ \sigma_{LT}\end{Bmatrix}^{\theta}=[Q_2]\begin{Bmatrix}\sigma_L\\ \sigma_T\\ \sigma_{LT}\end{Bmatrix}^{\theta} \quad (19)$$

The transformation matrix for the strains with fibre angle *θ*:

$$\begin{Bmatrix}\varepsilon_{11}\\ \varepsilon_{22}\\ 2\varepsilon_{12}\end{Bmatrix}=\begin{bmatrix}\cos^2\theta & \sin^2\theta & \cos\theta\sin\theta\\ \sin^2\theta & \cos^2\theta & -\cos\theta\sin\theta\\ -2\cos\theta\sin\theta & 2\cos\theta\sin\theta & \cos^2\theta-\sin^2\theta\end{bmatrix}\begin{Bmatrix}\varepsilon_L\\ \varepsilon_T\\ 2\varepsilon_{LT}\end{Bmatrix}=[Q_1]\begin{Bmatrix}\varepsilon_L\\ \varepsilon_T\\ 2\varepsilon_{LT}\end{Bmatrix} \quad (20)$$

3.5. Description of WiseTex software

Textile structures and textile reinforcements are defined by a distinct hierarchy of structure. The textile has a highly complex architecture, whereas the base product, the yarns or filaments are of the scale of 10^{-5} m. the end products that are made of the textile as reinforcement can reach a size of several meters. [14]

With the WiseTex software, under development in the MTM Department of K.U. Leuven, it is possible to create a truly integrated model of the internal structure and the deformability of textile reinforcements. With the WiseTex software package it is possible to model various textile architectures. Possible models are fibres, yarns, the topology of weaves, woven fabrics, 2D braids with and without inlays, UD preforms and stitched multi-axial multi-ply fabrics. The software edits, views, stores and retrieves textile fibre, yarn and fabric data, calculates the internal geometry of the fabric and analyses the behaviour of the fabric under compressive and tensile load and shear deformations. [22]

With the definition of the fibre, alternatively filament data, a model of the fibrous structure of the textile reinforcement is constructed. On the basis of this model and together with the yarn specifications, the fibrous structure is calculated, assuming an even distribution of the fibres over the cross-section of the yarn or roving. An average fibre volume fraction v_f is the result. The yarn structure depends on the yarn type, i.e. mono, multi-filament or spun yarn, the twist and the cross-section, mostly elliptical, with the dimensions d_1 and d_2.

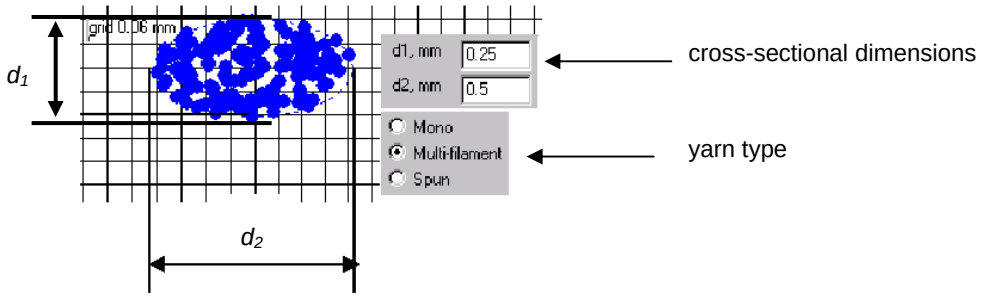

Figure 3.13: WiseTex, example of a yarn with filaments

Vectors, described by d_1 and d_2 for height and width and the vectors a_1, a_2 and b, define the cross-section of the filaments.

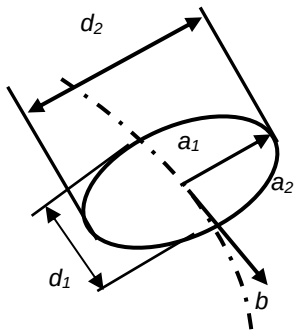

Figure 3.14: Vectors characterizing cross-section: elliptical d_1 and d_2

The topology of the textile is complex and can vary throughout the textile fabric. For this purpose, the yarn properties, the topology of the yarn interlacing pattern within the fabric repeat and the yarn spacing have to be defined.
Additionally, the bending rigidity of the individual yarns, or rovings, can be entered into the program.

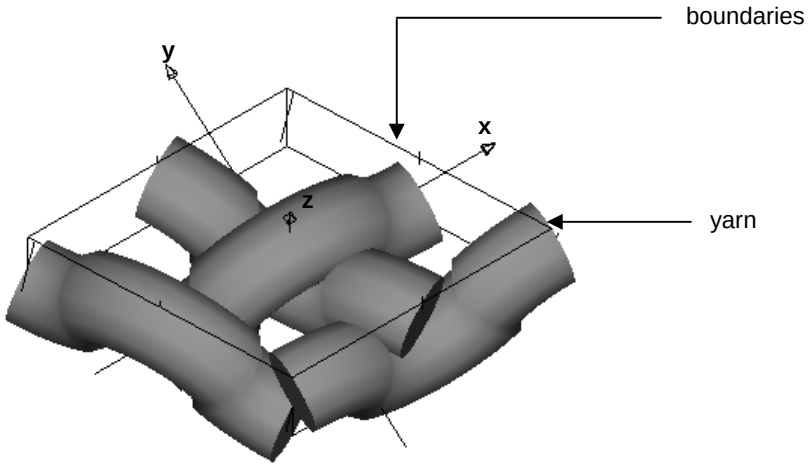

Figure 3.15: Example of WiseTex model, braid unit cell

The developed WiseTex model can then be deformed in-plane. The deformed states are considered under tension in x-direction, tension in y-direction or tension in the x- and y- directions.

In figure 3.16 the deformation of a woven fabric under tension is illustrated. The forces F_x and F_y attach at the woven structure and deform it under an angle γ. The biaxial deformation is described by the equations:

$$\varepsilon_x = \frac{\Delta X}{X_0} = \frac{X - X_0}{X_0} \qquad (21)$$

$$\varepsilon_y = \frac{\Delta Y}{Y_0} = \frac{Y - Y_0}{Y_0} \qquad (22)$$

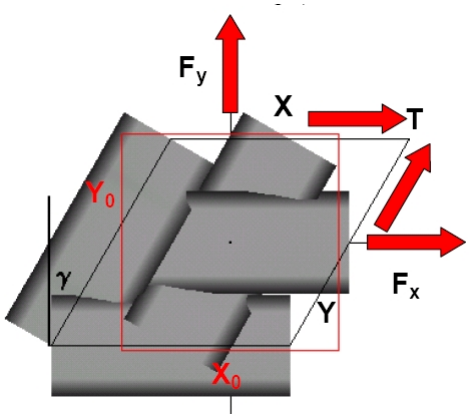

Figure 3.16: Example of WiseTex in-plane deformation

Additionally, the program predicts forces for uniaxial and biaxial loading conditions, shear forces, the presence of rupture and of wrinkling and the stress-strain behaviour.

3.6. Description of the LAP software

The LAP (Laminate Analysis Program) designed by anaglyph Ltd is a software tool used to design and analyse flat composite material laminates. The solutions are based on CLT (Classical Laminate Theory), discussed in section 3.2. The software is used in prime design for tailoring a stacking sequence. A complex analysis can be then obtained by other methods such as finite element analysis (FEA).

There are four different modules included; the Basic module and the other three modules, Non-linear, Design, Additional Failure Criteria, which are optional.

In this thesis, the Basic modulus is applied, providing linear analysis functionality to predict ultimate loads for testing.

For the design, the program requires the definition of the engineering properties of the basic material, the individual layers and the definition of the stacking sequence, the lay-up of the individual plies, including ply thickness and ply angle. Additional information on the various loadings enables the program to calculate and analyse the laminate. The subjection of loading to the laminate is e.g. in-plane load, like tension or compression, bending loads, deformations or loads considering curing, hygro, thermal or mechanical effects. The mechanical loading can be

additionally defined by load/moment and/or strain/curvature components. Effects like manufacturing deviations, e.g. actual fibre volume fraction or varying lay-up angle, are incorporated in the results. The main results include general results, stress-strain results, fail indices and displaced shape. This means effective stiffness constants for the laminate, expected in-plane laminate strength, failure criteria, maximum stresses and strains are computed. A laminate displaced shape in 3D visualises the laminate behaviour under load.

The example in figure 3.17 shows the stress distribution in YY-direction of a CF/epoxy material with an unbalanced CFRP lay-up.

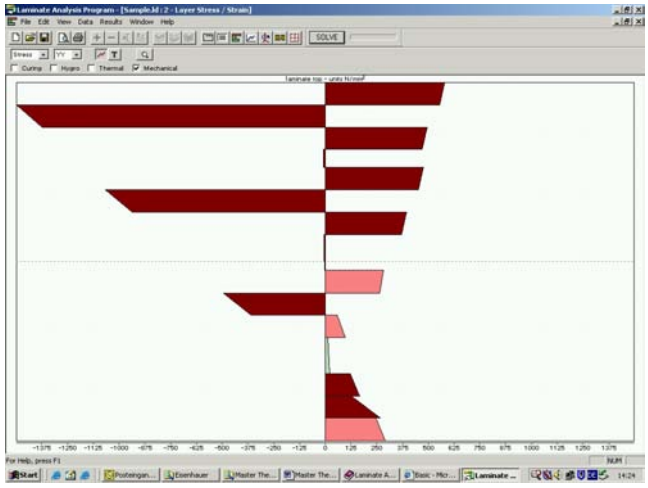

Figure 3.17: LAP of a lay-up with several plies, example

Based on this analysis, a prediction can be made for the ultimate load, which the UD-braid laminate can carry. This program is used in the later analysis for the determination of maximum loading and the behaviour of the laminate when exposed to load in chapter 10.

4. Reinforcement

The use of fibre reinforced plastic (FRP) as reinforcement of structures has been growing rapidly in recent years. This state-of-the-art report summarizes the current state of knowledge on the textile material used, i.e. the fibrous material, the braided textile, the braiding technology and the use of braids. In addition the production of the UD-braid and the UD-braid itself, used as reinforcement for the laminate to be tested, are described. Moreover, the material properties of the constituents for the laminate, i.e. resin, are discussed.

4.1. Type of material used for the UD-braid

The UD-braid to be tested is composed of two different kinds of rovings. One yarn system is a carbon roving, the HTS 5631 12 K by Tenax®. The other yarn is a matrix soluble yarn, the Grilon MS yarn developed by EMS-Chemie. The relative fineness of the carbon yarn and the Grilon MS yarn is 800 tex : 50 tex = 16 : 1. This textile reinforcement is infiltrated by an epoxy resin.
The technical data sheets of RTM6 and Grilon MS are attached in Appendix A.

4.1.1. General use of carbon fibres

In the mid 1960s there was a need for high-performance fibres, especially for aerospace applications. Conventional materials, like metal with a specific modulus of 250-300 GPa, have either a low elastic modulus or high density. In comparison, carbon fibres can reach an elastic modulus of 1200 GPa at a density close to 2. Therefore, carbon fibres show a high potential for the use of reinforcement.
In the late 1950s, carbon fibres were produced by thermal decomposition of natural fibres such as bamboo or cotton. The later carbon fibres were produced out of rayon by pyrolysis. These fibres had low mechanical strength. At around the same period, carbon fibres were also produced by the conversion of polyacrylonitril (PAN). These fibres were “strong” carbon fibres with high modulus. Another possibility to produce carbon fibres is out of pitch instead of out of PAN or rayon.
Carbon fibres consist out of at least 90 % carbon. This high percentage of the major element C is obtained by controlled pyrolysis of the above mentioned fibres, the precursors. These precursors give a high yield of carbon. During the conversion to carbon fibres, they maintain their morphology. Thereby, depending on the type of precursors, different types of morphologies and specific characteristics of the carbon fibres can be produced.
In the production of the laminates used later for the tests, carbon fibres out of PAN are used. These fibres have higher strength and modulus and lower volume fraction of voids than carbon fibres out of pitch or rayon. PAN fibres are already oriented and increase their orientation and parallelisation during processing. This process is divided into three successive stages:

- Oxidative stabilisation at 200-300 °C
- Carbonisation at about 1000-1500 °C
- Graphitisation at 1500-3000 °C [23]

Generally speaking, the higher the temperature, the better the quality of the carbon fibres.
The manufacturing stages are illustrated in figure 4.1.

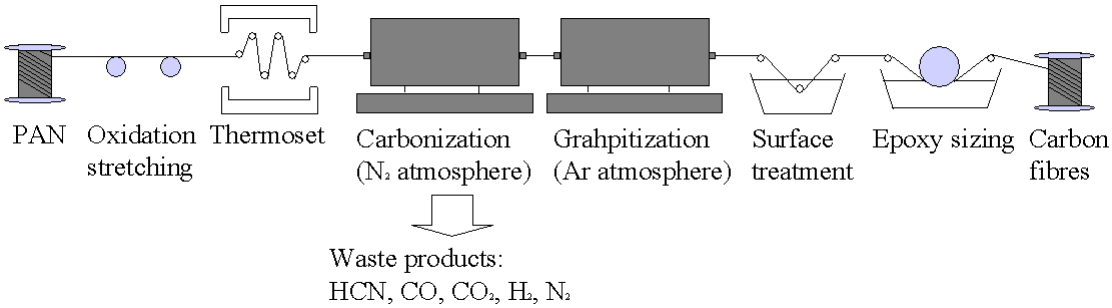

Figure 4.1: Manufacturing process of carbon fibres out of PAN

The polyacrylonitril fibres are first stretched and simultaneously oxidized. This process stabilises the PAN fibres by converting them into a non-plastic cyclic or ladder structure by cross-linking. During carbonisation at inert atmosphere, normally nitrogen, the non-carbon elements, that means HCN, NH_3 and H_2, are removed as volatiles and replaced by the carbon element. The result is a carbon yield of 50 %. The successive stage, graphitisation, is mainly a heat treatment at a temperature range of 1500-3000 °C. During this process, the structure becomes more ordered and the filaments turn into a graphitic form. The resultant filaments are of high tensile modulus. Hot stretching can additionally increase their strength. Therefore, the final morphology and properties of the carbon fibres depend strongly on the conditions of the manufacturing process.
The properties of the carbon fibres can be divided into the following parameters:

Table 4.1: Properties of PAN-based fibres [23]

Parameter	High strength (HS)	High modulus (HM)	Ultra high modulus (UHM)
Carbon component weight [%]	92 – 94	>99	>99.9
Filament diameter [μm]	5 – 8	5 – 8	6 – 8
Density [g/cm3]	1.7 – 1.8	1.8 – 1.9	1.9 – 2.1
Tensile strength [GPa]	2.5 – 7.0	2.2 – 2.4	1.8 – 1.9
Tensile modulus [GPa]	220 – 250	340 – 380	520 – 550
Tensile elongation [%]	1.2 – 1.4	0.6 – 0.7	0.3 – 0.4

4.1.2. Carbon fibres, used for UD-braid production

The main roving dominating the UD-braid is the carbon filament yarn HTS 5631 12 K produced by Tenax®. HTS is the fibre type, representing a classic Tenax® high performance carbon fibre yarn type with standard modulus and high tenacity (HT) providing excellent mechanical laminate properties. The number 5631 designates the fibre type. This type is a high strength aerospace grade carbon fibre used for reinforcement in high performance composites, produced out of PAN and surface treated with ca. 1.0% sizing based on polyurethane.
The characteristics are presented in table 4.2.

Table 4.2: Tensile properties of Tenax® HTS 5631

Type	Tenax® HTS 5631
Fineness [tex], without sizing	800
Number of filaments	12000
Twist	0/Z10
Filament diameter [µm]	7
Density [g/cm³]	1.77
Tensile strength [MPa]	4300
Maximum force [N]	2039
Tensile modulus [GPa]	240
Elongation at break [%]	1.8

The ideal stress-strain curve is linear:

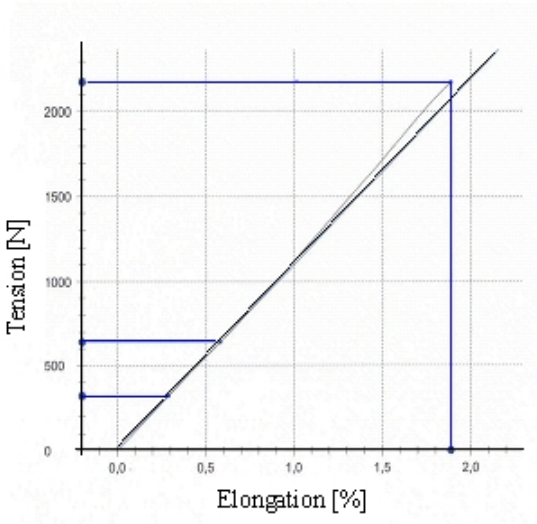

Figure 4.2: Stress-strain curve of carbon HTS 5631 (source: Toho Tenax)

4.1.3. Grilon yarn

As support yarn, the Grilon yarn MS, a polyhydroxyether developed by EMS-Chemie, is used. It is a fusible bonding yarn of a small fineness, which only provides stability during and after the braiding process. At 80 °C the yarn starts to melt and at 160 °C destruction follows, thereby dissolving in the epoxy matrix. Used only as support yarn, its mechanical properties are irrelevant. Its characteristics are shown in table 4.3.

Table 4.3: Data sheet, Grilon MS

Type	Grilon MS
Count [tex]	50
Twist	none
Linear density [g/cm³]	1.14
Tenacity [cN/tex]	10
Elongation at break [%]	50
Melting point [°C]	None, amorphous
Glass transition temperature [°C]	80

The data sheets for the HTS 5631 and Grilon MS can be found in the Appendix (attached CD).

4.2. Types of reinforcement structure

The structure of composite textile reinforcement can be of various types. It can be used, for example, non-axial fabrics. These fabrics are non-wovens, chopped fibre mats, bonded together. The parameters influencing the tensile strength are the fibre content in the laminate, the fibre direction and the orientation of the fibres. Woven fabrics, like plain, twill and satin weaves, are flat fabrics with integral stiffness. The basic yarn direction is in 0 ° and 90 °, interlacing two yarn systems, the warp and the weft yarns. However, they have limited drapability and show the disadvantage of undulation. Weft knitted fabrics are stretchable and therefore of a good drapability. The transformation of forces is in no specific direction due to the loop-structure. During application of tensile load, the loops change their shape in order to accommodate the applied load, resulting in resistance to impact and absorption of energy. Warp knitted fabrics are also drapable in a 3D-shape, showing good tensile strength in the warp direction. When used in composites, knitted fabrics are pre-stretched, so that the loops are already completely extended and the load is directly introduced into the fibres. Embroidery on a textile structure gives local reinforcement to a laminate. Reinforced knits, also called Direct Oriented Structures (D.O.S.), are made up of several layers of fabrics or rovings with different yarn angles. These multi-axial, non-crimp fabrics take-up loads in many possible directions, depending on the direction of the introduced layers. Most common are the systems Liba, Malimo and Meyer. It is also possible to introduce yarns or fleeces into a knitting

or stitch-bonding machine to produce more voluminous textile structures. Another, advantageous possibility for composite reinforcement is a braided textile.

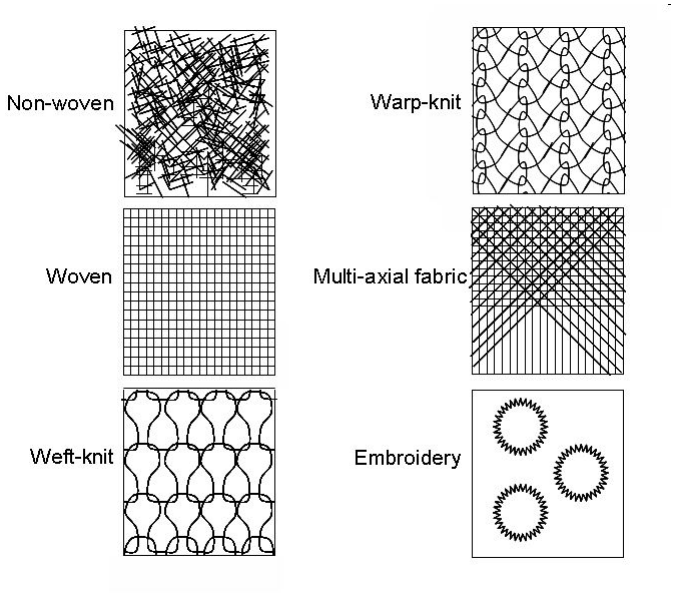

Figure 4.3: Types of reinforcement structures

Braiding is an established technology for the production of textiles used for shoe-laces as well as for ropes, tubes and hoses for technical end-use. High tech braids find application in the technical field, e.g. tow ropes, climbing ropes, seal ropes and biomedical hoses, for example artificial vascular grafts. Additionally, braids are used as preforms in composites in aerospace, automotive, industrial and medical applications and recreational equipment, like snowboards and tennis rackets. They also find application in wind energy. [1]

4.2.1. Braids

Braids consists of two or more yarn or roving systems intertwined, whereby at minimum two yarns cross each other alternately in a continuous way. The results are bias yarns in the textile structure, where the braiding angle can vary between 10° and 80°, depending on the take-down velocity. At low take-down velocity, a large braiding angel is obtained and vice versa, shown in figure 4.4. Braids have solid product selvages. [2]

Figure 4.4: Braid with altering braiding angel (source: ITA)

Interdependently, diameter or width, fibre angle and area weight can be engineered and changed during the braiding process.
Textile structures produced on a braiding machine result in 2D (planar)- or 3D (tube-like or T-shapes)-braids. 2D-braids only expand in the x- and y-direction.

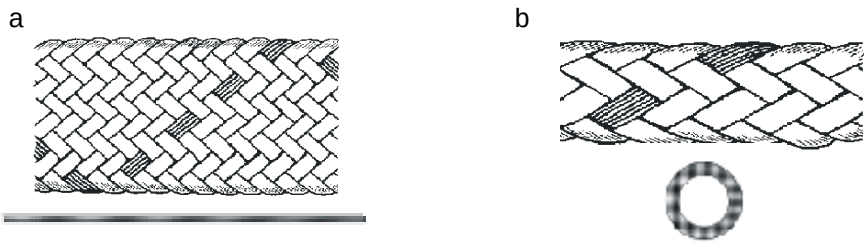

Figure 4.5: 2D- braids top view and cross-section, planar (a), tube-like (b) (source: ITA)

3D-braids stretch additionally in the z-direction, where the yarns penetrate through a three-dimensional structure, spanning a voluminous space. The process of the production and a 3D-braid is visualized in figure 4.6 a and b. [10]

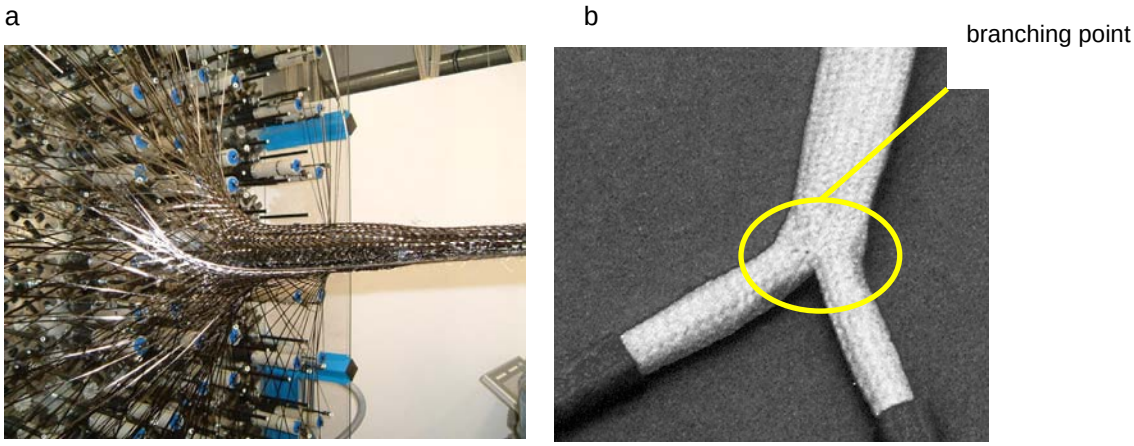

Figure 4.6: Braiding of a 3D-braid (a) (Source ITA)
3D-braid; branched structure (b) (Source ITA)

Only with the 3D-braiding process is it possible to produce a branched structure. The main part is a 2D-braid. At the branching point the yarns inside the braid also stretch in the third dimension.
Braids can also be directly manufactured onto a moulding tool or mandrel, which is known as overbraiding. The mandrel can be shaped in a complex form.

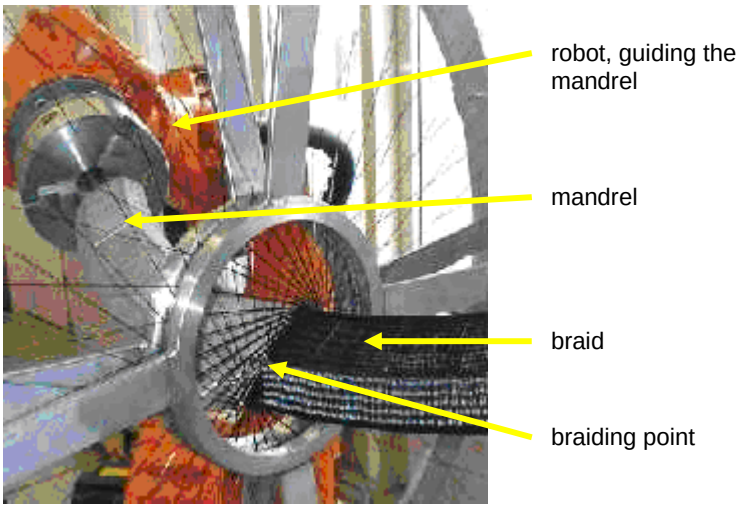

Figure 4.7: Overbraiding process (source: EADS)

The thickness of the braids is defined by the diameter of the yarn and the area weight. However, via overbraiding, a defined thickness can be realized by braiding several layers of fabric over each other.

It is also possible to introduce yarns in the production direction, so called standing-yarns, which are not active during production. They can be introduced at any position inside the braid. This leads to triaxial, multi-directional braids. [10]

Mechanically interlocking of rovings or yarns, the usage of continuous filaments and the coiling of filaments in a helix, make braids highly efficient in distributing loads evenly. Additionally, braids are impact resistant, absorptive of energy and have a high fatigue resistant, showing low cracks when being exposed to high fatigue cycles. Due to their low lateral stability, braids are bendable and adaptable to any shape, however in the technical field, through the use of special linings or resins, braids can become stiff and firm in composites. [30]

4.2.2. Braiding, the technology

Braiding technology has the potential of producing optimal design for braided composite structures by applying recent braiding processes.

Mainly, there are two different braiding procedures. The conventional braiding, which uses strand braiding machines, lace braiding machines and packaging braiders to produce 2-D braided textiles. Circular braiding and overbraiding also produce 2-D fabrics. The three-dimensional braiding technique uses the Four-Step-Braiding process, Two-Step-Braiding process and the 3-D rotary-braiding process. [9]

2D

In circular braiding machines the arrangement of the bobbins can be done in two ways. They can face in the direction of the centre, known as a radial braiding machine, produced by Herzog, figure 4.9. The bobbins follow a circular path around the centre in sinusoidal circles shifted by 180 ° on two pathways in opposite direction to obtain a crossing of the yarns.

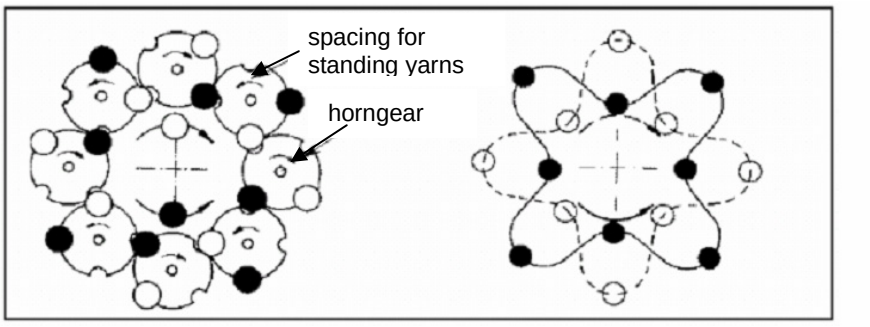

Figure 4.8: Scheme for circular braiding [2]

Due to their special alignment to the centre, the yarns on the bobbins are less stressed, as the distance between the bobbin and fell varies only a small amount. Thereby, the yarn is hardly pulled off the bobbin and back. Moreover, the yarns of the different bobbins converge in a very late state, which reduces friction. Standing yarns can be subjoined from release bobbins outside the machine, arranged at the circumference facing in the take-up direction.

In figure 4.9 the braiding robot from the KUKA company is shown, which is operated by a special computer sub-program, swaying the mandrel with a big freedom of movement, inside the braiding ring and forth.

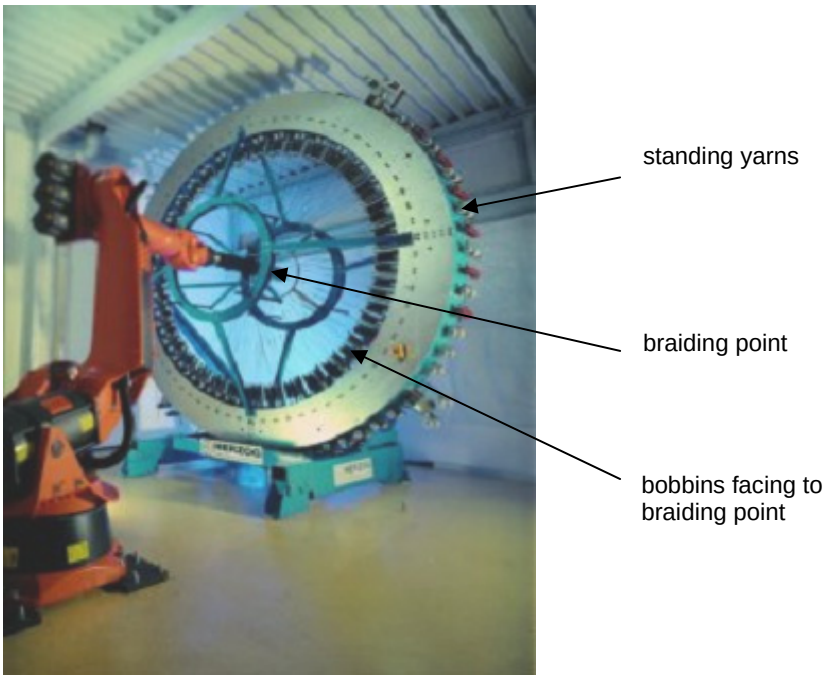

Figure 4.9: Radialbraider by Herzog (source: Herzog)

In the other arrangement the bobbins are facing in the direction of the take-down, moving on two concentric circular paths in opposite rotational direction. To realize a yarn crossing, the bobbins alternate between the inner and outer slide way, shown in figure 4.10.

Figure 4.10: Circular braiding

Further developments in circular braiding technology are sophisticated circular braiding machines being able to produce thin-wall branched structures with a bifurcated mandrel and improved near-net-shaped fibre preforms of complex shaped composite materials. [11]

3D

The architecture of 3D-braids can vary, creating outstanding properties for technical applications, achieving high impact tolerance levels and structural energy absorption. 3D rotary-braiding machines consist of a braiding bedplate with horngears arranged in rows and columns. Each horngear can carry up to four bobbins. Additionally, each horngear can be equipped with one yarn in the centre, forming axial yarns. The horngears are rotating in opposing directions, moving the bobbins from one gear to the other by switch points. The schematic drawing in figure 4.11 demonstrates the arrangement of a horizontal 3D-Rotary braiding machine, shown with the red arrow, the possible movement of the bobbins, being transferred from one horngear to an adjacent horngear. To avoid crashes of bobbins during the braiding process, a computer set-up is written for the movement of the bobbins and their transfer. [20]

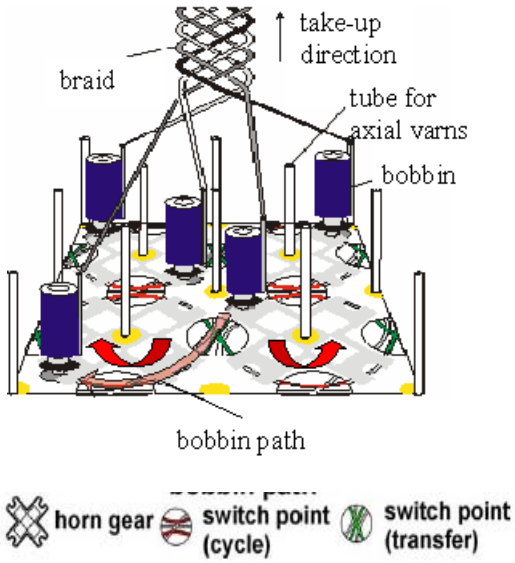

Figure 4.11: Principle of 3D–Rotary braiding machine (source: ITA)

Examples for 3D-Rotation machines are shown in figure 4.12, displaying two possible arrangements.

a

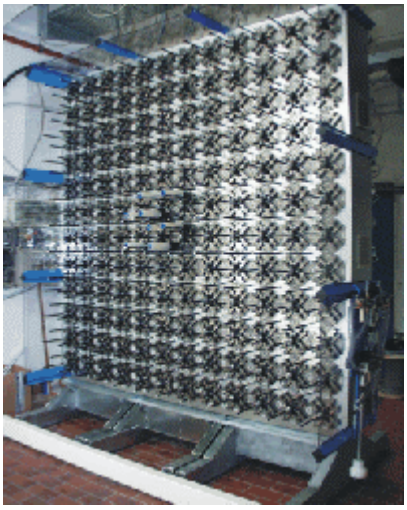

b

Figure 4.12: 3D-Rotation machine, vertical (a) horizontal (b) (source: ITA, EADS)

In an overall cost analysis, braiding is cost competitive in comparison to filament winding and cost effective considering advancements in technology, conformability of the braid and the predictability of the braid's architecture. Moreover, the need for cutting, stitching and the manipulation of fibre orientation is reduced.

4.2.3. UD-Braids in general and specific, used for tests

Traditional braids are normally symmetric braids with the same or similar yarn count of all yarn systems to provide strength and absorption of forces in the bias directions. However, several disadvantages of braids, like undulation resulting in reduced strength and stiffness, lead to attempts to invent new technologies. Recent developments of asymmetric braids already point in the direction of the development of UD braids.

A patent on asymmetric braiding of improved fibre reinforced products was applied for in 1992, with the patent number WO9215740 US. In asymmetric braiding the “cross-sectional areas of the fibres employed to form the diagonally crossing braids are substantially different”. [17]

Thereby, undulation of the yarns at the crossing points is decreased. The idea arose from filament winding, which offers advantages like better translation of fibre modulus by the elimination of undulation. However, the disadvantage is the slippage of the filaments sideways out of the geodesic path and the difficult manufacturing of wound fibre preforms with conventional lamination methods.

Braiding of self-stable, interlocked asymmetric fabrics overcomes large undulation angles and severe abrasion damage. The rovings, different in cross-sectional dimensions, are loaded in the braiding machine onto opposing yarn carriers. The primary reinforcement fibres of large tow size, with little or no twist, lie flat in the textile. The containment fibres of low tow size, influencing the undulation of the primary reinforcement fibres, perpetuate precisely the arrangement of the reinforcing fibres. [17]

Figure 4.13 is a scheme of an asymmetric braid, showing the reinforcement fibres, 212, and the contaminant fibres, 218 and 210, with an angle of 45 °.

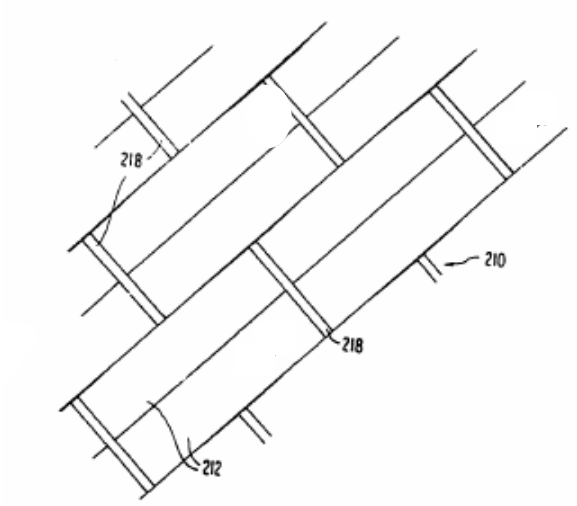

Figure 4.13: Asymmetric braid (source:[17])

The contaminant fibres of high fineness do not contribute to the stiffness and strength of the braid. Therefore a consideration is to disregard the mechanical properties of the contaminant fibres and use fibres with low tensile strength instead of high-strength fibres.

A further step is the development of unidirectional (UD) – braids, patented by EADS-G. [18]

Unidirectional braids are braids with parallel oriented rovings under a specific angle, fixed by thin yarns, melting in the matrix. The task of these containment yarns is only to fixate the primary reinforcement fibres on the mandrel; in the laminate they have no function anymore. The process of UD-braiding is similar to the conventional 2D-braiding technology. The resultant structure is different from the traditional braids but similar to the asymmetric braid. [15]
One example for the use of such a UD-braid is in the framework of a project for the development of a subscalar version of the Ariane main compartment motor.

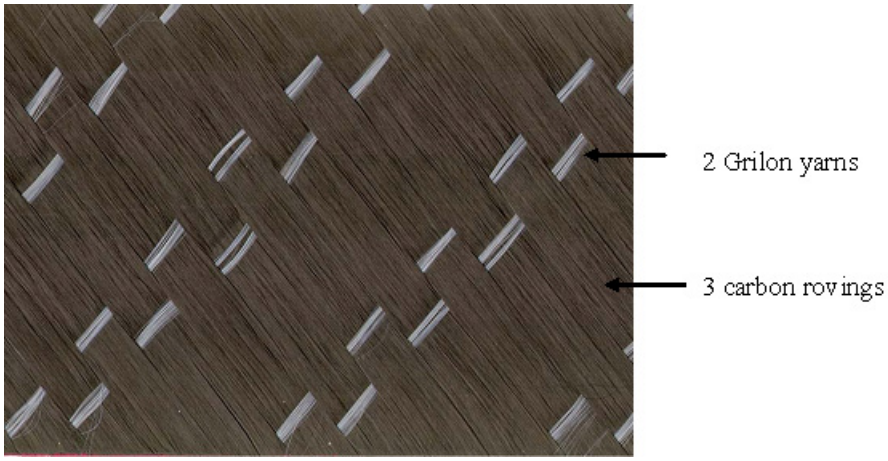

Figure 4.14: UD-braid, scan

The UD-braid, shown in figure 4.14 is used and characterised in this thesis. The black roving is the carbon yarn and the white one is a matrix soluble yarn with the brand name Grilon MS, melting in the matrix.
The main yarn system is of high tensile strength and the remainder is a yarn system of a similar type as the matrix. The latter gives stiffness during production and lamination and then “disappears” in the composite. As in asymmetric braiding, undulation on a mesoscopic scale is drastically reduced, providing greater strength and stiffness. Additionally, during infiltration the formation of resin cavities is decreased. The alignment of the braid in the composite is in the direction of the carbon filaments to take the greatest advantage of the tensile strength of the carbon.
The UD-braid out of the carbon roving and the Grilon yarn is braided onto a mandrel with the circular braiding technique by the overbraiding process, as described in chapter 4.2.2. The pattern of the UD-braid is according to a modified arrangement of the 144 bobbins of the braiding machine; three carbon rovings run parallel and are crossed by two additional yarns, the Grilon yarns. An additional characteristic is the pattern of the Grilon yarn. Two times two Grilon yarns cross the three carbon rovings and then the next two Grilon yarns are left out. The 144 bobbins on the braiding machine are assigned according to the following pattern:

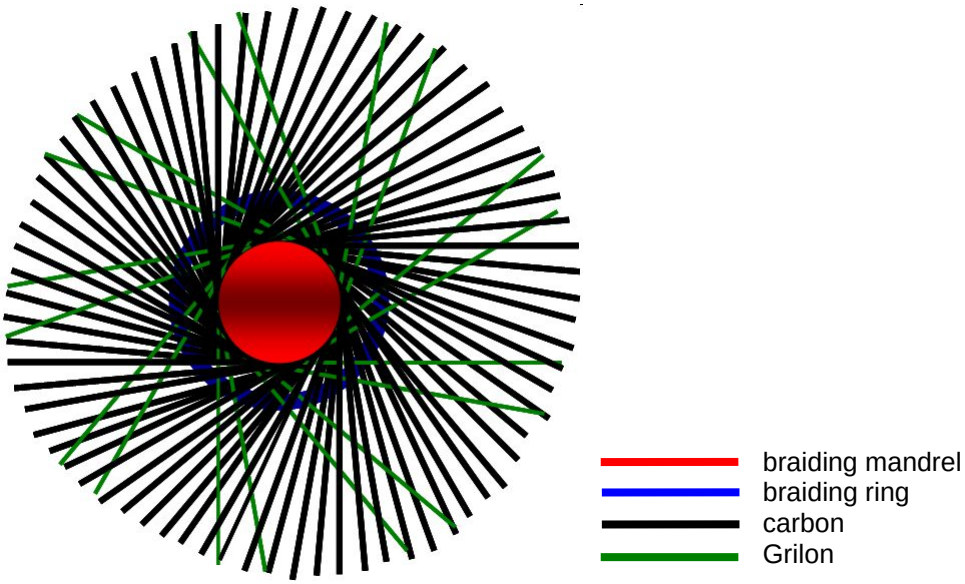

Figure 4.15: UD-braid, schematic drawing of the braiding process

The fabric is produced according to the following braiding scheme (figure 4.16), whereby the braiding angle is not 45 °, but slightly shifted as defined by the take-down velocity.

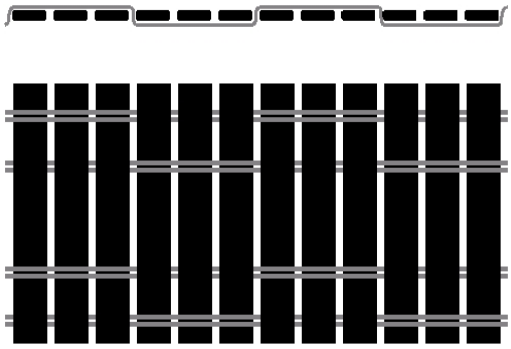

Figure 4.16: Braiding scheme

The dimensions of the hollow mandrel are: *u* (circumference) = 51 cm
d (diameter) = 16.2 cm

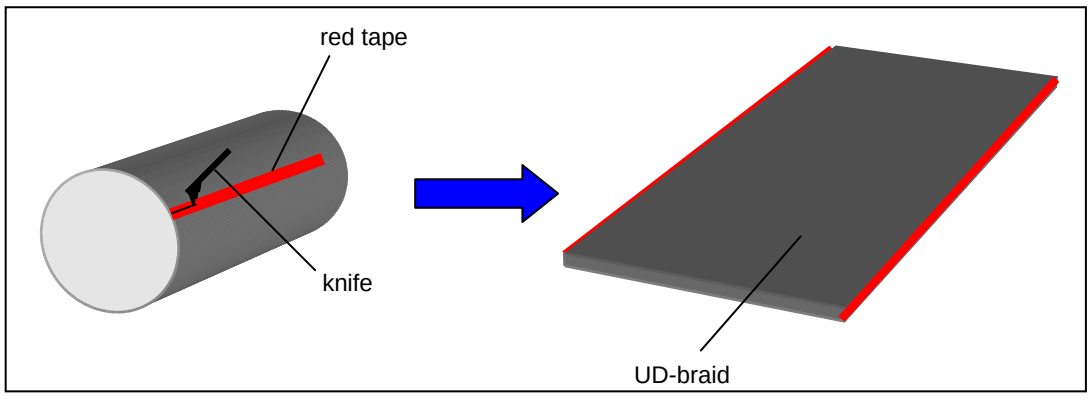

Figure 4.17: UD-braid cutting

The UD-braid is braided onto the hollow mandrel, whereby a robot guides the mandrel to assure planar movement of the mandrel. Then the braid is secured with a tape to avoid that filaments move and, as a result, misalign during the cutting of the braid, as shown in figure 4.17.
After cutting along the mandrel length, i.e. the braiding direction, a planar braid is obtained.

In figure 4.18, *d* stands for the thickness of the braid. One unit cell is defined as the distance between two Grilon yarns. The slight undulation seen in figure 4.18 is eliminated during lamination when applying pressure and temperature. The Grilon yarn melts and in the finished composite part the carbon fibres are completely straight.

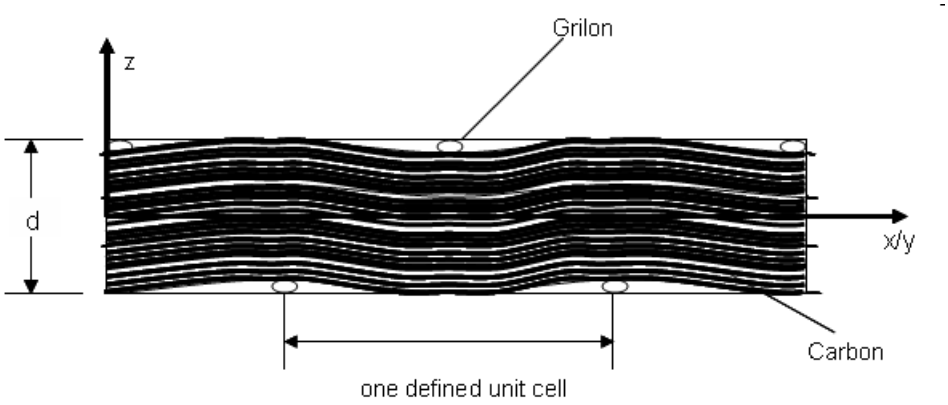

Figure 4.18: Schematic drawing of the undulation in the UD-braid

4.3. Epoxy resin, used for laminate production

Epoxy resin belongs to the group of duroplastic matrix systems with strongly interconnected chain molecules. In figure 4.19 the comparison of the viscosity of an epoxy resin and a PP matrix in an uncured state is shown. There is a strong decrease in viscosity dependent upon the temperature for the epoxy resin, with the lowest viscosity at ca. 150 °C.

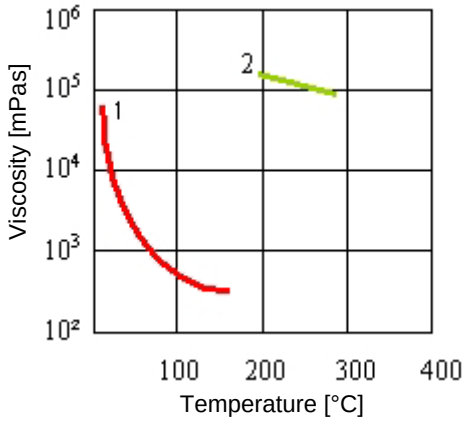

Figure 4.19: Viscous performance of epoxy (duromere) -1, and polypropylene (plastomere) -2, dependent upon temperature [4, p. 128]

The epoxy resin used in the production of the laminate, described in chapter 5, is RTM 6 manufactured by Hexcel. RTM 6 is a premixed epoxy/amine system developed for the needs of the aerospace industry in resin transfer moulding. Its curve of viscosity dependent upon temperature is shown in figure 4.20.

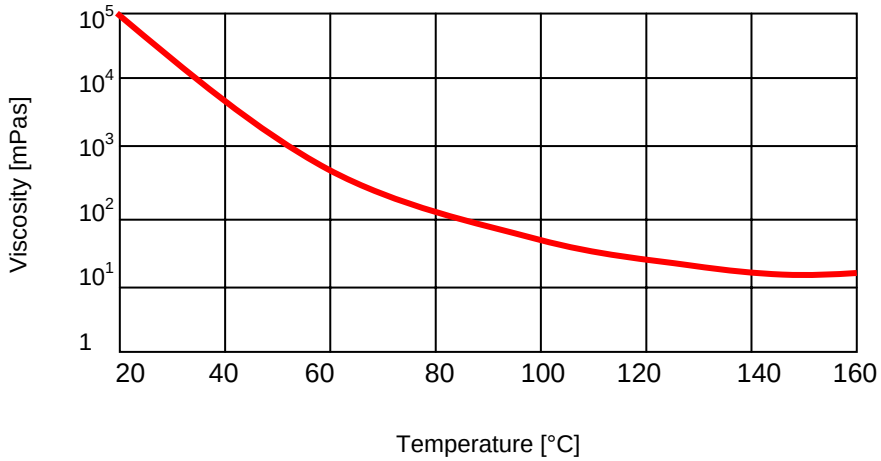

Figure 4.20: Viscosity of Hexcel RTM 6

The data sheet of RTM 6 can be found in the Appendix (attached CD)

5. Laminates

In the following chapters a short description of the current lamination methods used is given. Additionally, the preparation of the laminates and the quality testing of the laminates are described. Quality testing includes the H_2SO_4 test to determine the fibre volume fraction and a C-scan of the plates to detect voids or contamination inside the plate.

5.1. Lamination Methods in general

There are many manufacturing processes for producing fibre reinforced plastics. A few examples are spray lay-up, wet lay-up or hand lay-up, vacuum bagging, filament winding, the continuous process of pultrusion, RTM (resin transfer moulding), VARI (vacuum assisted resin injection), Resin Film Infusion (RFI) and prepreg moulding. Vacuum-Assisted Resin Transfer Moulding (VARTM) is widely used for large-scale composite manufacturing.
Another method is the VAP method, the Vacuum Assisted Process, developed and patented by EADS Germany for producing CFRP components. It is a special form of the VARTM. A gas-permeable membrane, forming a resin barrier, is placed over the fabric layers and sealed to work under low pressure. A connection to a vent allows uniform vacuum distribution and a continuous degassing of the resin. [19] One of the advantages is that no autoclave is needed, the pressure gradient is generated by vacuum and thereby gas and air inclusions are minimized. This method, described in more detail in chapter 5.2, is used in this thesis to produce the laminates for specimen production.

5.2. Laminate preparation for testing according to Ladevèze

The laminates are prepared for testing according to the testing program described by Ladevèze. The stacking sequence is defined for the five different test series, resulting in four laminates with different stacking sequences. [25]

5.2.1. Stacking

For the stacking of the UD-braid layers, each layer has to be cut to the desired dimensions. The fabric pieces are secured on the edges with a tape able to withstand high temperatures in order to restrict the filaments from moving out of their alignment. The stacking sequence is different for each plate.

The specimens, which have to be prepared for the tests, are cut out of four different plates. The specimens later obtained out of plate 1 are used for the 0° simple tensile test and the 0° simple compression test.

From the production process of the UD-braids a fabric is obtained where the carbon roving has an angle of 40° to the edge. To be able to produce unidirectional samples of 0 °, the eight layers of the braid are all cut and laid up at an angle of 40 ° in the same direction. The parameters of the laminate are as shown in figure 5.1:

- Dimensions: 400 x 500 mm
- Stacking: 8 layers at 40 ° (specimens will be cut under an angle to get 0 °- specimens)
- Weight of the eight layers: 510 g
- Weight of the layers after subtracting the weight of the tape and the Grilon yarn: 489.6 g.

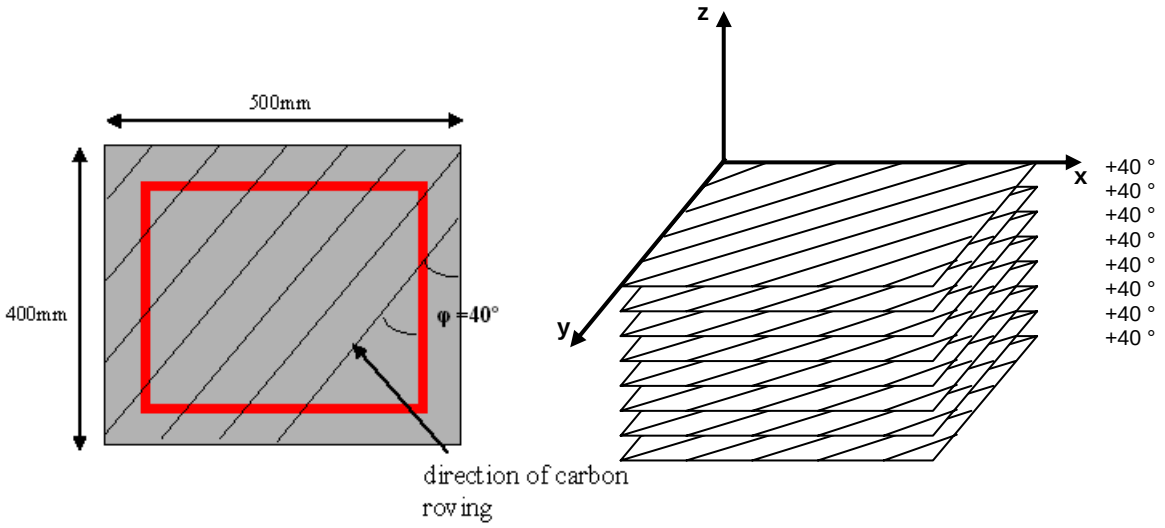

Figure 5.1: Cutting scheme of the layers for plate 1 and stacking sequence

Plate 2 is laid up in ±45° for the simple tension test with “load/unload” cycles on $[\pm 45]_{2S}$ laminates. For the cutting of the layers for plate 2, the edges are again secured by a tape and then cut out at an angle of 45 ° with the following parameters:

- Dimensions: 400 mm x 400 mm
- Stacking: 8 layers at ±45 °, symmetrically to centre line $[+\theta_1/-\theta_2/+\theta_1/-\theta_2/-\theta_2/+\theta_1/-\theta_2/+\theta_1]$
- Weight of the 8 layers: 401.8 g.

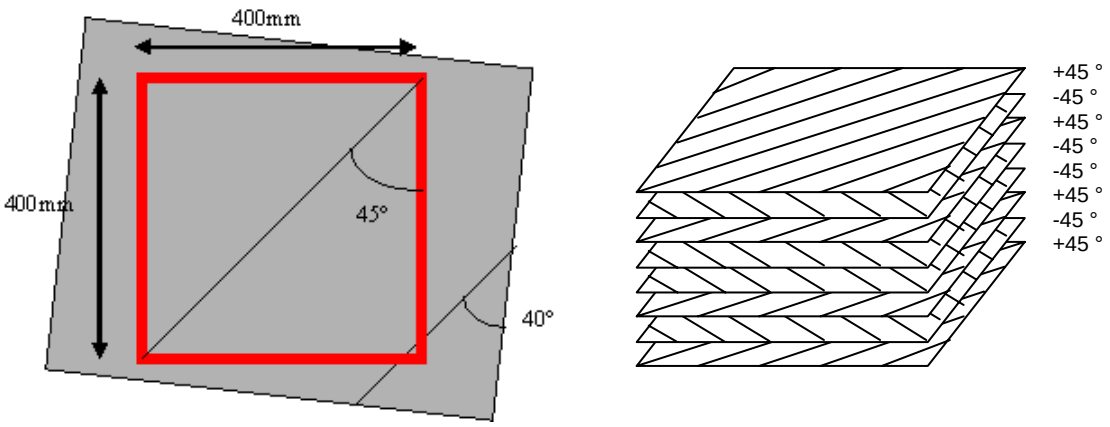

Figure 5.2: Cutting scheme of the layers for plate 2 and stacking sequence

Plate 3 contains eight layers with the alignment of +45°. The specimens out of this plate are used for the simple tension test with “load/unload” cycles on $[+45]_8$ laminates.

The cutting of the layers for plate 3 is analogous to plate 2.

- Dimensions: 400 mm x 400 mm
- Stacking: unidirectional with an angle of +45 ° of all 8 layers
- Weight of layers (weight of Grilon and tape subtracted): 371.8g.

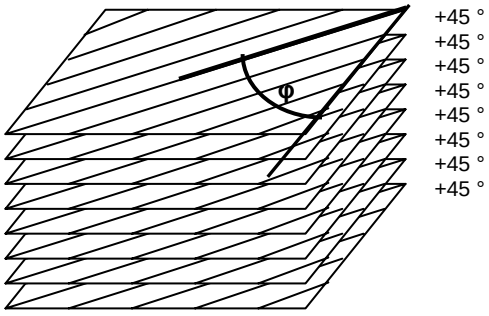

Figure 5.3: Stacking sequence of plate 3

Plate 4 in ±67.5° is used for the simple tension test with “load/unload” cycles on $[\pm 67.5]_{2S}$ laminates. The eight layers are cut out of the UD-braid layers, which have an angle of 40 º. The parameters are the following:

- Plate dimensions: 400 mm x 400 mm
- Stacking sequence: angle for the 8 layers +/-67.5 º
- Weight of the stacking: 380 g
- Weight of pure carbon fibres: 361.9 g.

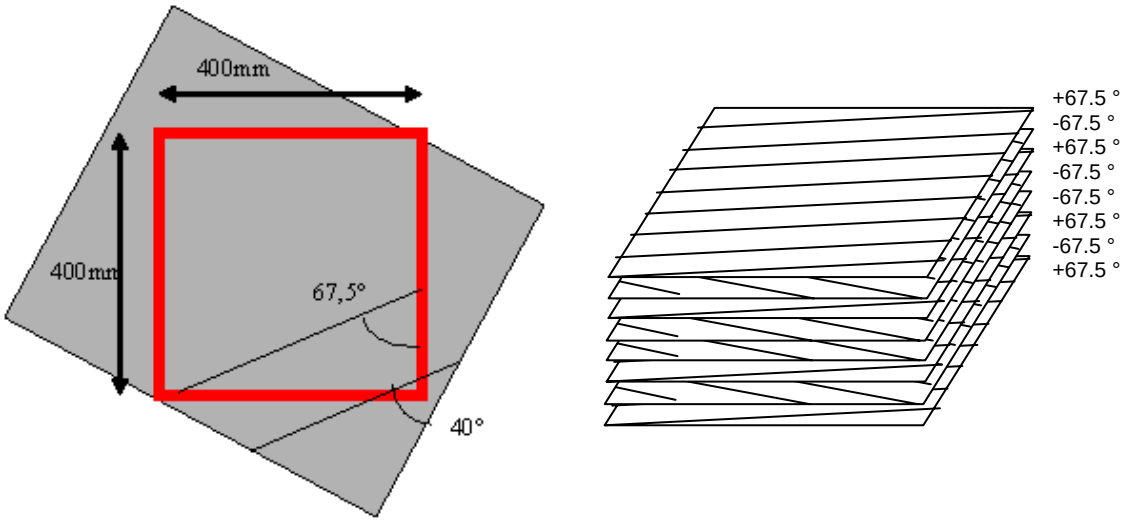

Figure 5.4: Cutting scheme of the layers for plate 4 and stacking sequence

5.2.2. Infiltration

All the four plates are infiltrated with the VAP (vacuum assisted process) in a convection oven from the company Heraeus. The set-up for the VAP method is illustrated in figure 5.5 with all the material used, listed in table 5.1.

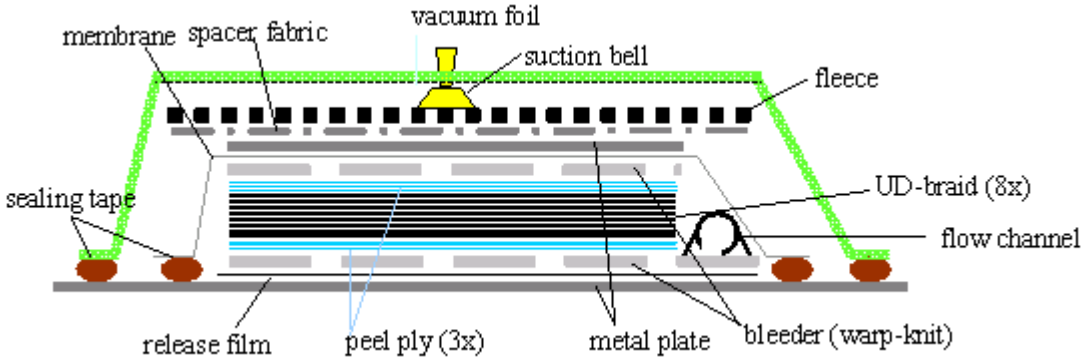

Figure 5.5: Set-up for the VAP method

Table 5.1: Material used for VAP method

Material	Manufacturer
Release agent	Release All #50 (Airtech advanced materials group)
Release film	FUS Tedlarfolie
Membrane	Goretex (semipermeable)
Peel ply	FUS Super Release Blue Code 51789/061
Bleeder	Werder Systems Polyesterfliesmedia
Vacuum fleece	Felt
Vacuum foil	FUS Vakuumfolie HS8171
Sealing tape	Aero Consultant CH GS-100 Sealant 1/8" x 1/2"
Flow channel	Gummi-Bauer Silikonprofil Art.-Nr. 242-717674190
Resin tube	Sahlberg PTFE Schlauch 6x1x8 mm
Others	Aluminium compression plate

Figure 5.6 shows a picture of the finished set up for the VAP method. Under the vacuum foil the eight layers of the UD-braid together with the infiltration auxiliaries are sealed airtight with the sealing tape.

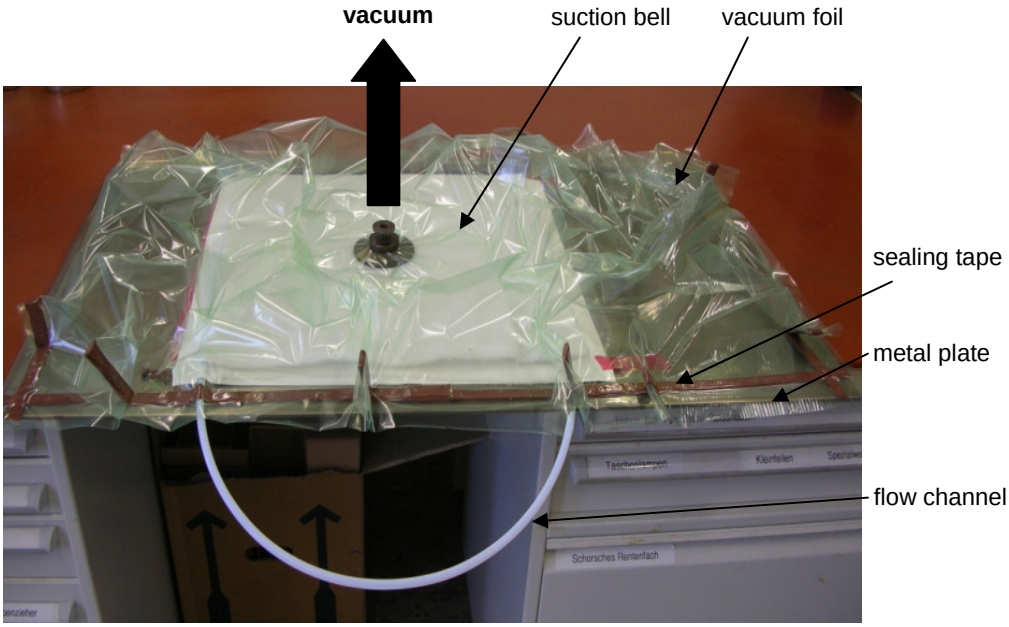

Figure 5.6: Finished VAP set-up

The set up is placed into the oven and vacuum is applied. The semi-permeable membrane allows air to penetrate, however the resin is held back. Into this “chamber” the resin is injected via a flow channel. The resin flows evenly into the “chamber” containing the eight layers of the UD-braid, with the help of the bleeder, which is a warp-knit out of polyester.

The desired amount of the preheated epoxy resin, is sucked into the preheated plate via a pipe and the flow channel at 100 / 120 °C. After letting the resin cure at a given time and temperature, the plate is removed from the oven to cool down before unwrapping the laminate out of the lay-up. The peel ply easies this process. The four finished plates are post cured, which means tempered at 180 °C for two hours to receive a homogeneous and identical degree of cure in the different laminates.

The infiltration of plate 1 is produced according to figure 5.5. During the infiltration process, the temperature of the resin and the plate in the oven is regulated according to the following scheme:

- Pre-heating of resin and lay-up: at 80 °C for 160 min
- Infiltration of resin into lay-up: at 100 °C
- Extra addition of resin: at 120 °C after 260 min
- Curing: at 180 °C for 60 min
- After-curing: at 120 °C for 640 min
- Total amount of resin infiltrated: 530 g; take-up by plate 310 g
- Absorption by the bleeder and a portion remaining in flow channel: 220 g
- Total weight of laminate: 800 g; 490 g fibres and 310 g resin
- Final average thickness of laminate: 2.31 mm

The infiltration of plate 2 proceeds like the following:

- Pre-heating of resin and lay-up: at 100 °C for 160 min
- Infiltration of resin: 480 g at 120 °C
- Curing of resin: at 120 °C for 60 min, and for 60 min at 180 °C
- After-curing: at 120 °C for 640 min
- Total weight of laminate: 655 g; 402 g fibres and 253 g resin
- Final average thickness of laminate: 2.37 mm

The laminate plate 3 is heated at a later state. Therefore, the temperature for heating is higher than the one for heating the resin:

- Pre-heating of lay-up: at 120 °C for 20 min
- Pre-heating of resin: at 70 °C for 120 min
- Infiltration of resin: 460 g at 100 °C
- Curing of resin: at 180 °C for 30 min
- After-curing: at 120 °C for 720 min
- Final weight of laminate: 580 g; 372 g fibres and 208 g
- Laminate thickness: 2.27 mm

For plate 4, the infiltration procedure follows this routine:

- Pre-heating of lay-up and resin: at 80 ºC for 120 min
- Infiltration of resin: 460 g at 120 ºC
- Curing: at 180 ºC for 60 min
- Final post-curing: at 120 ºC for 660 min
- Final thickness of laminate: 2.22 mm
- Final weight of laminate: 540 g, 362 g fibres and 178 g resin

As an example, the curve of the infiltration temperature is shown in figure 5.7.

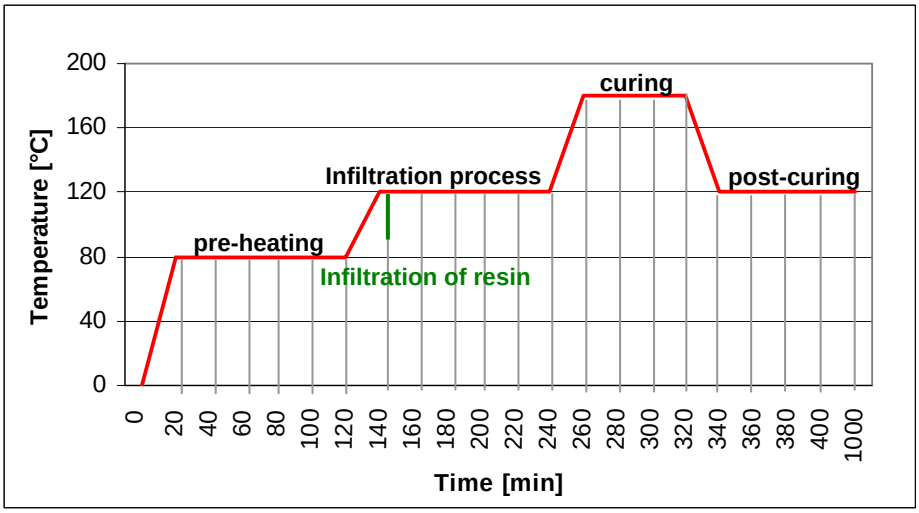

Figure 5.7: Infiltration temperature of plate 4

The detailed infiltration processes, including temperatures, are attached in the Appendix (additional CD).

The final examination of the plates after post-curing shows a slight warpage of plate 1 and plate 4. Especially when placed into cold water, the warping of the plate is aggravated. There could be several reasons for this effect.

One reason could be the strong water adsorption of the Grilon MS yarn. No shortening in length appears. However the water absorption by weight is 80 %, which evaporates completely after drying. The different post-curing rate of the resin due to the introduction of heat into the oven from above can be another reason. The epoxy resin at the top part of the plates cures at first and faster. This linking of the polymer chains in the resin causes the bending, most visible in plate 1 in the direction perpendicular to the fibre orientation. Another possibility could be small differences in layer thickness or in the layer orientation of the lay-up. A possible reason for the flexion of plate 4 could also be the different distances of the single layers to the middle axis, especially serious, as the plates are very thin. That means the layers with a negative angle are more concentrated around the centre, visualized in figure 5.8

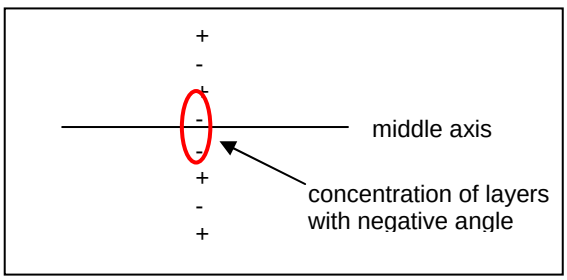

Figure 5.8: Stacking sequence, dependence of lay-up angle

However, the direction of the bending of the plates is in the direction of the smallest specimen dimension. Therefore, it can be neglected and the specimens can be used for the tests.

5.2.3. Ultrasonic test of the plates

The produced plates are tested with the ultrasonic test method (reflection method) in a water reservoir. The testing head has a frequency of 10 MHz with a focus at 15 mm, scanning with a grid distance of 1 mm in x- and y-direction.

The scanned data are displayed in an Ultrasonic C-diagram, the CSCAN, determining material characteristics of interest such as the presence of cracks, voids, inclusions, delamination, porosity, part thickness and misalignments of rovings. The sonic speed is measured inside the plates by sending and receiving ultrasound through the cross-section of the laminates, which means the shortest distance. The amplitude is colour coded; high amplitudes are displayed in bright (yellow) colours and low amplitudes in dark (blue) colours.

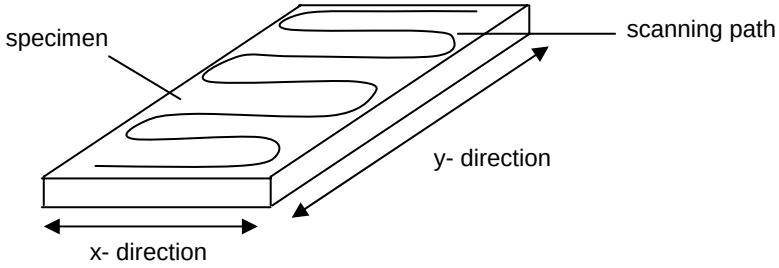

Figure 5.9: Ultrasonic C-scan, scanning path

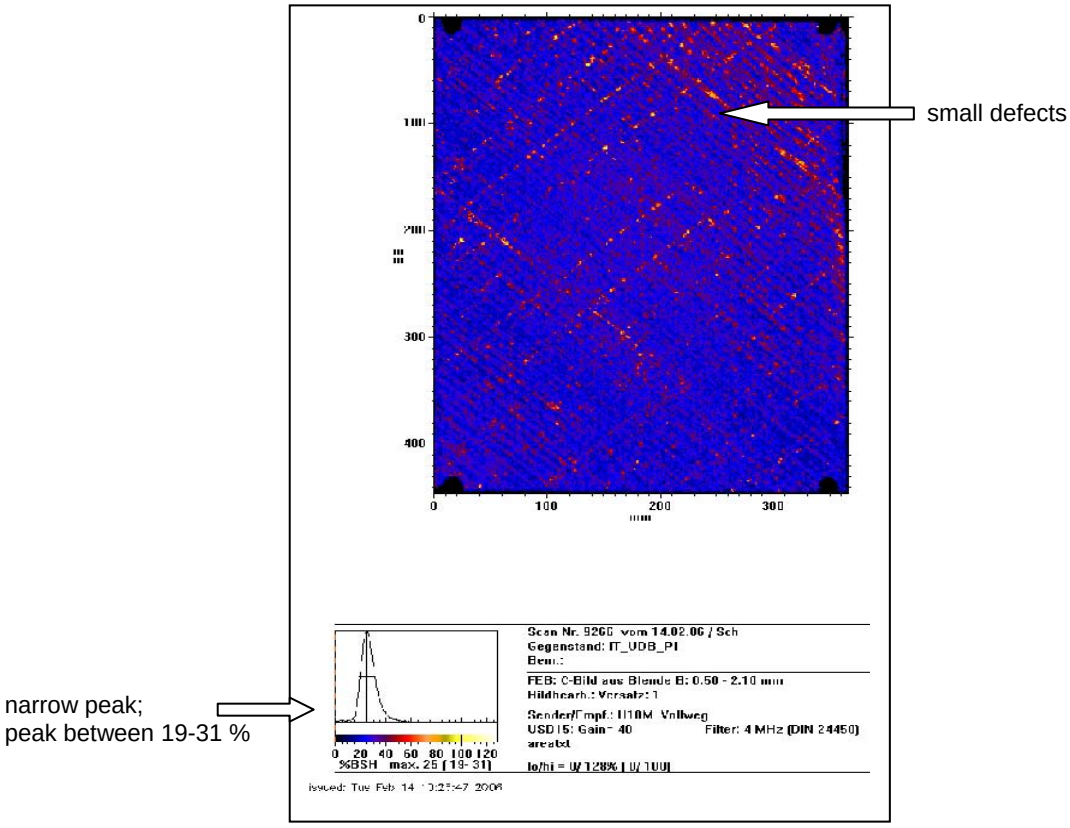

Figure 5.10: C-scan of Plate 1

The C-Scan mode or pulse-echo provides a planar view image at a specific depth. The ultrasonic scan of plate 1 (figure 5.10) shows the FEB (Fehlerecho Blende B = defect echo diaphragm B). This scan illustrates any defects inside the laminate. Small defects are visible, marked with a reddish colour. The narrow peak of the colour code represents a good quality of the laminate.
With the LZB (Laufzeitecho Blende B = delay echo diaphragm B) the depth of the failure is investigated. Additionally, a REA (Rückwandecho Blende A = rear panel echo diaphragm A) and a HEB (Hilfsreflektorecho Blende B = auxiliary reflection echo diaphragm B) can be produced, showing the ultrasonic waves reflecting from the rear panel, respectively an auxiliary plane.
The ultrasonic scan shows for plates 1 and 4 a few voids. Plates 2 and plate 3 do not show any specific incidents. All plates can be used for testing.
Detailed C-Scan results can be found in Appendix (attached CD).

5.2.4. Determination of the fibre volume fraction

The mechanical properties of a composite depend directly on the volume fraction of reinforcing fibres v_f. In reality, the fraction of the voids v_v also has to be taken into consideration. The sum of the fibre volume fraction v_f, of the matrix volume fraction v_m and the void volume fraction v_v is 1.

$$v_f + v_m + v_v = 1 \qquad (23)$$

The fibre volume fraction is determined as it presents the basis for the calculation for Classical Laminate Theory (CLT). In CLT, which is also used in the calculations of the LAP program, mechanical properties of the laminate are calculated. The mechanical properties depend, among other characteristics, on the fibre volume fraction. The fibre volume fraction also has to be considered when determining the Ladevèze parameters, describing the mechanical and the damage behaviour of a laminate.
For the determination a density of 1.14 g/cm^2 for the resin RTM 6 and 1.77 g/cm^2 for the carbon fibre is used. The void volume fraction is assumed to be zero. To determine the v_f a small sample of 10 mm x 20 mm is treated with H_2SO_4. The resin is dissolved with the sulphuric acid. From the weight and the density of the components of the laminate, the fibre volume fraction is determined. The results of the fibre volume fraction are summarized in table 5.2.

Table 5.2: Values of fibre fraction volume

Sample	v_f [%]
P 1	55.6
P 2	55.8
P 3	55.4
P 4	58.3

6. Mechanical textile characterisation of the UD-braid

Before using the textile in the composite structure it is important to know about the fabric, which means the UD-braid itself. The material architecture and the characteristics of the yarn materials have an influence on the properties of the composite part produced with it.
This chapter describes the tests, undertaken at the institute ITA of the RWTH Aachen University, to investigate and obtain the characteristics of the dry UD-braid.
For the characterisation of the UD braid in its dry form, tensile strength and tensile stiffness of the roving itself and the braid and bending stiffness of the braid are tested. All tests are performed under normal testing conditions, i.e. temperature of 20.2 °C and relative humidity of 65.0 %.

6.1. Cantilever beam test

The bending stiffness is measured using the cantilever beam test according the standard DIN 53362.
The cantilever test equipment has the following construction:

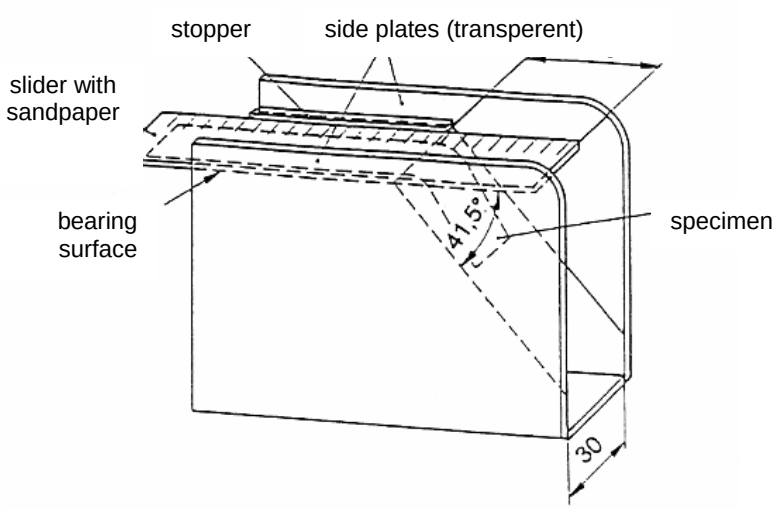

Figure 6.1: Cantilever test equipment

10 sample strips of 25 mm width and 250 mm length are placed onto the top of the test equipment. Within 10 sec. the specimen is pushed forward over the edge to bend over due to its own weight until reaching the marking on the cantilever, at an angle of 41.5°. The length of the overlapping fabric is measured and the sample is pushed back in the initial position. The test is repeated upside down and on the other edge of the sample, face- and backside. The resulting four values for each specimen are obtained. After the tests, the specimen is weighed.

The bending stiffness is equal to:

$$B = F_1 \left(\frac{l_{ü}}{2} \right)^3 \qquad (24)$$

with:

B: bending stiffness

F_1: length dependent weight ($F_1 = g_n \frac{m}{l}$)

$l_{ü}$: overlapping length of specimen

During the tests carbon filaments get caught between the ruler and the edge at the first test or at least the second one. In figure 6.2 a, the test is correctly performed, but already in figure 6.2 b it can be seen that filaments stick to the sandpaper at the bottom of the ruler. During further movement of the ruler, the filaments straighten and let the specimen deviate at a significantly earlier stage. Therefore, only some valid values are obtained.
Alternatively, the use of the Kawabata bending test would be suitable. However, the test equipment is very expensive and is not available at the ITA. [24]

a b

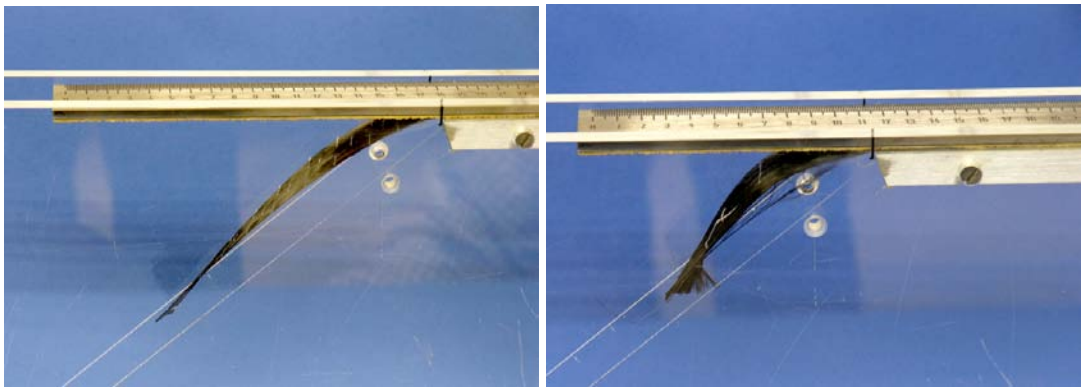

Figure 6.2: Cantilever test

The test results are attached in the Appendix (additional CD).

Table 6.1: Cantilever test results, statistics

Stiffness in bending B [nN*cm²]			
	Average	SD	CV [%]
FS; front/back	619.59	178.91	28.88
BS; front/back	545.51	124.55	22.83

An assumption for the problems of the given test is the destruction and breakage of the filaments under the given conditions during the test or already before testing due to the braiding process. When investigating the tested braided stripes under an REM microscope no excessive fractures of the carbon filaments and no breakage of the sizing can be featured. Also in the microscopic

analysis of the untested braided fabric, no outstanding breakages of filaments or sizing are exhibited. This is positive evidence for the quite gentle braiding process.
The conclusion is that the filaments do not break during the testing, but get stuck and distort the results. Therefore, only the results of some tests, where the filaments do not get stuck, can be used. The results will only be used as guide values.

6.2. Tensile test of roving

The longitudinal yarn behaviour should be determined from tension tests on single rovings in the filament direction. However, there is still no perfect method available to test dry carbon rovings. The transmission of load into the fibre does not happen in the same way as in a laminate. Therefore, the results obtained from the test do not give the maximum of tensile strength and stiffness, but only provide a basis for the comparison of the carbon roving from the bobbin and the roving dissected out of the braided fabric. As the same test method is used, a direct comparison can be made. However, the experimental results are not comparable with the values given by the manufacturer. The testing method of the manufacturer results in higher values for both tensile and stiffness properties.
The standard procedure is to embed the whole carbon roving into a resin. Through the matrix a perfect transmission of the load is possible. As such a piece of equipment is not available, another testing method is used.
The tests are based on the standard DIN EN ISO 2062 and ISO 3341; however, they vary due to the special properties of the carbon filaments. Carbon can take up extreme forces, is very brittle and has a smooth surface; therefore the filaments would not stay in the clamps during testing, but slide out of the clamps during standard testing. Therefore, a special method was developed at the RWTH Aachen University to perform these tests. The carbon rovings with a length of 250 mm, either from the bobbin or prepared out of the UD-braid, are placed into a mould in a threefold way. This means that three rovings are put together. The edges are embedded into a matrix, a two-component epoxy resin. One component of the matrix is EP 210-2, an epoxy laminating resin, and the other one is EPH 412-2, an epoxy-hardening agent. The part to be tested, in the middle of the specimen, with a test length of 125 mm, stays free, without matrix, while ensuring with plasticine that none of the still fluid resin reaches this part. The epoxy resin mix out of a proportion of 100:40 results in a non-tacky, glossy surface with 8 mm thickness and a length of 75 mm after a hardening time of 24 hours
The 10 specimens, shown in figure 6.3, are then taken out of the mould and can be tested.

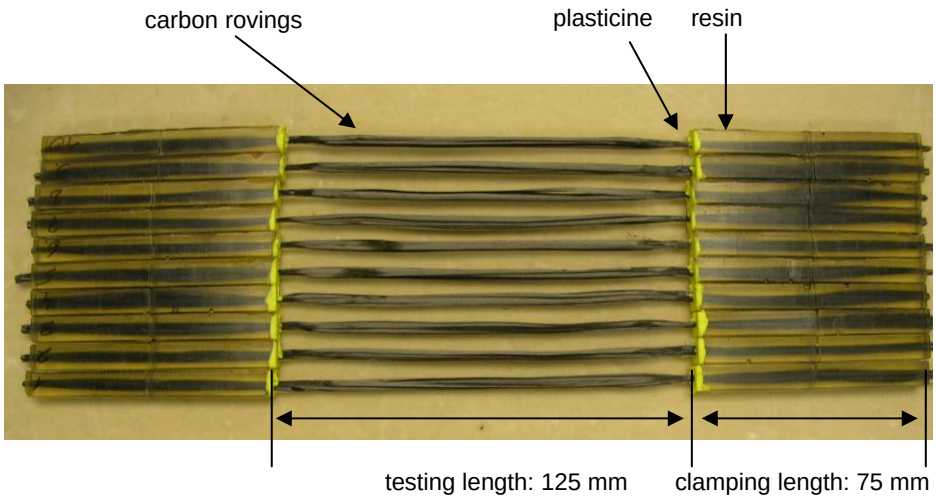

Figure 6.3: Carbon rovings, embedded in epoxy resin

The investigation of the tensile properties is carried out via the traverse way, which means according to the change in position along the whole clapming length. The rovings of Tenax® HTS 5631 are tested at a universal tensile testing machine (Zwick/Roell Z100), clamping the embedded edges into the cotter pin. According to the specimen fineness of 2400 tex (3 x 800 tex) and the density of 1.76 g/cm³, the preliminary tension of 0.5 cN/tex and the constant rate of extension with a velocity of 10 mm/min is chosen, stressing under static continuous loading conditions. Here, it has to be mentioned that three rovings are tested together in one specimen to obtain a direct comparison between the rovings prepared out of the braid and from the bobbin. The roving inside the braid is threefold and cannot be divided as they already went through a process together.

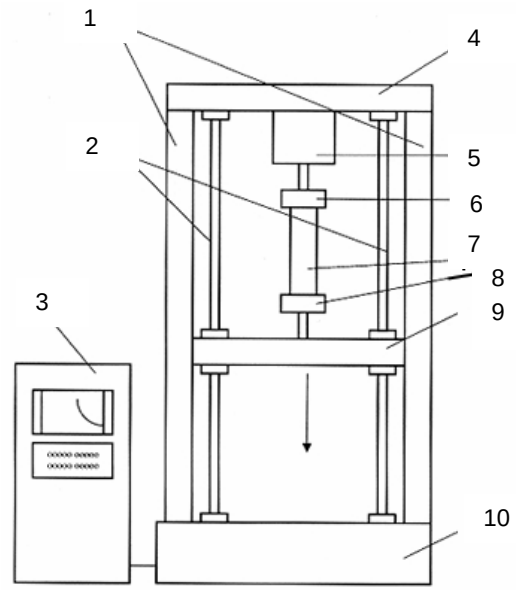

1	frame
2	mandrel
3	control module and evaluation unit
4	upper crossbar
5	load cell
6	upper clamp
7	specimen
8	lower clamp
9	lower crossbar
10	base with drive

Figure 6.4: Schematic drawing of a tensile tester [20]

In figure 6.4 a tensile tester is schematically drawn, showing the various components. The specimen is fixed between the two clamps; the lower clamp is moved downwards during testing by the lower crossbar. The load cell measures the mechanical power, i.e. the tensile force.

6.2.1. Carbon roving from bobbin, threefold

The results can be seen in table 6.2 and figure 6.5:

Table 6.2: Results of tensile test, Tenax® HTS 5631, threefold

Series n=10	Tensile strength [N/mm²]	Force max [N]	ε-Force max [%]
Average	1819	2481	2.53
Stand. dev.	93.67	93.67	0.19
CV [%]	3.78	3.78	7.35
Min	1709	2330	2.33
Max	1923	2622	2.79

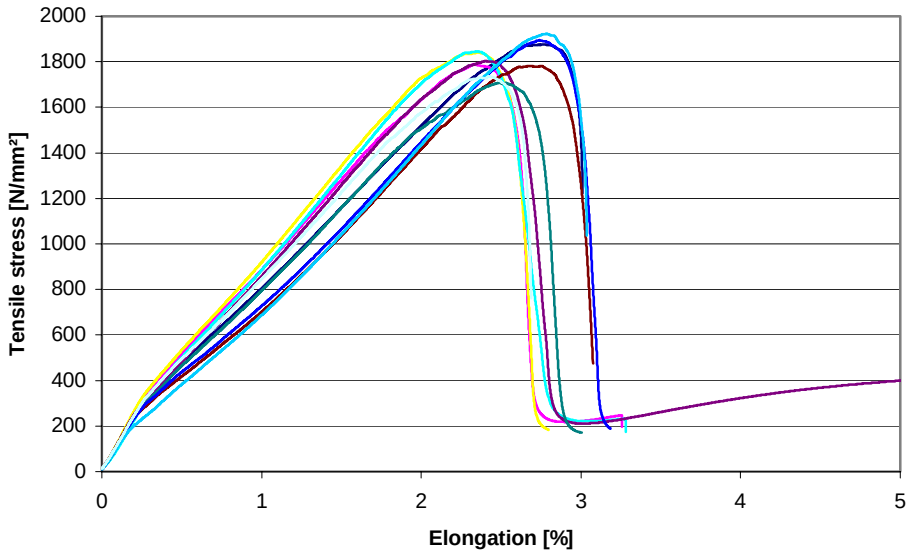

Figure 6.5: Stress-strain graph, carbon roving HTS 5631, threefold

In the graph, a two-part division can be recognized. There is a drop of stiffness after an elongation of 0.25 %. Additionally, the tensile strength is very low compared to the values given by the manufacturer. This is due to the fact that the test on a dry roving cannot be performed perfectly. The transmission of load into the fibre does not happen in the same way as in a laminate.

6.2.2. Carbon roving out of braid, threefold

Additional tests are realized on the roving Tenax® HTS 5631 prepared out of the braid. Table 6.3 shows the results.

Table 6.3: Results of tensile test, Tenax® HTS 5631 out of braid

Series n=10	Tensile strength [N/mm²]	Force max [N]	ε-Force max [%]
Average	1805	2461	2.47
Stand. dev.	104	142.26	0.23
CV [%]	5.78	5.78	9.46
Min	1666	2271	2.09
Max	1985	2706	2.88

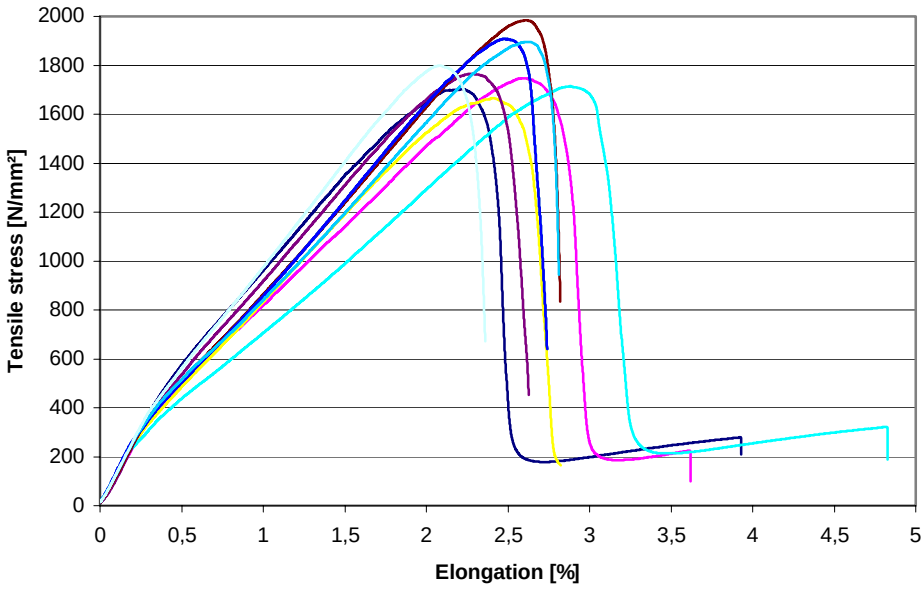

Figure 6.6: Stress-strain graph, carbon roving HTS 5631 out of braid

Just as in the graph for the HTS 5631 threefold roving from the bobbin, a bending at 0.25 % of the elongation is shown in figure 6.6. The performance of the two threefold rovings is extremely similar. The roving out of the braid shows lower values for the elongation, but slightly higher tensile strength. Moreover, the elongation of the specimen is relatively high and does not lie beyond 2 %. Therefore, the assumption is made that the filaments break one after another. This theory is based on the form of the stress-strain curve. Already before the maximum elongation at breakage, individual filaments start to break. This effect, also known as the zipper-effect, is illustrated in figure 6.7.

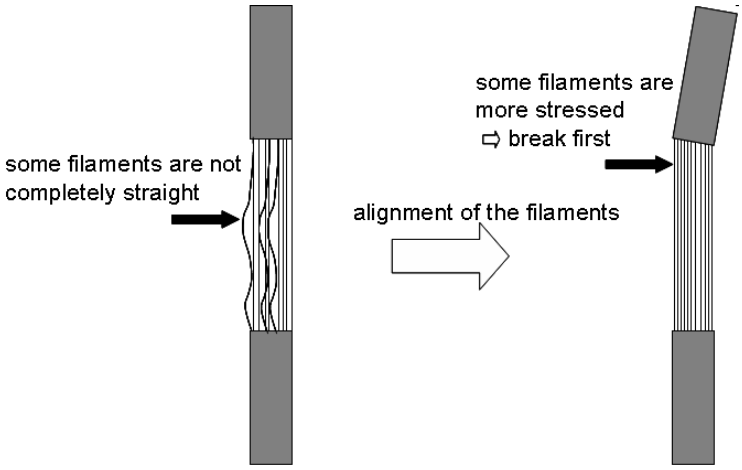

Figure 6.7: Extrapolated illustration of the type of breakage of the carbon filaments

During embedding, not all filaments lie straight. When applying the load, the filaments align in the direction of the load. The other filaments, already in a straight state are stressed and break first. Therefore, no maximum of tensile strength can be reached with this test method. The transmission of power from filament to filament in the specimens is hardly possible in yarn tension tests of carbon filaments in dry state.

Table 6.4: Tensile strength [N], comparison

Series n=10	Roving from bobbin, threefold	Roving out of braid, threefold
Tensile strength [N]	1819 ±94	1805 ±104
Elongation [%]	2.53 ±0.19	2.47 ±0.23

The comparison shows that the values of the tensile strength are not far from each other. The tensile strength for the rovings, taken out of the braid, is slightly lower than the ones taken from the bobbin with the same fineness indicating a very small amount of damage to the roving during rewinding from bobbin to bobbin and during the braiding process.

6.3. Tensile test of braid, dry

The influences of the geometric parameters, as well as the braiding process are investigated by applying tensile tests on the braid itself. With the test of the dry braid, maximum force (F max [N]) and maximum elongation per force (ε-F max [%]) are determined.
Just as for the carbon roving the stripe of the braid is embedded into a matrix to avoid slippage out of the clamps.

Figure 6.8: Embedded stripes of braid, after tensile test

The edges of the braided stripes are embedded in a two component epoxy resin, composed of 100 parts of weight of Araldite 2011/A laminating resin and 80 parts of weight of Araldite 2011/B hardening agent. A squared plate of an area of 25 cm² is placed onto the embedded parts of the braid on the front- and backsides, where the braid is clamped in for the tests. This method was also developed at the RWTH Aachen University.

The tensile strength is determined according to the standard DIN EN ISO 13934-1, determination of tensile properties of fabrics. This standard is normally used for woven textiles and is not common for fabrics out of carbon fibres. The direction of the test, on the Zwick/Roell Z100, is in the direction of the carbon yarn. In the standard it is specified that if the ε-F max [%], the elongation at maximum force, is expected to be lower than 8 %, then the testing length is 200 mm at a velocity of 20 mm/min. A preliminary force of 5 N is applied, determined by the area weight of the specimen. Two samples are tested, due to a lack of material. No clamp slippage or break at the edge of the clamp appeared.

Table 6.5: Results of tensile test, braid

Series n=2	Area [mm²]	Force max [N]	ε-Force max [%]	ε-break [%]
Average	8.864	13541	4.30	4.69
Stand. dev	0.9642	82	0.13	0.07
CV [%]	10.88	0.60	3.11	1.42
Min	8.182	13483	4.20	4.64
Max	9.545	13598	4.39	4.73

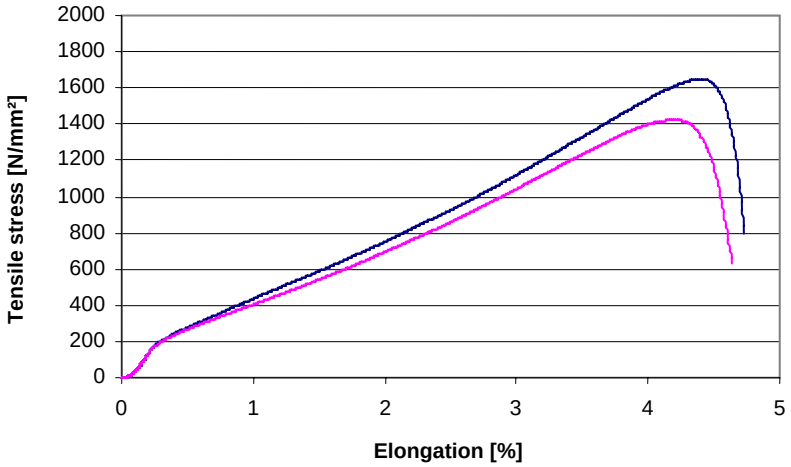

Figure 6.9: Stress-strain graph, carbon braid

The initial section of the curve shows, just as in the roving threefold, a decrease in tensile stress at low elongation (at around 0.25 % of elongation), having a high initial stiffness. The average tensile strength is lower than the tensile strength of the roving itself. Either the rovings get damaged during the braiding process or not each roving in the fabric is nicely stretched before adding the epoxy end tabs. An about 2 % higher elongation, in comparison with the roving out of the braid, is notable.

7. Geometrical characterisation of the dry UD-braid

To be able to build a WiseTex textile model of the UD-braid, the braid has to be geometrically characterised. In section 7.1, the area weight is measured, in section 7.2, the thickness is determined. The structural geometrical characterisation of the textile reinforcement, described in 7.3, enables one to find the textile structure of an individual ply, i.e. yarn width, yarn spacing and the braiding angle. All of those values are obtained from an evaluation of the top view of a textile scan with high resolution.

7.1. Area weight measurement

The mass per unit area is determined according the standard DIN EN 12127. The two specimens are stamped out of the textile to be tested according to the standard. Due to the availability of only a small amount of test material, only two specimens can be prepared out of the 2 different sample pieces, instead of 5 specimens as prescribed in the standard.
The area *A* of the samples is 100 cm². The results are shown in table 7.1.

Table 7.1: Results of weight and area weight of the braid

Sample number	Weight of sample *m* [g]	Area weight *M* [g/m²]
1	3.294	329.48
2	2.931	293.08
Average	3.113 ±0.257	311.28 ±25.74

The area weight *M* is calculated from the weight of the sample according to the following equation:

$$M = \frac{10000m}{A} \qquad (25)$$

7.2. Thickness determination

The tests are performed according to the standard EN ISO 5084. The testing area chosen is, contrary to the standard, 25 cm² due to the size of the testing machine and the number of tests are two, instead of five as defined in the standard. According to the definition, the thickness is the distance between the two plates of reference, whereby a pressure of 1 kPa is applied to the textile. The fabric is placed onto the lower plate. The upper plate, a circular pressure stamp, applies the pre-defined pressure. After 30 seconds the value, describing the thickness, is read from the measuring instrument, the Frank thickness measurement device 16502. This apparatus uses a calliper for the determination of the thickness. The results are shown in table 7.2.

Table 7.2: Results of thickness of the braid

Sample number	Thickness a_x conform the standard [mm]
1	0.369
2	0.424
Average	0.40 ±0.04

Sample 1 is taken out of a piece with greater carbon roving width. Therefore, the thickness is lower than in sample 2, due to position of the individual filaments. In sample 2 more overlapping of the filaments is assumed.
Additionally, the influence of the Grilon yarn has to be considered. In the composite, the Grilon yarn is smelted inside the resin and does not contribute to the thickness of the braid anymore. The expected thickness of the UD-braid in the composite is slightly lower, see chapter 8.1.

7.3. Textile geometric characteristics

For the geometric characterization of the UD-braid a 200 mm x 300 mm piece is scanned with an HP Scanjet 4600 at 1200 dpi. On the magnified image 200 pixels at positions, where the Grilon yarn and the Carbon roving cross, are marked. The image coordinates are listed and the coordinates of these pixels are further processed in Microsoft Excel to obtain yarn width, fibre orientation, braiding angle and yarn spacing. The distance on the picture is calculated from the fact that 1200 dpi stands for 1200 dots per inch, which is recalculated into centimetres.

7.3.1. Yarn orientation

For the yarn orientation, the points (e.g. *P*, *Q*, *R* in figure 7.1) are found along the yarn edges and are averaged to find the midpoints of the yarn (e.g. *Q* in figure 7.1). The yarn orientation provides information about the braiding angle.

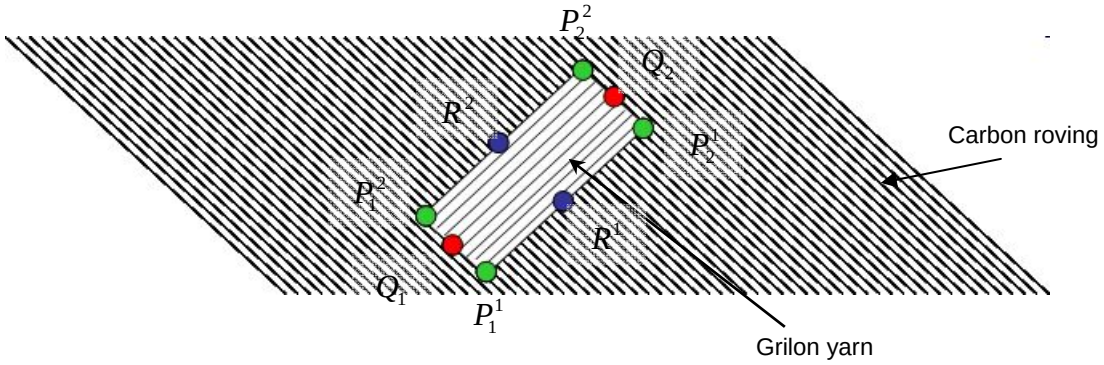

Figure 7.1: Measuring points for fibre orientation

The middle points Q_x and Q_y are calculated according to the following equations, with P_1^1, P_1^2, P_2^1 and P_2^2 as the crossing points along the Grilon yarn:

$$Q_{1_x} = \frac{P_{1\,x}^1 + P_{1\,x}^2}{2};\ Q_{2_x} = \frac{P_{2\,x}^1 + P_{2\,x}^2}{2};\ \ldots\ldots Q_{i_x} \quad (26)$$

$$Q_{1_y} = \frac{P_{1\,y}^1 + P_{1\,y}^2}{2};\ Q_{2_y} = \frac{P_{2\,y}^1 + P_{2\,y}^2}{2};\ \ldots\ldots Q_{i_y} \quad (27)$$

For each set of the middle points Q_i belonging to a yarn, a linear fitting curve is calculated. The parameters *a* and *b* in $y = ax + b$ can be calculated with the following equations [31]:

$$a = \frac{Y \cdot XX - X \cdot XY}{n \cdot XX - X^2} \quad (28)$$

$$b = \frac{nXY - X \cdot Y}{n \cdot XX - X^2} \quad (29)$$

With:

$$X = \sum_{i=1}^{n} Q_{i_x} \quad (30)$$

$$Y = \sum_{i=1}^{n} Q_{i_y} \quad (31)$$

$$XY = \sum_{i=1}^{n} \left(Q_{i_x} \cdot Q_{i_y} \right) \quad (32)$$

$$XX = \sum_{i=1}^{n} \left(Q_{i_x} \cdot Q_{i_x} \right) \quad (33)$$

From all of the yarns, the average is taken to get a mean value for the whole fabric. The resultant slope for the Grilon yarn is 0.938, which means an angle of 43.1 °. For the Carbon yarn, the slope is – 0.741, representing the angle of – 36.9 °. The resultant braiding angle is 80 °.

7.3.2. Yarn width

The width of the carbon roving and the Grilon yarn are again calculated from the points along the yarn edges, *P, Q* and *R*, see figure 7.1. It has to be noted that the result of the width of the carbon roving has to be divided by three, as three rovings lie in between the measuring points *A* and *B*. The same is necessary for the Grilon yarn; between the measuring points *1* and *2*, there are two Grilon yarns. Therefore, the value has to be divided by two.

Between Q_1 and Q_2 is L_g, the length of the Grilon yarn in the direction of the Grilon filaments $\overrightarrow{D_g}$. The straight line between R^1 and R^2 is L_c, the length of the Grilon yarn in the direction of the carbon filaments $\overrightarrow{D_c}$.

The dimensions of the Grilon yarn are then calculated according to:

$$L_g = \sqrt{\Delta x_{Q_1}{}^2 + \Delta y_{Q_1}{}^2}\,; \qquad \Delta x_{Q_1} = Q_{1_x} - Q_{2_x} \qquad (34)$$

$$\Delta y_{Q_1} = Q_{1_y} - Q_{2_y}$$

$$L_c = \sqrt{\Delta x_{R^1}{}^2 + \Delta y_{R^1}{}^2}\,; \qquad \Delta x_{R^1} = R^1{}_x - R^1{}_x \qquad (35)$$

$$\Delta y_{R^1} = R^1{}_y - R^2{}_y$$

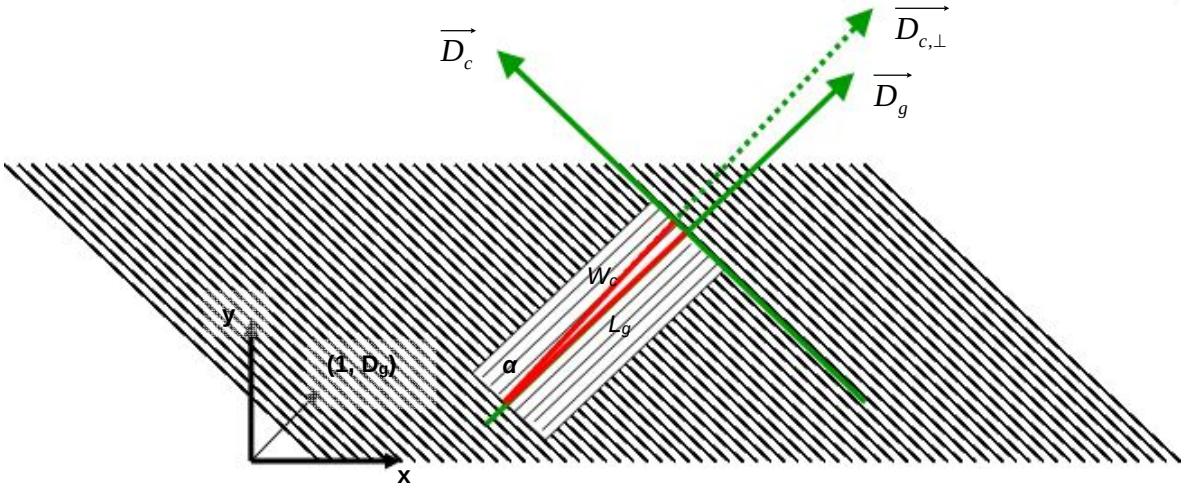

Figure 7.2: Model for calculation of yarn width

As the direction $\overrightarrow{D_g}$ is not perpendicular to the carbon fibre orientation, L_g does not directly represent the width of the carbon roving. To find the correct width of the carbon yarn the length L_g is projected onto a line perpendicular to the direction of the carbon yarn (represented by $\overrightarrow{D_{c,\perp}}$).

$\overrightarrow{D_{c,\perp}}$ is assumed to be perpendicular to $\overrightarrow{D_c}$. From that results the scalar product:

$$\overrightarrow{D_{c,\perp}} \cdot \overrightarrow{D_c} = D_{c,\perp_x} \cdot D_{c_x} + D_{c,\perp_y} \cdot D_{c_y} = 0 \qquad (36)$$

With:

$$\overrightarrow{D_c}\left(D_{c_x}, D_{c_y}\right) \qquad \text{and} \qquad \overrightarrow{D_{c,\perp}}\left(D_{c_y}, -D_{c_x}\right)$$

The angle α, the angle between the vectors $\overrightarrow{D_g}$ and $\overrightarrow{D_{c\perp}}$, is calculated from the following equation to calculate the width of the carbon roving W_c.

$$\cos\alpha = \frac{\overrightarrow{D_g} \cdot \overrightarrow{D_{c\perp}}}{\left\|D_g\right\| \cdot \left\|D_{c,\perp}\right\|} \qquad (37) \quad \_\,1)$$

$$\cos\alpha = \frac{D_{g_x} D_{c,\perp_x} + D_{g_y} D_{c,\perp_y}}{\sqrt{\left(D_{g_x}\right)^2 + \left(D_{g_y}\right)^2}\sqrt{\left(D_{c,\perp_x}\right)^2 + \left(D_{c,\perp_y}\right)^2}} \qquad (38)$$

$$W_c = L_g \cos\alpha \qquad (39)$$

Analogous is the determination of the values for the Grilon yarn.
The resultant average widths are summarised in table 7.3.

7.3.3. Yarn spacing

For the determination of the yarn spacing S_x, again the points along the yarn edges are used and their position is defined. In contrary to the yarn width, the three carbon rovings floating above and, respectively, below the Grilon yarns are regarded as one unit for the definition of the yarn spacing.

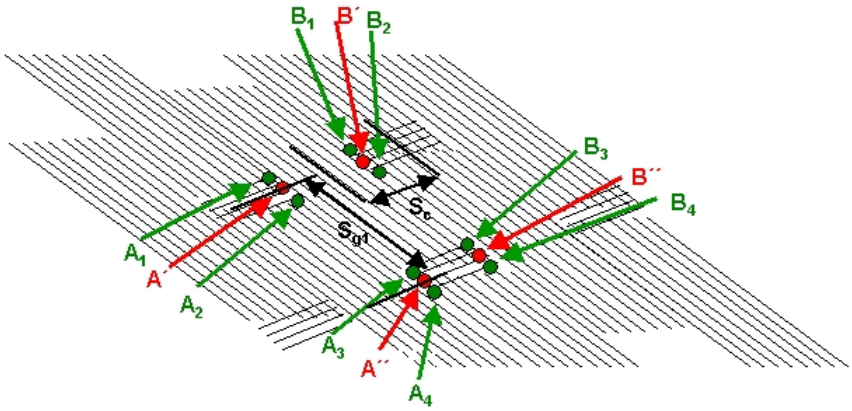

Figure 7.3: Model for calculation of Grilon yarn spacing

1) $\vec{A} \cdot \vec{B} = A_x B_x + A_y B_y$
$= \left\|\vec{A}\right\| \cdot \left\|\vec{B}\right\| \cdot \cos\alpha$

Then the average points at the edges are identified as middle points according to:

$$A' = \frac{A_1 + A_2}{2} \qquad (40)$$

$$A'' = \frac{A_3 + A_4}{2} \qquad (41)$$

The distance is calculated according to:

$$S_A = \sqrt{\Delta A_x^{\,2} + \Delta A_y^{\,2}} \qquad (42)$$

with: $$\Delta A_x = A_x'' - A_x' \qquad (43)$$

$$\Delta A_y = A_y'' - A_y' \qquad (44)$$

The average of S_A, S_B, …., S_N ends up in a yarn spacing of 8.32 mm and 27.12 mm between the Grilon yarns and 9.07 mm between the carbon rovings. There is only one value for the spacing of the carbon roving calculated. The second value, which represents the spacing of the carbon rovings at the crossing with the Grilon yarn, cannot be exactly calculated, but is assumed to be slightly higher.

7.4. Results of the geometrical characterisation of the dry UD-braid

The geometrical properties are summarized in table 7.3 and figure 7.4.

Table 7.3: Textile geometric parameters

Parameters		
Yarn orientation [°]	Grilon	43.1 ±2.2
	Carbon	-36.9 ±0.5
Yarn width [mm]	Grilon W_g	0.90 ±0.17
	Carbon W_c	2.93 ±0.20
Yarn spacing [mm]	Grilon S_{g1}	8.32 ±0.18
	Grilon S_{g2}	27.12 ±0.14
	Carbon S_c	9.07 ±0.41

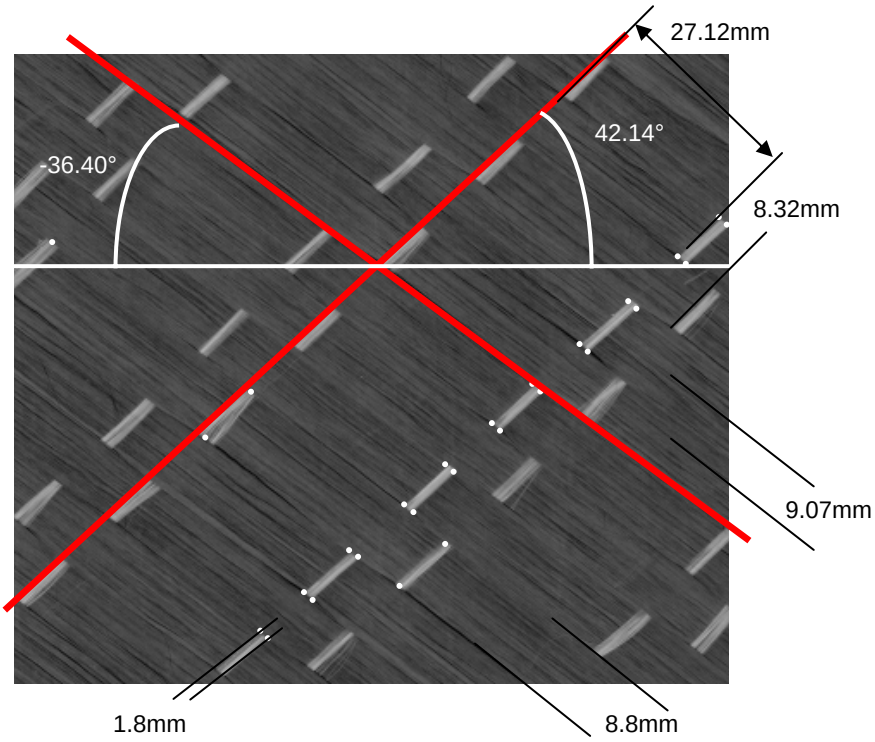

Figure 7.4: Scan of UD-braid

8. Geometrical characterisation of the laminate

In this chapter, the textile reinforcement is geometrically characterised inside the laminate, as the textile structure undergoes geometrical changes during the laminate production. Due to the application of pressure during the infiltration process, the individual ply becomes compressed. The analysis of the cross-section of the laminates is undertaken by investigating the polished micrograph sections in section 8 to find yarn thickness and fibre undulations.

With the cross-section analysis of the laminates, the thickness of the plies inside the laminates, the undulation of the rovings and the dimensions of the rovings can be measured. Additionally, the defined angle of each individual ply can be calculated from the cross-section scan.

For this purpose, a sample of 10 mm x 25 mm is cut out of each plate, whereby the longer side runs along the carbon filaments. Each specimen is embedded into an epoxy resin, from the company Struers, is brushed and polished. The polished specimens are observed under the light-microscope Polyvar and put on record with various magnifications. The range of magnification is between 25 and 1000 times. A digital camera records the image.

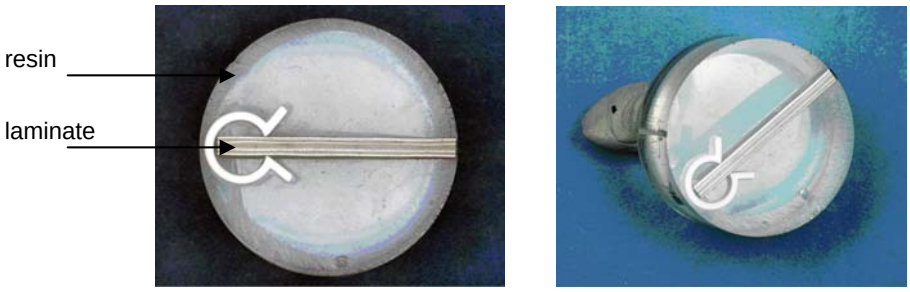

Figure 8.1: Laminate plate, embedded for cross-section analysis

From these polished micrograph sections, the various parameters are measured.

The cross-section of the specimens of plates 2 and 4 show the eight plies very precisely separated from each other. However, it is difficult to define the boarder between the 4th and the 5th plies, due to their identical orientation. From these cross-sections, the thickness of the single ply, the undulation of the roving inside the laminate and the precise angle of the plies to each other can be determined. Additionally for plate 2, the roving size can be measured.

As plates 1 and 3 have a unidirectional stacking, it is barely possible to see the boarder line between the various layers. This is a positive sign for the unidirectional stacking. Therefore, on the cross-section of these laminates, only a rough value of the thickness of each ply can be stated.

8.1. Ply thickness

Figure 8.2 presents the cross-section of the laminate P 1. It can be seen that the plies lie unidirectional inside the laminate. The single plies can be barely seen. However identification of the various layers was attempted as illustrated in figure 8.3.

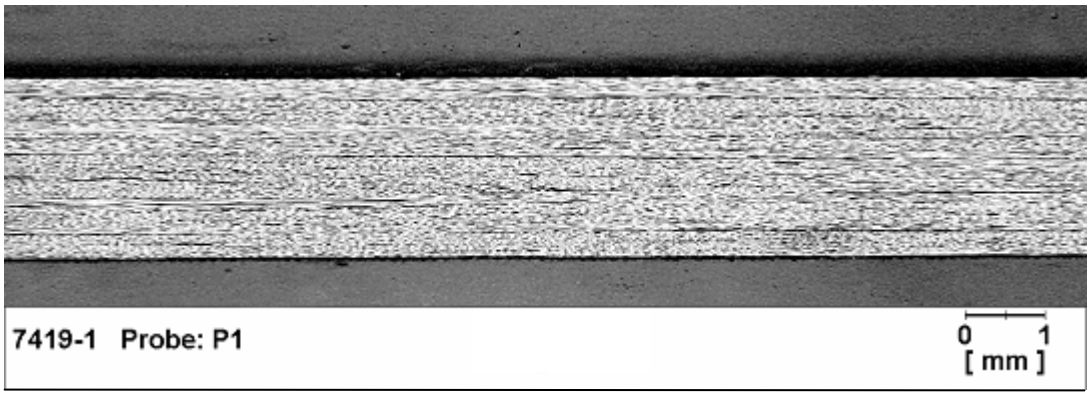

Figure 8.2: Cross-section of plate 1

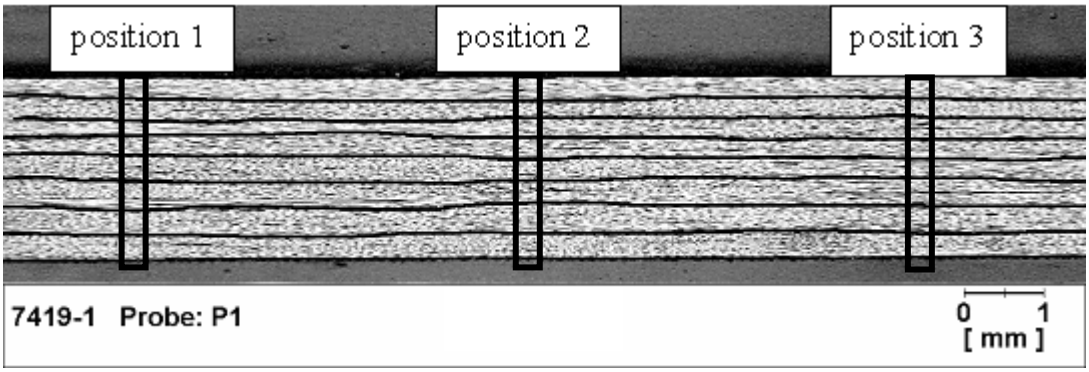

Figure 8.3: Thickness measurement, P 1

The identified plies are measured in three positions. The results are presented in table 8.1.

Table 8.1: Thickness values, P 1

	Position 1 [mm]	Position 2 [mm]	Position 3 [mm]	Average [mm]
Ply 1	0.216	0.275	0.255	0.249
Ply 2	0.275	0.255	0.255	0.262
Ply 3	0.255	0.196	0.255	0.235
Ply 4	0.216	0.255	0.235	0.235
Ply 5	0.294	0.353	0.294	0.314
Ply 6	0.353	0.314	0.314	0.327
Ply 7	0.353	0.314	0.353	0.340
Ply 8	0.353	0.333	0.314	0.333
Sum	2.315	2.295	2.275	2.295

In figure 8.4, showing the cross-section of the plate P 2, the various plies can be clearly seen. Due to the stacking, which is symmetrical to the centre line, plies 4 and 5 cannot be clearly identified. Therefore, again measuring the plies in three positions, one value of the thickness for ply 4 and 5 is given, summarised in table 8.2.

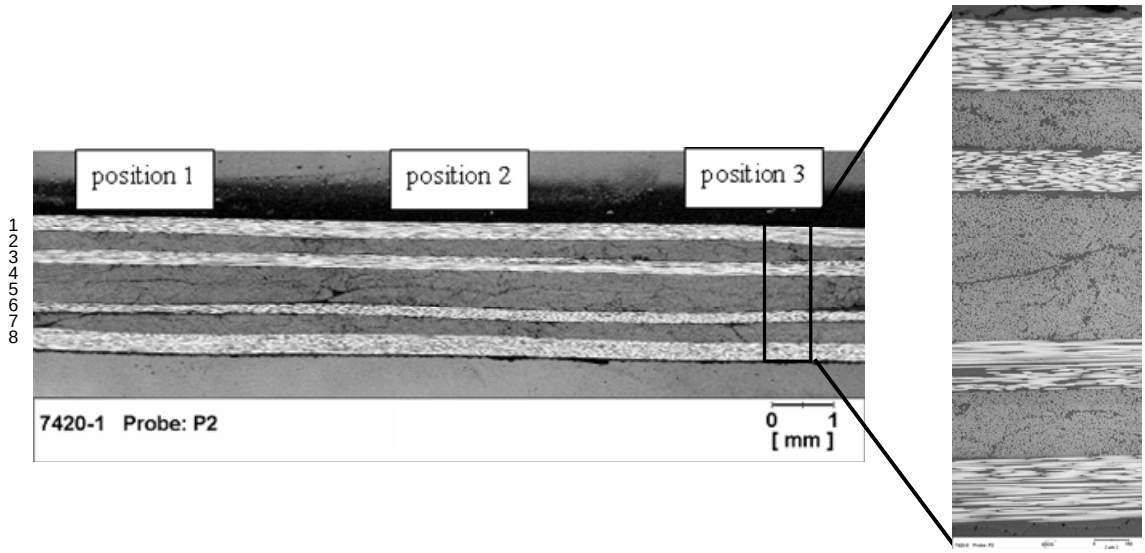

Figure 8.4: Thickness measurement of single plies, P 2

Table 8.2: Thickness values of single plies, P 2

	Position 1 [mm]	Position 2 [mm]	Position 3 [mm]	Average [mm]
Ply 1	0.269	0.278	0.259	0.269
Ply 2	0.306	0.273	0.338	0.306
Ply 3	0.227	0.227	0.222	0.225
Ply 4 / Ply 5	0.611	0.606	0.593	0.603
Ply 6	0.176	0.185	0.176	0.179
Ply 7	0.319	0.282	0.329	0.310
Ply 8	0.310	0.310	0.278	0.299
Sum	2.218	2.161	2.195	2.191

For plate P 3 no differentiation of the plies can be made. Therefore, the thickness of the plies cannot be determined.

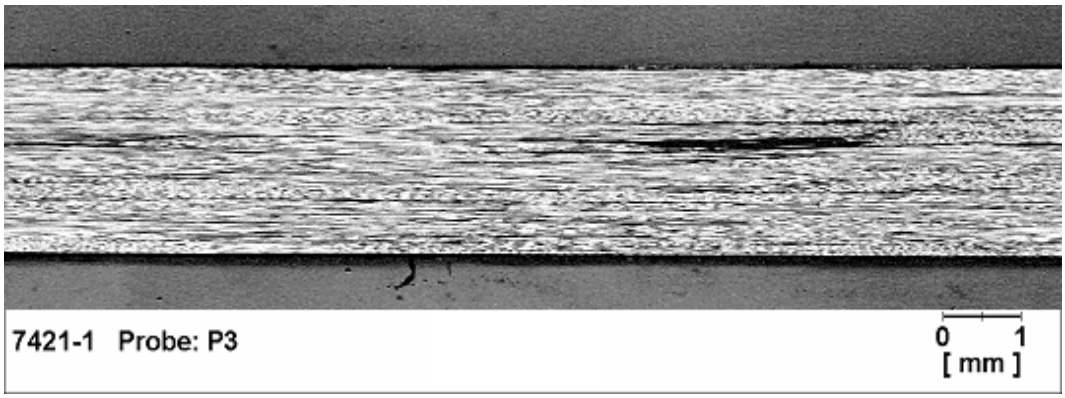

Figure 8.5: Cross-section of plate 3

Just as for plate P 2, plate P 4 shows defined borderlines between all plies, except between plies 4 and 5. The results are individual thickness values for plies 1, 2, 3, 6, 7 and 8 and one value for plies 4 and 5.

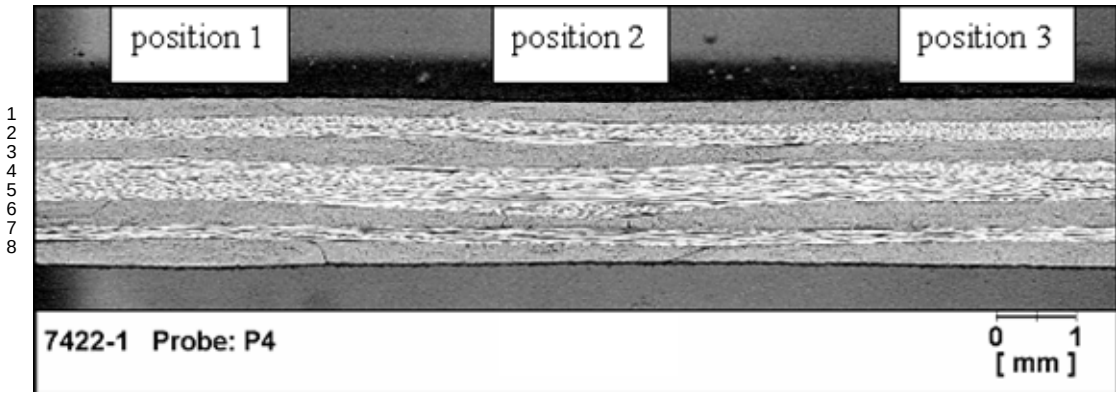

Figure 8.6: Thickness measurement of single plies, P 4

Table 8.3: Thickness values of single plies, P 4

	Position 1 [mm]	Position 2 [mm]	Position 3 [mm]	Average [mm]
Ply 1	0.235	0.255	0.275	0.255
Ply 2	0.294	0.314	0.275	0.294
Ply 3	0.216	0.235	0.216	0.222
Ply 4 / Ply 5	0.529	0.608	0.549	0.562
Ply 6	0.294	0.196	0.314	0.268
Ply 7	0.216	0.216	0.216	0.216
Ply 8	0.353	0.196	0.314	0.288
Sum	2.137	2.020	2.159	2.105

8.2. Undulation

The position of the rovings inside the laminates is important for stress transmission during the tension and compression test. The desired case is that the rovings lie completely straight and rectilinear. Already the smallest deviation from the ideal straight line causes a decrease in strength and stiffness of the composite. Therefore, the undulation has to be precisely investigated.
The undulation of the individual plies in a laminate is determined by creating lines parallel to the edge of the laminate, pulled up alongside the highest point of each ply, illustrated in figure 8.7:

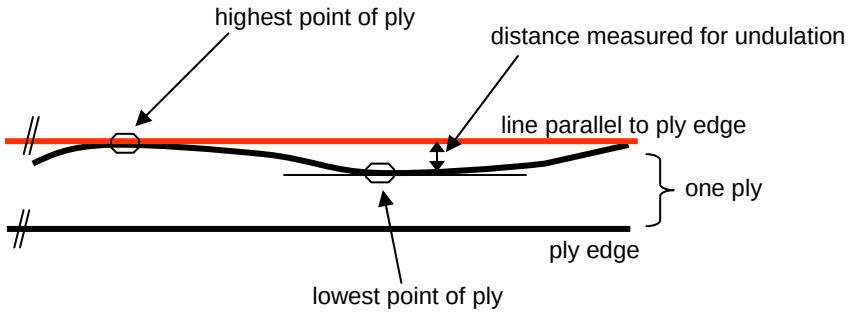

Figure 8.7: Schematic drawing for the measurement of undulation

As the laminates P 1 and P 2 are unidirectional, it is impossible to define the undulation.
In the cross-section scan of plate P 2, the undulation is determined as seen in figure 8.8.

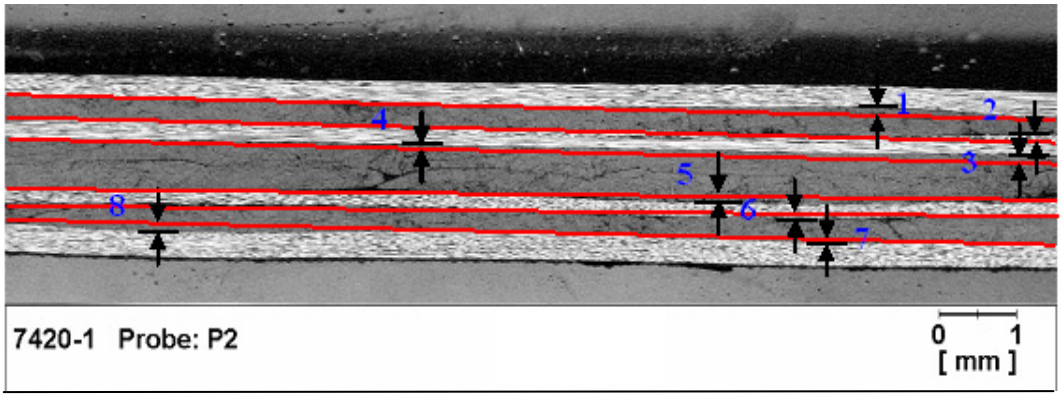

Figure 8.8: Undulation, P 2

Table 8.4: Values for undulation of rovings, P 2

Number	Distance [mm]
1	0.118
2	0.137
3	0.118
4	0.078
5	0.091
6	0.078
7	0.059
8	0.098

It can be clearly seen that plies 1, 2 and 3 undulate the most. However, the deviations are quite small.

Also for plate 4, the undulation is small, as shown in figure 8.9 and table 8.5.

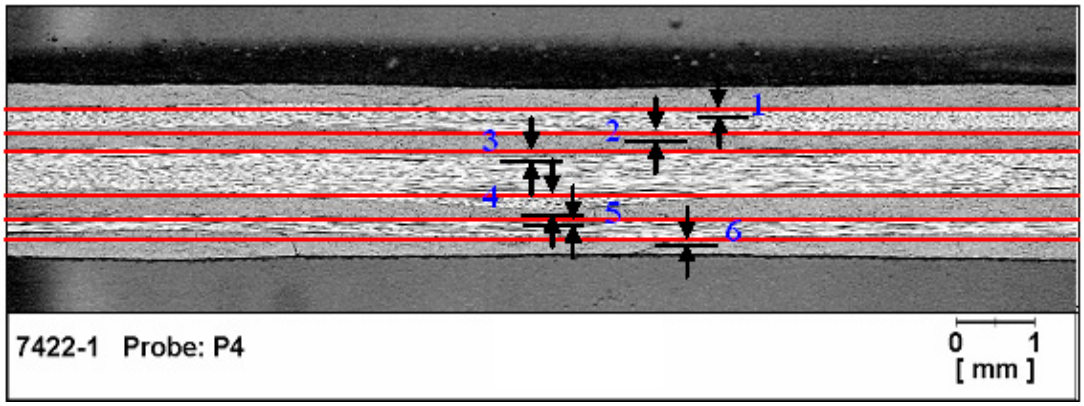

Figure 8.9: Undulation, P 4

Table 8.5: Values for undulation of rovings, P 4

Number	Distance
1	0.098 mm
2	0.118 mm
3	0.137 mm
4	0.216 mm
5	0.098 mm
6	0.098 mm

8.3. Rovings

Through the infiltration process, the Grilon yarn dissolves completely in the matrix. It is smelted into the epoxy resin. The carbon rovings become compressed during the infiltration process due to the pressure applied to the laminate. Therefore, it is almost impossible to differentiate the rovings from each other. In plate P 2, five rovings can be identified. These carbon rovings are measured according to the length and width of their cross-section.

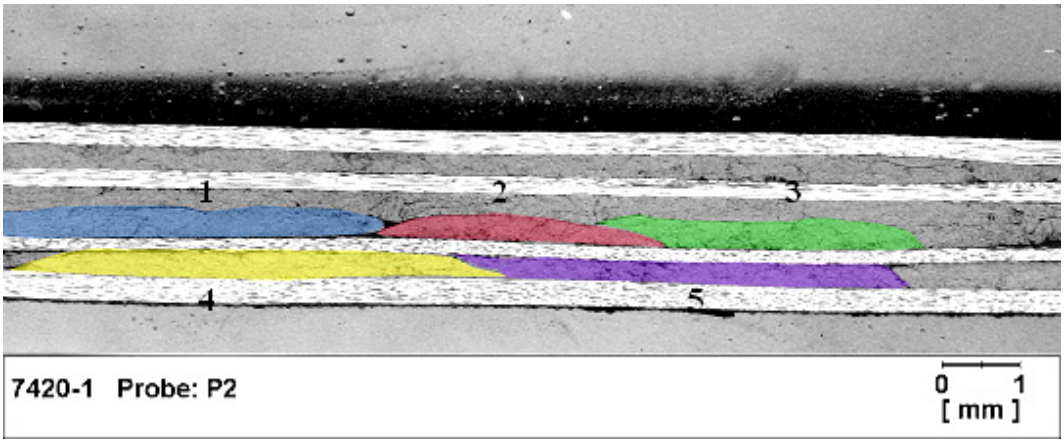

Figure 8.10: Measurements of roving size, P 2

Table 8.6: Values of roving size, P 2

	width [mm]	thickness [mm]
Roving 1	4.946	0.387
Roving 2	3.753	0.344
Roving 3	4.215	0.355
Roving 4	6.054	0.333
Roving 5	5.634	0.290
Average	4.920 ±0.956	0.342 ±0.035

From the values it can be clearly seen that a strong compression of the rovings during the infiltration process takes place when compared with the geometrical measurement on the dry UD-braid (section 7.3). Additionally, the rovings merge, resulting in fewer voids. The results of the geometrical characterisation provide a validation for the favourable load transmission during loading.

8.4. Ply angles

The evaluation of the angles in the laminate is an important step. For validation of a perfect stacking, this means that the eight plies lie under the correct angle, the ply angle of the laminates is determined. A prerequisite for testing under tensile and compressive load is that the angle deviation is not bigger than 5 °.

The angel of the filaments is determined by measuring the filament cross-section in the x- (width *w*) and y- (height *h*) direction on the picture of the polished micrograph section.

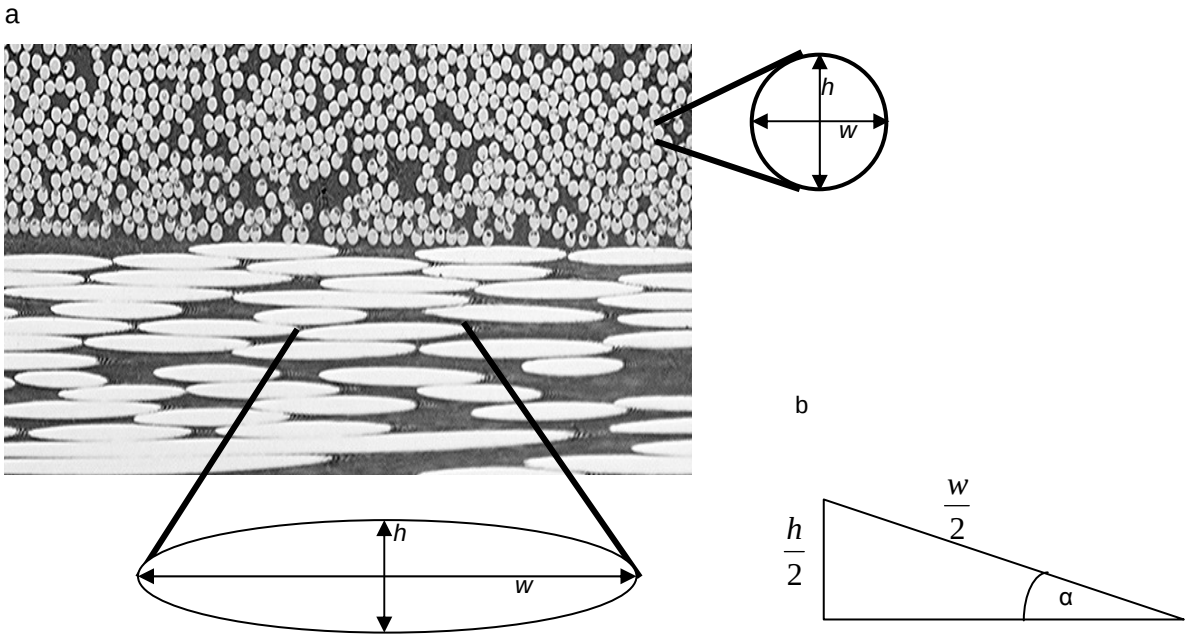

Figure 8.11: Schematic measurement of width and height (a)
Resultant ply angle *α* (b)

With:
$$\cos\alpha = \frac{h}{2}\cdot\frac{2}{w} = \frac{h}{w} \qquad (45)$$

The measurements are recalculated from pixel into µm.

With the equation:
$$\alpha = \arcsin\frac{h}{w} \qquad (46)$$

the angle α is calculated.

If the cut is directly perpendicular to the filaments, the angle is 0 ° and sin 0 is 0. Then the cross-section of the filaments is completely round. If the cut is along the filaments, a complete line is visible. The angle is then 90 ° with sin 90 = 1

For the cross-section analysis of plate 2, the cut is done along the length of the carbon rovings in +45 °. Therefore, the filaments of these rovings are expected to lie under an angle of $\alpha = 0$ °, this means $w \approx \infty$.

For the determination of the angle α, 160 filaments are measured for each of eight plies with plies 2, 4, 5 and 7 as reference, resulting in the average values:

Table 8.7: Length and width of ply 1-8 of plate 2

	heigth [µm]	width [µm]	angle deviation [°]
Ply 1	6.934	177.895	2.2
Ply 2	w = l	l = w	0
Ply 3	6.461	81.184	4.6
Ply 4	w = l	l = w	0
Ply 5	w = l	l = w	0
Ply 6	5.967	601.053	0.6
Ply 7	w = l	l = w	0
Ply 8	5.987	463.289	0.7

The filaments of the plies in the direction of –45 ° are completely round, that means $h = w$, i.e. $\alpha = sin^{-1} 1 = 90$ °.

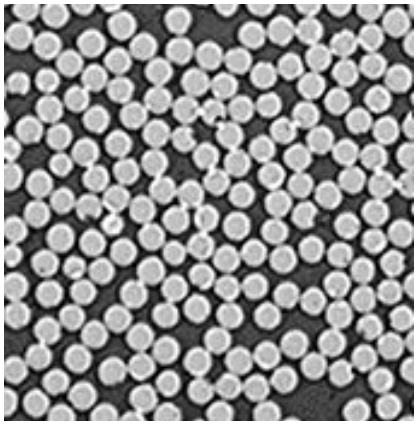

Figure 8.12: Filaments of plies 2, 4, 5, 7 of plate 2, completely round

Therefore, the angle between the two plies in ±45 °-direction is, instead of 90 ° for:

ply 1 / 2 92.2 ° alternatively 87.8 °
ply 3 / 4 94.6 ° / 85.4 °
ply 5 / 6 90.6 ° / 89.4 °
ply 7 / 8 90.7 ° / 89.3 °.

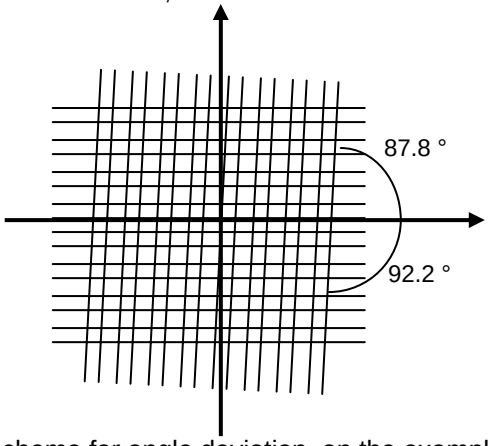

Figure 8.13: Scheme for angle deviation, on the example of ply 1

As the deviation is smaller than the limit of 5 °, the laminate can be used for testing.

In plate 4, with the stacking sequence of ±67.5 °, the cut for the polished micrograph section is done along one direction of the plies, in +67.5 °. The plies lied up in the other direction in the stacking sequence should have a correlating angle of 45 °, respectively 135 °. 20 filaments of each ply are measured according to their height and width.
The average results are:

Table 8.8: Length and width of ply 1-8 of plate 4

	height [µm]	width [µm]	α [°]
Ply 1	7.203	10.547	43.1
Ply 2	6.152	402.875	0.9
Ply 3	6.291	9.375	42.1
Ply 4	7.031	221.842	1.8
Ply 5	6.353	204.737	1.8
Ply 6	7.031	9.745	46.2
Ply 7	7.031	91.974	4.4
Ply 8	7.031	9.375	48.6

Plies 2, 4, 5 and 7, which should have an angle of 0 °, are slightly rotated. The same is valid for plie 1, 3, 6 and 8. Again the deviation of the angle is lower than 5 °. Therefore, the plate can be used for testing.

9. WiseTex model of the UD-braid

The WiseTex model provides a geometrical description of a textile structure. On the basis of the geometrical properties, an idealised model is constructed for the UD-braid as a fibrous reinforcement structure, using the WiseTex software. Another model is generated for the UD-braid in a compressed state which means simulating the textile reinforcement after the infiltration process. This model represents the textile reinforcement inside the laminate. On the basis of the model of the compressed textile the software tool FETex can be used to convert the WiseTex model into a FE model. This FE model will provide a full description of the material properties and fibre orientation.

The FE model will be built with using the commercial available FE tools of MSC. [34]

The geometrical properties of the UD-braid measured and described in the previous chapter are used to produce the model.

9.1. WiseTex of the dry UD-braid

The object shown in figure 9.4 is created in WiseTex 2D braided fabric.

The pattern of the fabric, i.e. the topology is shown in figure 9.1. “+” yarns are the carbon rovings, with three rovings brought together. “-“ yarns are the Grilon yarns, with two yarns together.

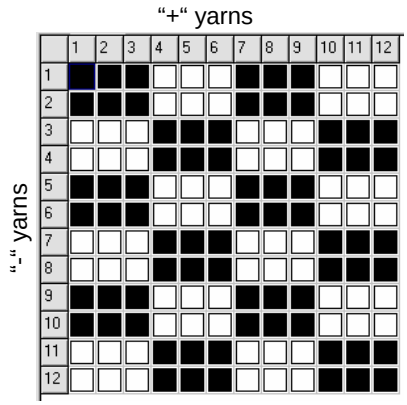

Figure 9.1: Topology of the UD-braid

To get the right pattern, the spacing is defined according to the measurements from the geometric characterization, summarized in table 7.3.

Table 9.1: Yarn spacing

	"+" yarns [mm]	"-" yarns [mm]
1	2.93	0.93
2	2.93	7.42
3	3.21	0.93
4	2.93	26.22
5	2.93	0.93
6	3.21	7.42
7	2.93	0.93
8	2.93	26.22
9	3.21	0.93
10	2.93	7.42
11	2.93	0.93
12	3.21	26.22

A braiding angle of 78 ° between the carbon roving and the Grilon yarn is used as defined in section 7.3.1.

For the description of the yarns the following parameters are defined:

Table 9.2: WiseTex parameters for yarns

Grilon MS			
	Twist and cross-section	twist	none
		elliptical	d_1, mm 0.05
			d_2, mm 0.9
	Fibres	fineness	50 tex
		N fibres	28
		Diameter, mm	0.0446
		Density, g/cm³	1.18
		Colour	white
Carbon			
	Twist and cross-section	twist	none
		elliptical	d_1, mm 0.37
			d_2, mm 2.9
	Fibres	fineness	800 tex
		N fibres	12000
		Diameter, mm	0.007
		Density, g/cm³	1.77
		Colour	black

The parameter d_1 is assessed for the Grilon yarn and the carbon roving, as these values cannot be exactly measured with the available equipment.

According to the parameters of table 9.2, the yarns are simulated in the WiseTex program, reproducing the individual filaments in a given grid. The carbon roving is in a wide state in the braid, this means lying in the braid elliptically and flat, called spread tow application. The simulated Grilon yarn and carbon roving are shown in figure 9.2.

a b

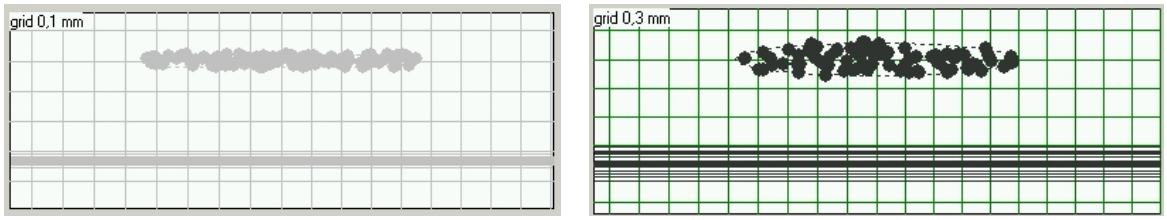

Figure 9.2: WiseTex, a Grilon yarn (a) and carbon roving (b)

Combining the yarn parameters and the spacing dimensions, the WiseTex model can be built (figure 9.3), assuming additionally the crimp height and the crimp of 90 % for the Grilon yarn.

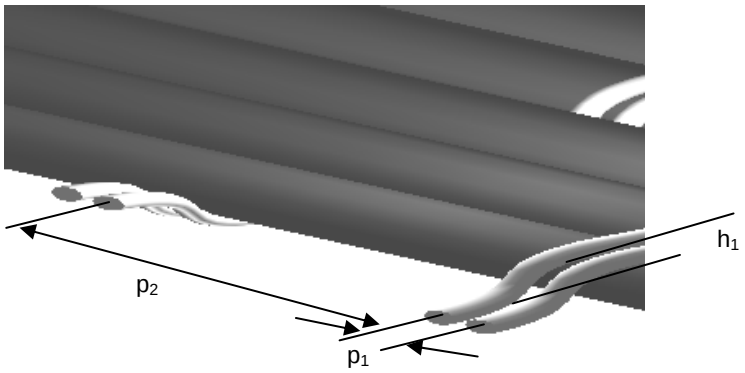

Figure 9.3: Yarns in UD-braid: spacing *p*, crimp height *h*

The final result of the modelling of the UD-braid in the WiseTex model is shown in figure 9.4. Same as in the original braid, the Grilon yarn is in white and the carbon roving in black.

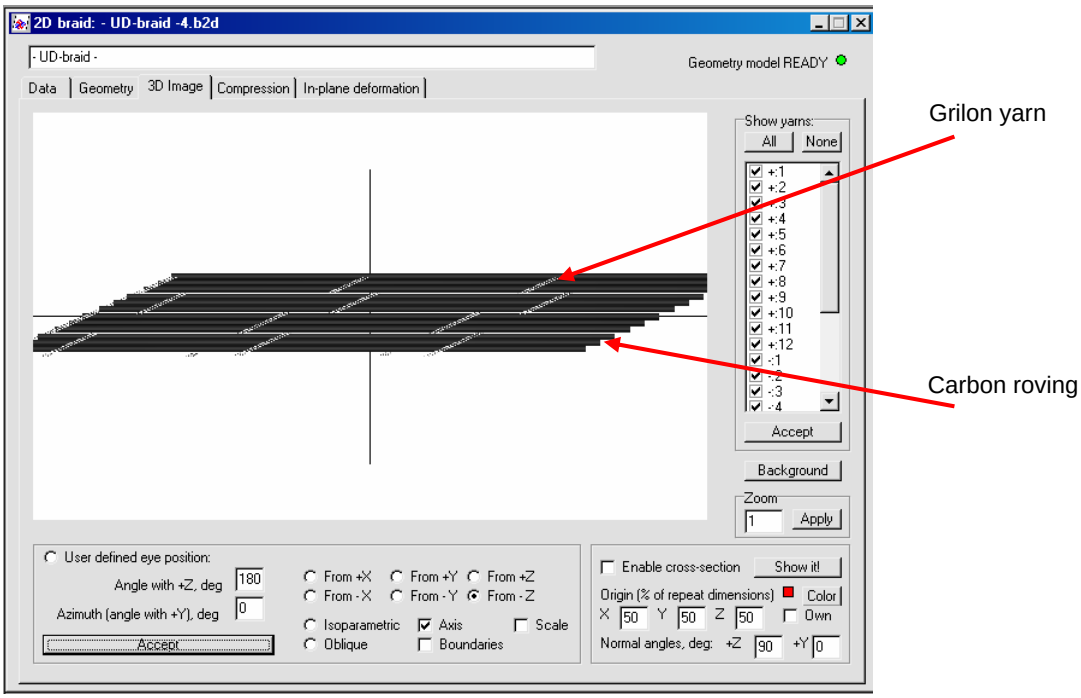

Figure 9.4: WiseTex model, geometry of UD-braid

Even in a detailed view, the simulated UD-braid and the scan of the UD-braid are quite identical in comparison.

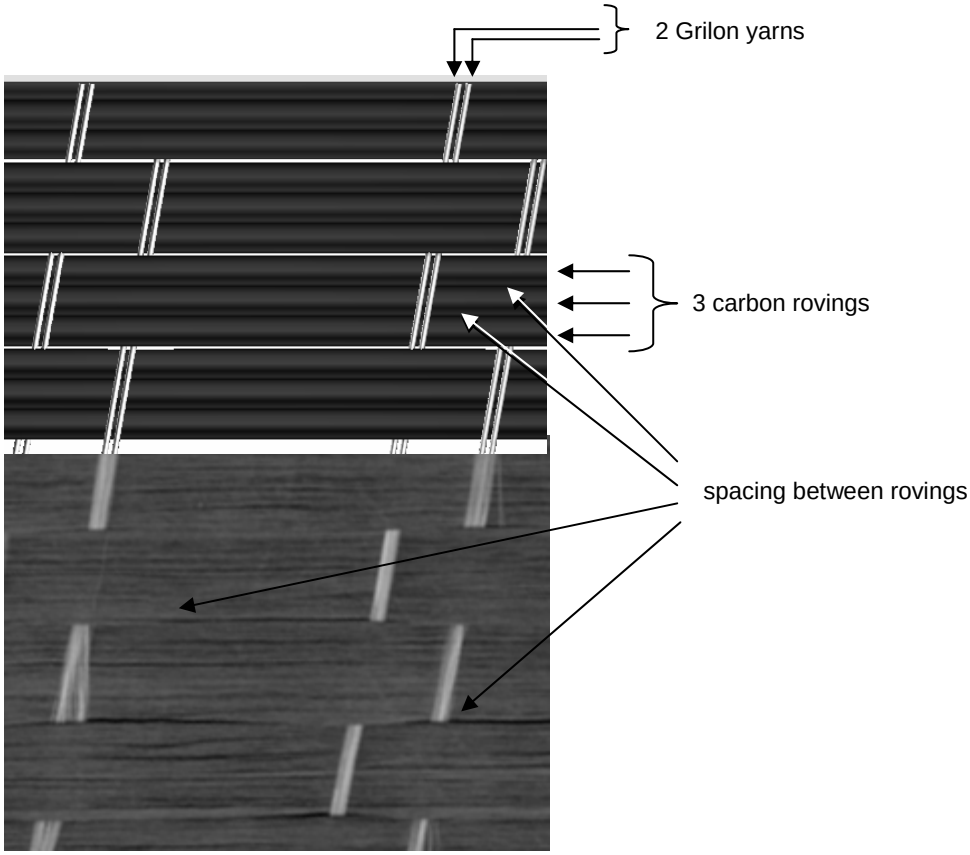

Figure 9.5: Comparison WiseTex model and original textile

9.2. WiseTex model of the compressed UD-braid

The WiseTex model of the compressed dry UD-braid is different to the non-compressed UD-braid in yarn dimensions. As a result of compression, the carbon rovings increase in width and decrease in thickness. Therefore, the rovings merge and slightly overlap each other. There are hardly any voids between the carbon rovings, observable from the microscopy as described in section 8.3. This is the desired state to reach a high volume fraction in the laminate. Compression also takes place for the Grilon yarn. The dimensions of the compressed carbon roving and the Grilon yarn are presented in table 9.3. The compression in the direction of the thickness of the Grilon yarn is an estimated value. As the non-compressed dimension in the direction of the thickness is already assessed, only a rough value for the compressed dimensions can be given. The compression of the carbon yarn is defined from the cross-section measurements of the laminate in section 8.3.

Table 9.3: Dimensions of the compressed rovings

Grilon MS			
	Twist and cross-section	twist	none
		elliptical	*d_1, mm 0.01*
			d_2, mm 0.5
Carbon			
	Twist and cross-section	twist	none
		elliptical	d_1, mm 0.342
			d_2, mm 4.920

The compression coefficients $\eta_1 = \frac{d_1}{d_{10}}$ and $\eta_2 = \frac{d_2}{d_{20}}$ are presented in table 9.4:

Table 9.4: Compression coefficients for WiseTex model

Compression	$\eta_1 = \frac{d_1}{d_{10}}$	$\eta_2 = \frac{d_2}{d_{20}}$
Grilon yarn	*0.85*	*1.40*
Carbon roving	0.92	1.70

On the basis of the figures shown above, a WiseTex model is created.

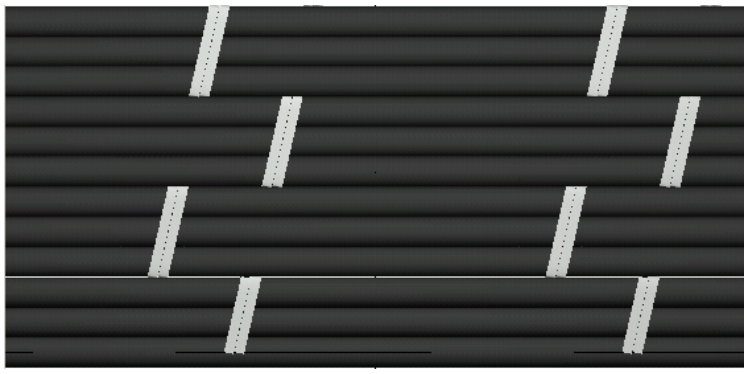

Figure 9.6: WiseTex model of compressed dry UD-braid

For the prediction of deformability of the UD-braid and the rovings tension and bending can be included in the WiseTex model. The bending rigidity results from the cantilever test in section 6.1. The value is a rough estimation as problems occurred with the test equipment. However, it can be used for a orientation.

Bending rigidity B: 583 nN*cm²

The tensile parameters are obtained from the data received from the producer of the carbon robbing HTS 5631 and pasted into the WiseTex data of the yarns. The trend of the tension curve is obtained from the tensile tests in section 6.2.

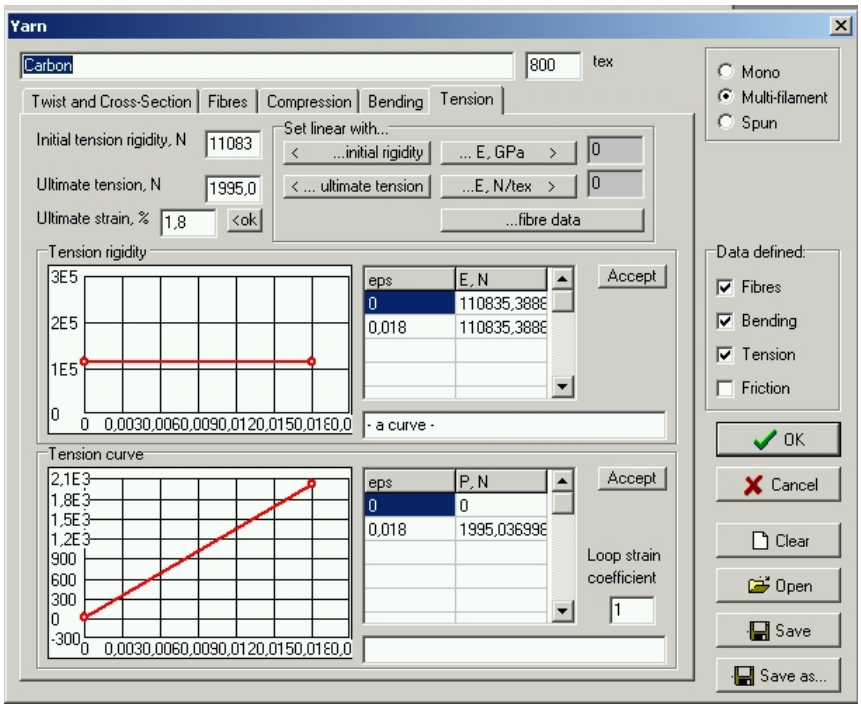

Figure 9.7: WiseTex, tension parameters of carbon roving

In-plane deformation can thus be predicted.

10. Ladevèze characterisation of the laminates

In this chapter, the infiltrated UD-braids in the form of four laminates with different stacking sequences are tested. Hereby, the mechanical and the Ladevèze damage properties of the UD-braid laminate are desribed. First the Ladevèze testing program is described in section 10.1. In section 10.2, the preparation of the specimens for the tests is illustrated. The test set-up and the performance of the tests are described in section 10.3. Additionally, the results of the tests and the calculated Ladevèze parameters are presented in sections 10.4, 10.5 and 10.6

10.1. Testing programme according to Ladevèze model

The tests are carried out according to the experimental test series developed by Ladevèze. The Ladevèze parameters result from the following tests, described in the PAM-CRASH/SAFE^{TM} 2004, SOLVER NOTES MANUAL. [21]:

- simple tension test on $[0]_8$ laminates
- simple tension test with “load/unload” cycles on $[\pm 45]_{2S}$ laminates
- simple tension test with “load/unload” cycles on $[+ 45]_8$ laminates
- simple tension test with “load/unload” cycles on $[\pm 67.5]_{2S}$ laminates
- simple compression test on $[0]_8$ laminates

With the tensile tests of the $[0]_8$ laminates fibre modulus E_1, Poisson ratio υ_{12}, critical strain threshold of ε and the damage parameter d are obtained. Shear properties, like G_{12}, and matrix damage Y are gained with the cyclic tests on the $[\pm 45]_{2S}$ laminates, whereby transverse properties E_2 are received with the cyclic tests on the $[+ 45]_8$ laminates. With the cyclic tests on the $[\pm 67.5]_{2S}$ laminates, transverse-shear coupling factor b and transverse damage Y' are examined.
The compression test series are done to collect data on the fibre compression properties, like the compression modulus E_1, with the corrective factor γ, and damage parameters ε_i^{ft}, ε_u^{ft} and d_u^{ft}.

10.1.1. Simple tension test on $[0]_8$ laminate

This test is a tension test on the unidirectional laminate, with all fibres in 0 °- direction, parallel to the applied load. With this test the following parameters are determined:

- E-modulus in fibre direction of the undamaged material E_1^{0t}
- Poisson’s ratio in plane (1,2) υ_{12}^0
- Critical strain threshold ε_i^{ft} and ε_u^{ft}

- Ultimate damage factor due to fibre rupture d_u^{ft}

From the parameters, the following functions for the fibre damage can be illustrated:

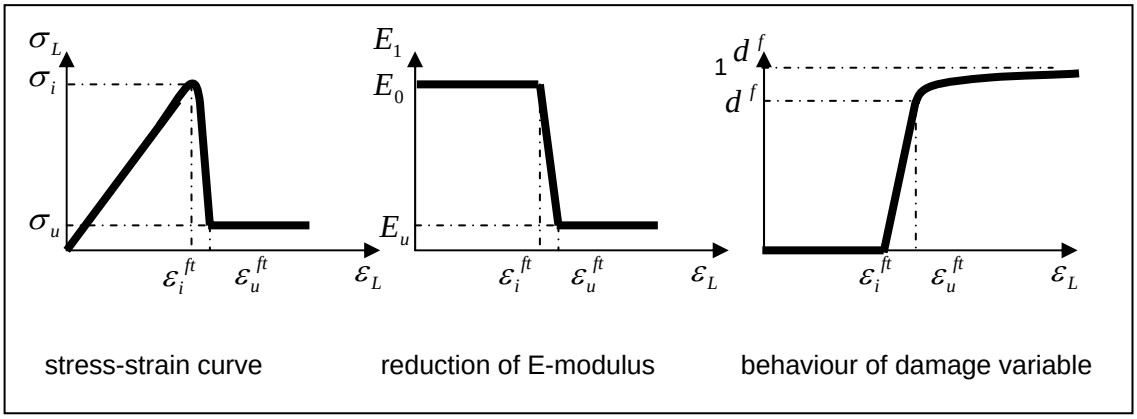

Figure 10.1: Fibre damage function

The reference direction of the global coordinate system and the fibre direction are the same. Therefore, stresses and strains can be obtained from:

$$\begin{Bmatrix}\sigma_{11}\\ \sigma_{22}\\ \sigma_{12}\end{Bmatrix}=\begin{Bmatrix}\sigma_L\\ 0\\ 0\end{Bmatrix} \quad \text{and} \quad \begin{Bmatrix}\varepsilon_{11}\\ \varepsilon_{22}\\ 2\varepsilon_{12}\end{Bmatrix}=\begin{Bmatrix}\varepsilon_L\\ \varepsilon_T\\ 0\end{Bmatrix} \qquad (47)$$

where:

σ_L : stress in the longitudinal direction

ε_L : strain in the longitudinal direction

ε_T : strain in the transverse direction

In accordance to the material law and the measured stress-strain curves, the material constants are defined by:

$$E_1^{0t}=\frac{\sigma_L}{\varepsilon_L} \qquad (48)$$

$$\upsilon_{12}^{0}=-\frac{\varepsilon_T}{\varepsilon_L} \qquad (49)$$

ε_i^{ft} , ε_u^{ft} and d_u^{ft} are defined from the functions in figure 10.1.

10.1.2. Cyclic simple tension test on $[\pm 45]_{2S}$

This test is performed on the laminate with a lay-up of ±45 ° to the global coordinate system. It gives prior information about the elastic shear behaviour of the material. The parameters to define are:

- Shear modulus in plane (1,2) G_{12}^0
- Critical shear damage limit Y_{12}^c
- Initial shear damage limit Y_{12}^0
- Elementary shear damage fracture limit Y_{12}^R

For the stacking sequence of ±45 ° the stresses and strains in the fibrous plies can be obtained from the following relation:

$$\begin{Bmatrix} \sigma_{11} \\ \sigma_{22} \\ \sigma_{12} \end{Bmatrix} = \begin{Bmatrix} 0 \\ 0 \\ \sigma_L / 2 \end{Bmatrix} \quad \text{and} \quad \begin{Bmatrix} \varepsilon_{11} \\ \varepsilon_{22} \\ 2\varepsilon_{12} \end{Bmatrix} = \begin{Bmatrix} 0 \\ 0 \\ \varepsilon_L - \varepsilon_T \end{Bmatrix} \qquad (50)$$

For the calculation of the material constants, at least 5 cycles with increasing load are needed. The first cycle, cycle 1, starts at half of the maximum expected load. The load of the following cycles *i* increases constantly. One cycle is described by a maximum load and the following minimum load. For cycle *i* with the applied maximum load higher than in cycle *i* – 1 it is assumed that the material damages more. Therefore a decrease of shear stiffness is expected. G_{12}^0 and G_{12}^i, and the elastic strain $2e_{12}^{i\ e}$, are shown in figure 10.2.

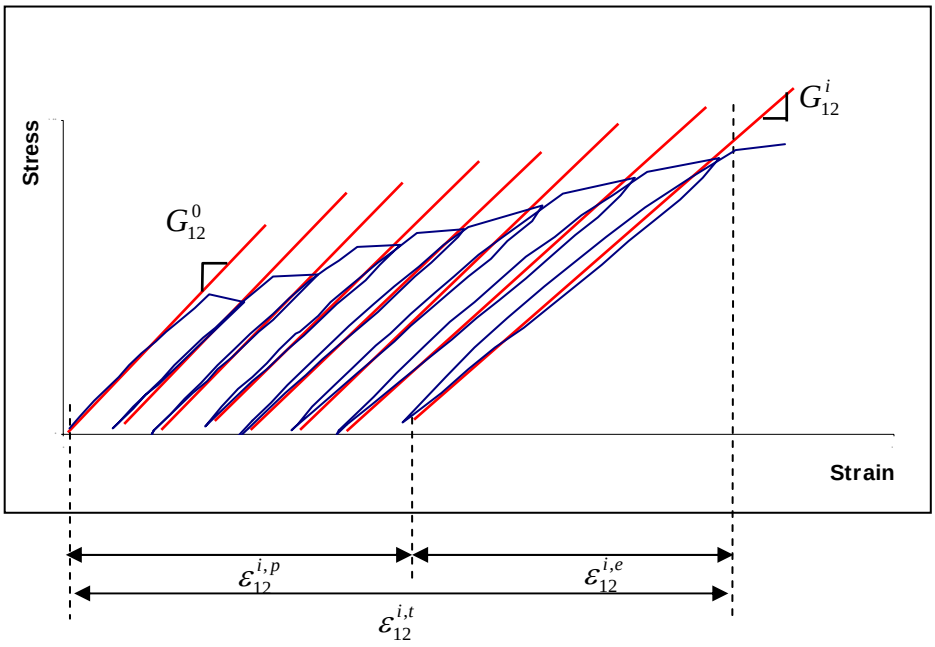

Figure 10.2: Extrapolated graph of cyclic tests

The damage factor d_i, is calculated according to the following equation:

$$d_{12}^{i} = 1 - \frac{G_{12}^{i}}{G_{12}^{0}} \qquad (51)$$

The evolution of the damage is described by the shear damage value *Y*, with:

$$Y_{12}(t_i) = \sqrt{\frac{1}{2} G_{12}^{0} \left(2\varepsilon_{12}^{i\ e}\right)^2} \qquad (52)$$

$$Y_{12}^{R} = \max\left(Y_R(t_i)\right) \qquad (53)$$

By plotting $Y(t_i)$ against the damage factor d_i and then adjusting a linear fitting curve, the initial and the critical shear damage threshold values are obtained.

$$Y_{12}(t_i) = Y_{12}^{c} d_{12}^{i} + Y_{12}^{0} \qquad (54)$$

10.1.3. Cyclic simple tension test on [+45]₈

With this test on the +45 °- laminate, the transverse properties of a laminate are tested and the coupling between transverse and shear plastic strains are determined. Therefore, the following parameters are obtained from the tests:

- Coupling factor (degree of plasticity of matrix) $a^2 = A$
- Initial transverse elastic modulus E_2^0

The fibre direction is +45 °, from which the stress and strain in the UD-ply are put into relation as follows:

$$\begin{Bmatrix} \sigma_{11} \\ \sigma_{22} \\ \sigma_{12} \end{Bmatrix} = \begin{Bmatrix} 0 \\ \sigma_L / 2 \\ \sigma_L / 2 \end{Bmatrix} \quad \text{and} \quad \begin{Bmatrix} \varepsilon_{11} \\ \varepsilon_{22} \\ 2\varepsilon_{12} \end{Bmatrix} = \begin{Bmatrix} 0 \\ \varepsilon_L + \varepsilon_T \\ \varepsilon_L - \varepsilon_T \end{Bmatrix} \qquad (55)$$

The transverse stiffness E_2^0 is obtained from the first cycle:

$$E_2 = \frac{\sigma_{22}}{\varepsilon_{22}} \qquad (56)$$

The plastic behaviour is investigated from the two curves:

$$\sigma_{22} = f\left(\varepsilon_{22}\right) \quad \text{and} \quad \sigma_{12} = f\left(2\varepsilon_{12}\right) \qquad (57)$$

and:

$$A = a^2 = \frac{\left(\varepsilon_{22}^{i\ p} - \varepsilon_{22}^{i-1\,p}\right)\left(1-d_i^{'}\right)^2}{\left(2\varepsilon_{12}^{i\ p} - 2\varepsilon_{12}^{i-1\,p}\right)\left(1-d_i\right)^2} \qquad (58)$$

If *A = 0*, there is no plasticity and can be neglected.

10.1.4. Cyclic simple tension test on [±67.5]$_{2S}$

These tests give information about the transverse damage behaviour and shear-transverse damage coupling. As input they use values obtained from the tests described above. E_1^o and ν_{12} are used from the test on the 0 °- laminate, G_{12}^o from the cyclic tests on the ±45 °- laminate and E_2^0 from the cyclic tests on the +45 °- laminate.

With these tests, the following values are defined:

- Critical transverse damage limit Y_2^c
- Initial transverse damage limit Y_2^0
- Brittle transverse damage limit for fibre-matrix interface Y_2^S
- Coupling factor between transverse and shear damage *b*

With the following matrices, the stresses and strains in the global coordinate system are transformed to local values inside the plies:

$$\begin{Bmatrix}\varepsilon_{11}\\ \varepsilon_{22}\\ 2\varepsilon_{12}\end{Bmatrix} = \left[Q_1\right]^T \begin{Bmatrix}\varepsilon_L\\ \varepsilon_T\\ 0\end{Bmatrix} \quad \text{and} \quad \begin{Bmatrix}\sigma_{11}\\ \sigma_{22}\\ \sigma_{12}\end{Bmatrix} = \left[C^0\right]\ \left[Q_1\right]\ \left[\overline{C^0}\right]\begin{Bmatrix}\sigma_L\\ 0\\ 0\end{Bmatrix} \qquad (59)$$

with:

$$\left[C^0\right]^{-1} = \begin{bmatrix} \frac{1}{E_1} & -\frac{\upsilon_{12}^0}{E_1} & 0 \\ -\frac{\upsilon_{12}^0}{E_1} & \frac{1}{E_2} & 0 \\ 0 & 0 & \frac{1}{G_{12}} \end{bmatrix} \qquad (60)$$

$$\left[Q_1\right] = \begin{bmatrix} \cos^2\alpha & \sin^2\alpha & \cos\alpha\sin\alpha \\ \sin^2\alpha & \cos^2\alpha & -\cos\alpha\sin\alpha \\ -2\cos\alpha\sin\alpha & 2\cos\alpha\sin\alpha & \cos^2\alpha - \sin^2\alpha \end{bmatrix} \qquad (61)$$

The matrix is solved for an angle α = +67.5 °, respectively –67.5 °.

The material constants are again obtained from the experimental curves with at least 5 “load/unload” cycles:

$$\sigma_{12} = f\left(2\varepsilon_{12}\right) \qquad \text{and} \qquad \sigma_{22} = f\left(\upsilon_{12}^{0}\varepsilon_{11} + \varepsilon_{22}\right) \qquad (62)$$

From each cycle *i*, the transverse and the shear damage factors are defined. Y_c and Y_0 result from the tests on the ±45 °- laminate. From these the coupling factor between transverse and shear damage for each cycle is calculated.

$$\left.\begin{aligned} d_{12}^{i} &= 1 - \frac{G_{12}^{i}}{G_{12}^{0}} \\ d_{2}^{i} &= 1 - \frac{E_{2}^{i}}{E_{2}^{0}} \end{aligned}\right\} \Rightarrow \qquad \begin{aligned} Z_{12}^{i} &= \frac{1}{2} G_{12}^{0}\left(2\varepsilon_{12}^{i\ e}\right)^{2} \\ Z_{2}^{i} &= \frac{1}{2} E_{2}^{0}\left(\upsilon_{12}^{0}\varepsilon_{11}^{i\ e} + \varepsilon_{22}^{i\ e}\right)^{2} \end{aligned}$$

$$\Rightarrow \quad b_i = \frac{\left(Y_{12}^{c} d_{12}^{i} + Y_{12}^{0}\right)^{2} - Z_{12}^{i}}{Z_{2}^{i}} \qquad (63)$$

The linear fitting curve of the graph of d_2^i versus $Y_2\left(t_i\right)$ gives the values Y_2^c and Y_2^0:

$$Y_2\left(t_i\right) = Y_2^c d_2^i + Y_2^0 \qquad (64)$$

The last parameter to define is:

$$Y_2^S = \max\left(\sqrt{Z_2^i}\right) \qquad (65)$$

10.1.5. Simple compression test on $[0]_8$

This test is assessed to obtain parameters to define the compressive material behaviour of a UD-laminate. The parameters obtained are:

- Compressive initial Young’s modulus in fibre direction E_1^{0c}
- Correction factor for non-linear compressive behaviour γ
- Initial critical strain corresponding to fibre damage ε_i^{fc}
- Ultimate critical strain corresponding to fibre damage ε_u^{fc}
- Ultimate damage factor corresponding to fibre failure d_u^{fc}

The fibre angle of each ply is 0 °: The same laminate as for the tension test on the 0 °- laminate is used. The transformation relationship for the individual UD-plies, the laminas, and the measured values is as follows:

$$\begin{Bmatrix}\sigma_{11}\\ \sigma_{22}\\ \sigma_{12}\end{Bmatrix}=\begin{Bmatrix}\sigma_L\\ 0\\ 0\end{Bmatrix} \qquad \text{and} \qquad \begin{Bmatrix}\varepsilon_{11}\\ \varepsilon_{22}\\ 2\varepsilon_{12}\end{Bmatrix}=\begin{Bmatrix}\varepsilon_L\\ \varepsilon_T\\ 0\end{Bmatrix} \qquad (66)$$

The material constants are obtained from the experimental stress-strain curve:

$$\sigma_L = f(\varepsilon_L) \qquad (67)$$

The initial slope of the experimental curve gives the initial elastic compressive modulus of the UD-ply in the fibre direction E_1^{0c}. The reduction of the modulus due to non-linear material behaviour is described as in figure 10.1 where γ can be calculated from:

$$\gamma = \frac{E_1^{0c} - E_1^{\gamma}}{E_1^{\gamma} E_1^{0c} \left|\varepsilon_{11}\right|} \qquad (68)$$

The parameters corresponding to the fibre damage are defined by the curve in figure 3.12.

10.2. Specimen preparation

Test specimens are prepared in accordance with EN 2565 method B for carbon fibre reinforced laminates.

10.2.1. Cutting

Cutting of the specimens out of the plates is done using an automatic wet diamond saw. The velocity chosen is 2 m/min. The cutting plan for each plate is shown in figure 10.3 and figure 10.4.

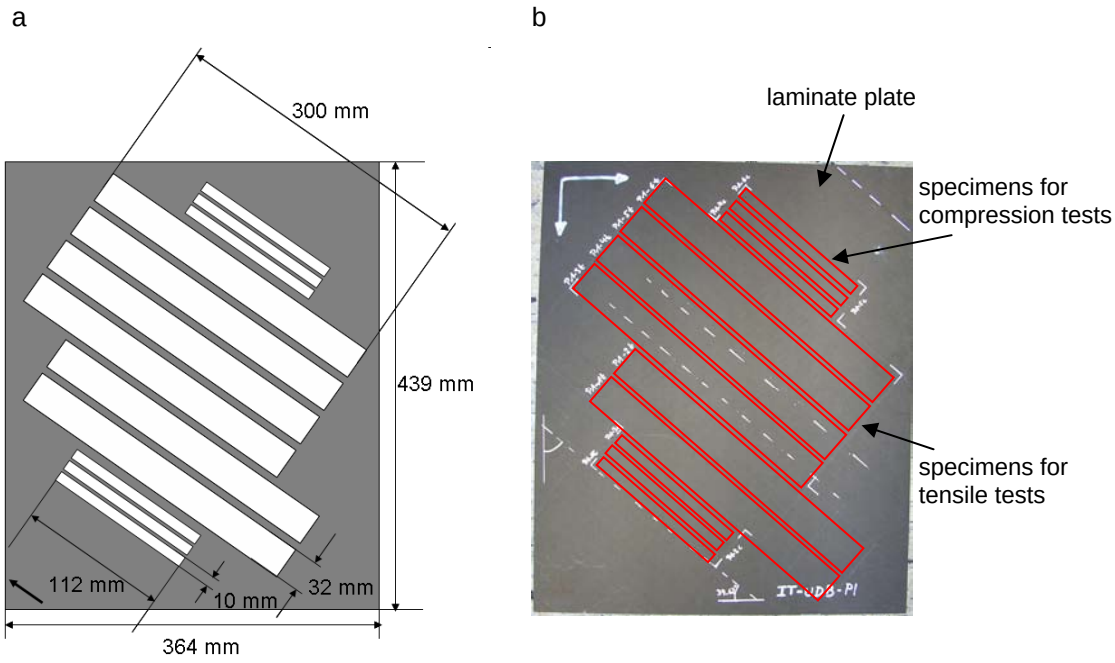

Figure 10.3: Cutting plan plate 1; model (a), photo of the laminate with schematic drawing of the cut outs (b)

The labelling of the specimens is from bottom left to top right: P1-1c (compression) until P1-3c, P1-1t (tension) until P1-6t, P1-4c until P1-6c.

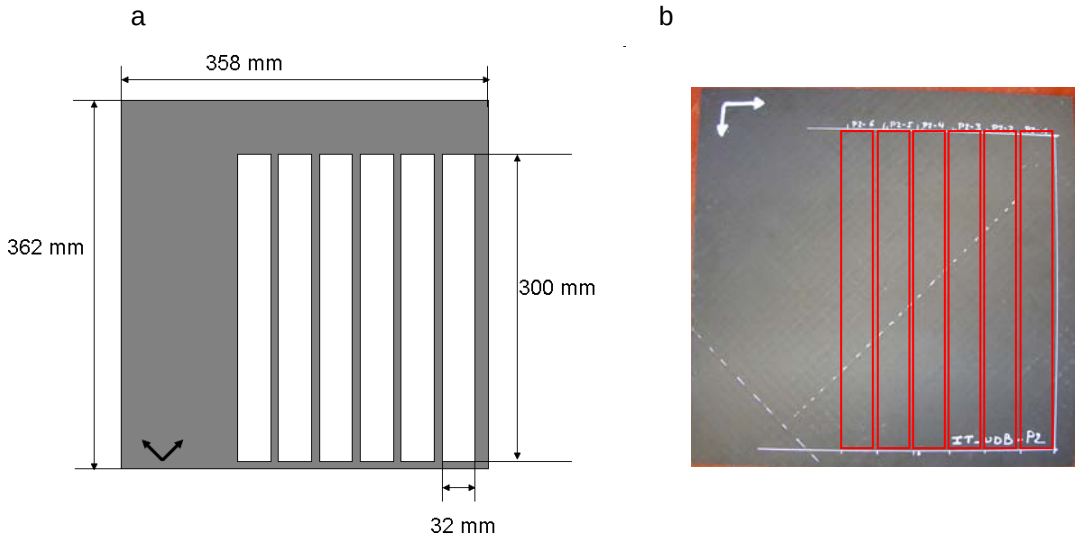

Figure 10.4: Cutting plan plate 2; model (a), photo of the laminate with schematic drawing of the cut outs (b)

The cut out specimens are marked from right to left by P2-1 until P2-6.

The same method is applied for plates 3 and 4.

10.2.2. End tabs

For each specimen four tabs are mandatory to avoid stress concentrations near the jaws, two on each edge on the top and rear sides are applied. They are cut out of a GFRP-plate (glass fibre reinforced plastics) plate, with a lay-up of 0 º and 90 º. The specimen dimensions for the tension tests are 32 mm x 60 mm x 2.4 mm and for the compression tests 10 mm x 51 mm x 2.4 mm. The end tabs are champered at one edge with an angle of 45 °, illustrated in figure 10.5.

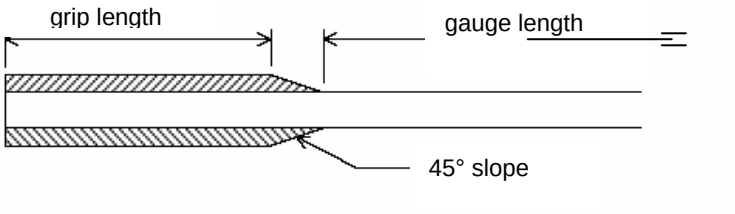

Figure 10.5: Tab geometry

The tabs are bonded to the laminate specimens with the two component adhesive Scotch-Weld™ 9323 B/A with a mixing ratio of 100/27.

10.2.3. Strain gauges

Strain gauges in both transverse and longitudinal direction are glued to the specimens for the registration of the strain during testing. A strain gauge of type LY11 manufactured by the company HBM, a linear strain gauges with one measuring grid and a gauge length of 10 mm, is used.

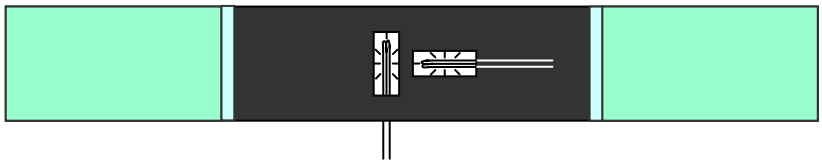

Figure 10.6: Specimen with strain gauges, transverse and longitudinal

For compression tests, one strain gauge is attached to the specimens in the longitudinal direction, i.e. in fibre direction, on each side, front and back. The strain gauges type KFG, by the company Kyowa, have a gauge length of 1 mm.

Figure 10.7: Specimen with strain gauge, longitudinal

10.2.4. Contrast grid for optical strain measurement

Additionally, for increased precision and validation of the results, a stochastic pattern is printed onto the backside of the specimens for the tensile test. First a dull white lacquer is sprayed onto the surface and then with a stamp a pattern out of 49 black points per cm^2 is printed evenly onto the lacquer. Thereby, a high contrast is realised.

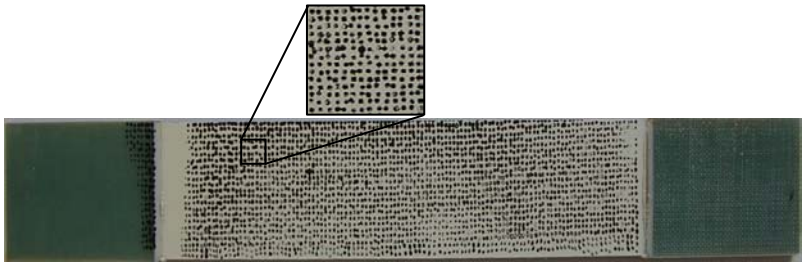

Figure 10.8: Stochastic pattern for strain mapping with Aramis

The in situ deformation strain mapping system Aramis is used for the inspection of the deformation and strain during loading. The Aramis system, an optical inspection system, measures 3D deformation using stereo high-resolution video cameras by photogrammetry. These cameras record the strains according to the contrast pattern on the specimen. Individual images of the pattern are taken at different load stages using CCD cameras.
Figure 10.9 shows the Aramis system, consisting of a computer with special software and two CCD cameras, to take a left and a right picture for strain mapping with coinciding focus. [26]

Figure 10.9: Aramis system, camera set-up [26]

10.2.5. LAP calculations of expected strength

Before the performance of the tests, an analysis of the expected strength is necessary; on the one hand the expected strength is calculated to be able to define the type of machine with the suitable load cell and on the other hand to define the individual load for each cycle, when performing the cyclic tests for plates 2, 3 and 4.

The expected ultimate load is calculated with the LAP (Laminate Analysis Program) by anaglyph Ltd, UK using the micromechanical equations according to Chamis. [16] The material data for the input into the LAP are obtained from former mechanical test on the UD-braid and from reference data of an epoxy resin / CF-woven fabric, using RTM 6 and G 1157 D 1300 Injectex®E01 2F. The parameters to determine the expected strength at ultimate load [+Nx] are additionally compared with test results of UD-braids out of HTS 6531 and Grilon K85, 16 layers, +/- 45° and 0/90°.

Table 10.1: Expected strength for testing, obtained from LAP calculations

Expected strength	$[0°]_8$	$[\pm 45°]_{2S}$	$[+45°]_8$	$[\pm 67.5°]_{2S}$
Ultimate load	4531 N/mm	288.7 N/mm	193.3 N/mm	168.5 N/mm
Maximum strength	145 kN	9.2 kN	6.2 kN	5.4 kN

Additionally, when considering the data obtained from the geometrical characterisation of the laminate, including the deviations from the angle of each ply and the various ply thickness, the expected maximum load is then slightly lower.

10.2.6. Testing machinery

According to the Ladevèze testing program, the tests are performed on four different testing machines. The tensile tests are executed according to the standard AITM 1-0007. For testing of the [0°] -laminate, plate 1, the expected forces are above 100 kN. Therefore, the machine Instron 8803 with a maximum load of 500 kN is used. For the hysteresis tests of plate 2, the [±45] –laminate, the machine Instron 5566 is used with a maximum load of 10 kN as the calculated maximum load is less than 10 kN. However, during the first test (P2-1), the specimen does not break. Additional testing results in a maximum load bearing of 10.9 kN. Therefore, the following tests, from P2-2 through P2-6, are performed on the testing machine Zwick 2071 with a load cell of maximum 100 kN. For testing the laminate P3 [+45°], the testing machine Zwick 2071 is also used. The first two specimens of plate 4, the [±67.5°] –laminate, are also tested on the machine Zwick 2071, but the machine has difficulties controlling the cycles of such a small loading. As a result, the following tests are performed on the testing machine Instron 5566, with a load cell of maximum 10 kN.
The Celanese compression tests on plate 1, the [0°] –laminate, are executed on the testing machine Zwick 1494 according to the standard DIN EN 2850.
The summary of the tests is shown in figure 10.1.

Table 10.2: Summary of testing machines used for each specimen

	Specimen	Testing machine, type	Load cell
P1	1t-6t	Instron 8803	500 kN
	1c-6c	Zwick 1494	500 kN
P2	1	Instron 5566	10 kN
	2	-	-
	3-6	Zwick 2071	100 kN
P3	1-6	Zwick 2071	100 kN
P4	1	Zwick 2071	100 kN
	2	Zwick 2071	100 kN
	3	-	-
	4-6	Instron 5566	10 kN

10.2.7. Stress / Strain mapping

The test set-up allows a parallel mapping of the strains with two different measuring methods. During the testing, the strains are measured with the two strain gauges, attached to the specimen. For the tensile tests, they are in longitudinal and transverse direction, measuring the elongation ε [%] of the specimens in the predefined directions, i.e. ε_L = longitudinal strain and ε_T = transverse strain. The specimens for the compression tests contain two strain gauges, both in longitudinal direction.

Additional, the Aramis system is used for strain mapping of the tensile test. The specimens of the compression tests are too small to use the Aramis system. Therefore, the strain mapping of the compression tests is not performed with the Aramis system.

The load cell of the testing machine measures directly the applied load.

10.3. Performance of the tests

The tensile tests are based on the standard AITM 1-0007 by Airbus®. The compression tests are performed according to the German standard for aerospace DIN EN 2850. The performance of the tests according to the Ladevèze testing program is described in the following sections.

10.3.1. Simple tension test on $[0]_8$ laminate

This test is a standard test in laminate testing. The tests of the 6 specimens are all performed on the testing machine Instron 8803, with a load cell of maximum 500 kN. Before testing, the testing machine is calibrated and the strain gauges on the specimens are connected with the testing machine by soldering the strain gauges to the input cables of the machine. The strain gauges measure transverse and longitudinal strains. Additionally, the Aramis system is set up and calibrated for additional measurement of the strains. The application of the load and the recording

of the Aramis start at the same time for time validation. The testing velocity is according to the standard AITM 1-0007. Every second, a picture is taken by the Aramis cameras.
The breakage of the specimens happens in brush like form due to the explosive behaviour during failure. Also due to a difference in stiffness of the fibre and the matrix, the phenomena of matrix cracking, followed by a debonding of the two components and then fibre rupture is observed.

10.3.2. Cyclic simple tension test on $[\pm 45]_{2S}$ laminate

This test is not a standard test and, due to the cyclic loading and unloading, the test puts higher demands on machine control.
The cyclic tests, also called hysteresis tests, are executed on different machines. The maximum load calculated in LAP is 9.2 kN. Therefore, the testing machine Instron 5566 is chosen, with a maximum load cell of 10 kN. The first specimen, P2-1, is tested with 10 cycles starting at half of the expected load. As the calculated load in the LAP is 9.2 kN, a slightly lower load is expected for the testing. Therefore, the maximum load of the first cycle is 4 kN. Then the machine drops back to a minimum load of 0 kN to complete the first cycle. The stepwise increase of the load per cycle is 0.5 kN for each cycle. Each cycle takes 6 minutes, in order not to over steer the machine motor. The “loading/unloading” of the testing machine is programmed in the machine software. The maximum cycle number is 10. Therefore, the maximum of the last cycle is 9 kN.
The time needed for the whole test is about 60 min. For the Aramis, a shooting time of one picture every four seconds is chosen due to the limitation of storage capacity of the Aramis PC. The strain gauges are connected to the machine.
However, at maximum load of 9 kN, the specimen does not break. An additional cycle is added until 10 kN, the limit of the load cell. Again, the specimen does not break. To test the ultimate maximum load of the specimen, the machine Instron 8803 is used. The result is a maximum strength of 145 MPa at maximum load of 10.9 kN. The results of the testing cycles on the different machines are summed up and put together in one stress-strain curve, see figure 10.10.

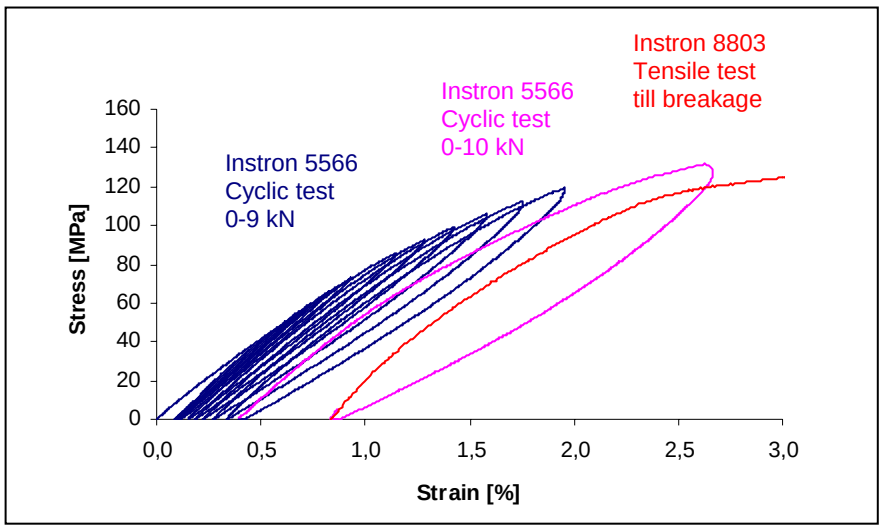

Figure 10.10: Stress-strain curves of specimen P2-1

As no other load cell than 10 kN and 100 kN is available, the further tests are performed on the testing machine Zwick 2071 with a maximum load cell of 100 kN.
Following scheme of the performance of the tests is chosen:

- Maximum load of the first cycle: 4 kN
- Minimum load of all cycles: 0 kN
- Increase of maximum load per cycle: 1 kN
- Time per cycle: 4 minutes
- Expected breakage of specimens between 10 kN and 11 kN

P2-2 breaks unintentionally due to an incorrect control of the machine motor.
The specimens P2-3 through P2-6 are tested as specimen P2-2. The only problem is the vibrating of the machine during loading and unloading. The measuring points show slight variations.
At cycle 8, while testing specimen P2-3, both strain gauges disconnect from the specimen surface and do not measure the strains anymore. Therefore, the results are used only through cycle 7.
The kind of breakage is a brittle failure.

10.3.3. Cyclic simple tension test on $[+45]_8$ laminate

To get a better comparison and as the test results of plate 2 and plate 3 are used in the test on the ±67.5 °-laminate, these tests are also performed on the testing machine Zwick 2071. The testing program is as follows:

- Maximum load of first cycle: 3 kN
- Minimum load of all cycles: 0 kN
- Increase of maximum load per cycle: 0.5 kN
- Time per cycle: 2 minutes
- Expected breakage of specimens between 5.1 kN and 6.3 kN

During testing, the stresses are measured by the machine. The strains in transverse and longitudinal direction are recorded by the two strain gauges and the Aramis system.
The small load and the cyclic control of the testing machine motor is problematic. This results in strong vibrations of the machine and big variations in the stress-strain diagram (figure 10.11).

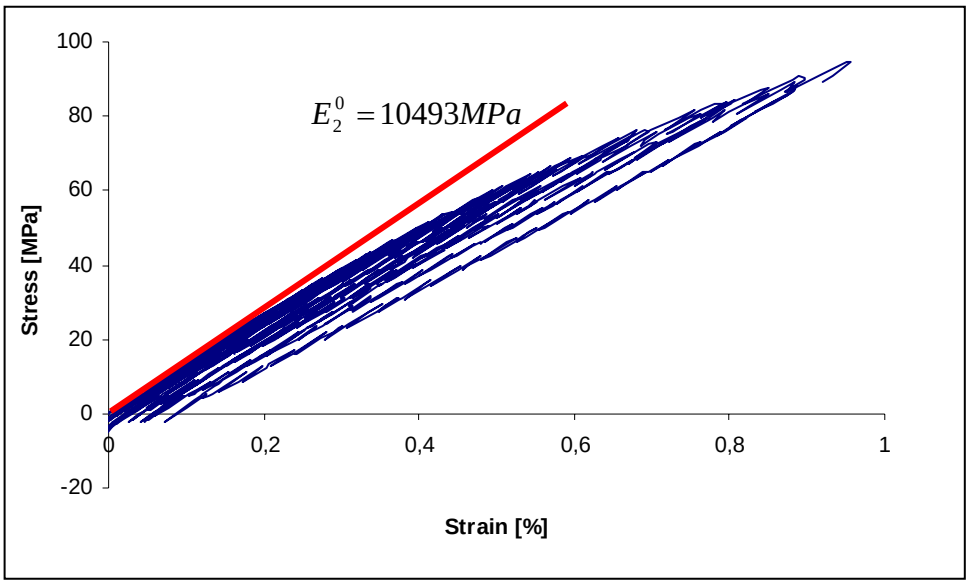

Figure 10.11: Stress-strain diagram of P3-1, vibrating motor during testing

10.3.4. Cyclic simple tension test on $[\pm 67.5]_{2S}$ laminate

The ±67.5 °- laminate can take up the lowest load. The maximum force necessary to break the specimen barely exceeds 4 kN. The UD-plies are almost tested in transverse direction as the angle is close to 90 °. This has a huge influence on the tensile strength of the laminate. For validation of the test results, the testing machine Zwick 2071 with a load cell of maximum 100 kN is used again. The testing program concerning the software programming of the testing machine is as follows:

- Maximum load of first cycle: 2.5 kN
- Minimum load of all cycles: 0 kN
- Increase of maximum load per cycle: 0.5 kN
- Time per cycle: 2 minutes

While testing the first specimen, P4-1, the machine shows high vibrations. The breakage of the specimen is at 4.1 kN. Therefore, the program of the cycles for the next tests is changed. The maximum load of the first cycle is at 1.5 kN, with an increase of 0.5 kN per cycle. Due to the extremely small load and the cyclic movement during loading and unloading, the motor of the machine vibrates very strongly. During testing of P4-3, the machine cannot control the small forces. Therefore, this test is not useable and the machine is changed. Specimens P4-4 through P4-6 are tested on machine Instron 5566 with a load cell of maximum 10 kN. The cycles are described in the testing program:

- Maximum load of first cycle: 1.5 kN
- Minimum load of all cycles: 0 kN
- Increase of maximum load per cycle: 0.5 kN
- Time per cycle: 4 minutes

10.3.5. Simple compression test on $[0]_8$ laminate

This test, a standard test in testing laminates, puts completely different demands on the testing machine than tensile tests. The problem of buckling of the specimen has to be eliminated. To avoid a wrong recording of the strains in the case of bending, two strain gauges are attached to the specimens at front and backside.
An average value for the compressive strains of the measured values of both sides is taken.

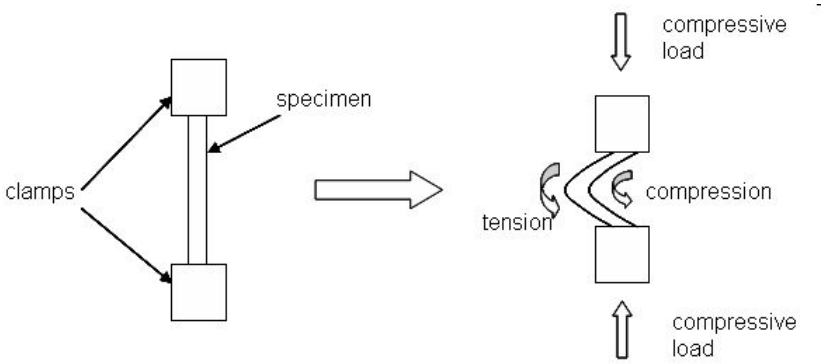

Figure 10.12: Compressive and tensile strains during compressive load

The machine used for testing is the Zwick 1494 with a load cell of maximum 500 kN.

10.4. Test results from strain gauges

In the following sections, the results of the Ladevèze testing programs are presented. All the parameters are based upon the measurements of the strain gauges and the testing machine data, as described in chapter 10.3.

10.4.1. Simple tension test on $[0]_8$ laminates

For the simple tension test, eight layers are built up in the laminate, each in 0 °-direction.
With the LAP, it is possible to simulate the behaviour of the UD-plies during testing and the change in shape of the laminate. The light blue is the original shape of the laminate, illustrated in figure 10.13. Due to the application of load in y direction, the carbon filaments become elongated and decrease in x- direction, shown in red colour. Therefore, the longitudinal strain ε_L is positive and the transverse strain ε_T is negative.

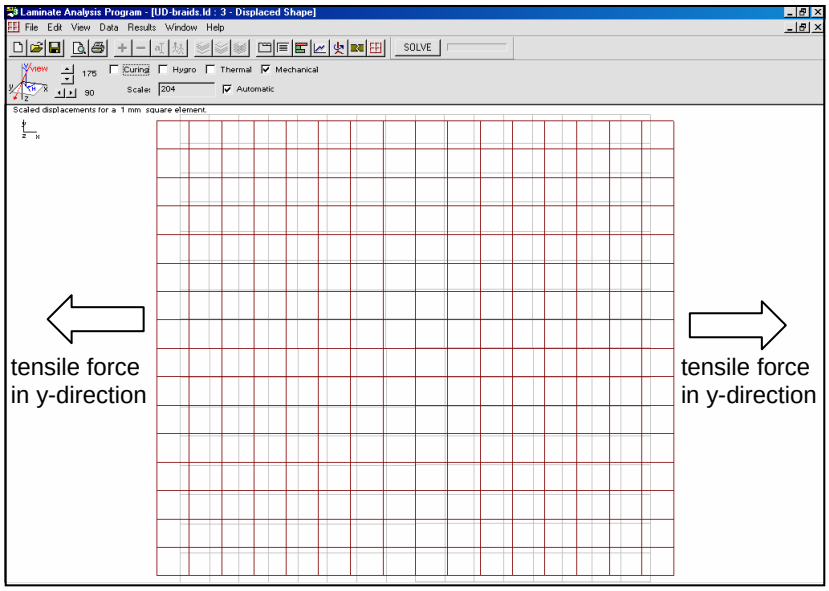

Figure 10.13: LAP displacement shape at simple tension test $[0]_8$

According to the transformation relationship, described in section 10.1.1, the longitudinal stresses σ_L are transformed in stresses σ_{11} in the local ply frame and the longitudinal ε_L and the transverse strains ε_T are transformed in the strains ε_{11} and ε_{22}.

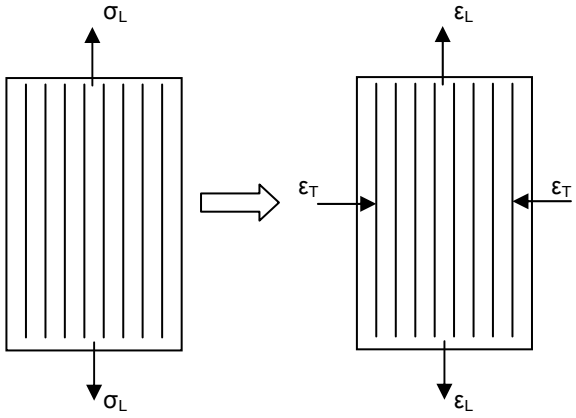

Figure 10.14: Schematic drawing of tensile test $[0]_8$ laminate, stress and strain on one layer

This transformation is needed for the analysis of the experimental test data. For this purpose, the MS Office application Excel is used, following a routine, described below:

- Collection of the raw data from the testing machine
- Reading the raw data into the program Excel
- Transforming stresses and strains for the individual UD-ply: $\sigma_L = \sigma_{11}$, $\varepsilon_L = \varepsilon_{11}$ and $\varepsilon_T = \varepsilon_{22}$
- Ascertaining the E-modulus of the undamaged material: $E_1^{0t} = \frac{\Delta\sigma_{11}}{\Delta\varepsilon_{11}}$ from the first 10 measuring points
- Calculation of modulus in fibre direction E_1 and d_i for each measuring point i

- Calculating the initial Poisson's ratio in ply plane direction: υ_{12}^{0}
- Determination of initial and ultimate threshold level of elongation, ε_i^{ft} and ε_u^{ft}, and the ultimate value of damage d_u^{ft} at tensile load from the curve: $\varepsilon_L = f(d_i)$, see figure 10.1 and figure 10.15
- Recalculation of the results from the actual fibre volume fraction of 55.6 % to a standard volume fraction of 60 %

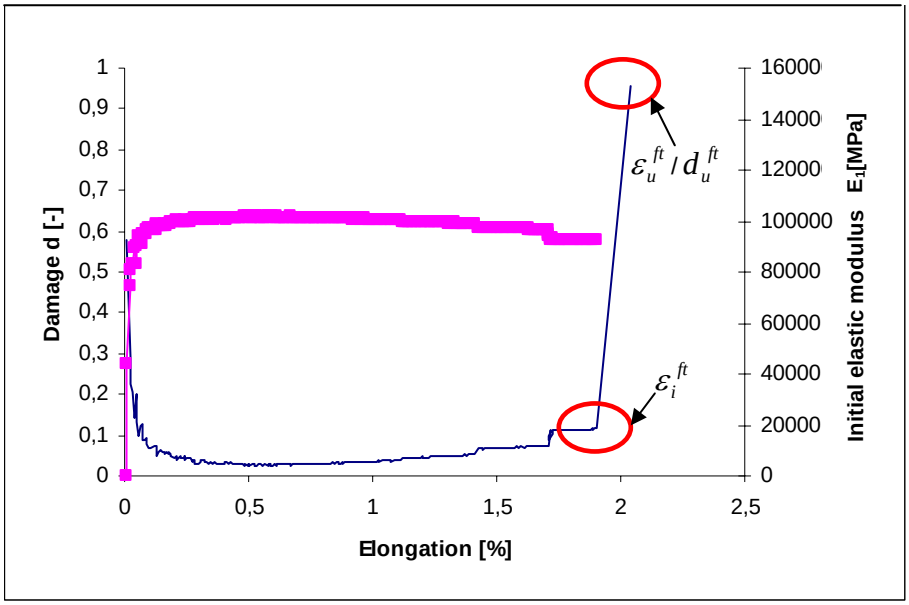

Figure 10.15: Tensile test of P1-1t

The blue line in figure 10.15 represents the damage factor *d* dependent of the tensile strain ε_L. From this graph, the initial elongation at damage ε_i^{ft} and the ultimate elongation at damage ε_u^{ft} are derived. The pink line is the elastic modulus E_1 for each state of elongation. In the graph it can be seen that the fibre breakage and the damage of the laminate is very small until a sudden breakage of filaments and matrix occurs, directly followed by the complete failure of the laminate.

The results of the analysis of the experimental data is summarised in table 10.3.

Table 10.3: Results of simple tension test on $[0]_8$- laminate

Test	E_1^0 [MPa]	υ_{12}^0 [-]	ε_i^{ft} [%]	ε_u^{ft} [%]	d_u^{ft} [-]
P1-1	112643.4	0.250	1.907	2.039	0.955
P1-2	118035.2	0.320	1.902	1.968	0.847
P1-3	141187.8	0.316	1.952	2.042	0.874
P1-4	147438.1	0.280	1.860	1.874	0.989
P1-5	165824.9	0.281	1.810	1.916	0.875
P1-6	146348.4	0.275	1.907	2.039	0.955
Average	**138579.6**	**0.287**	**1.890**	**1.980**	**0.916**
Stand. dev.	19913.3	0.027	0.049	0.073	0.058
Max	165824.9	0.320	1.952	2.042	0.989
Min	112643.4	0.250	1.810	1.874	0.847
CV	14.4	9.3	2.6	3.7	6.3

a

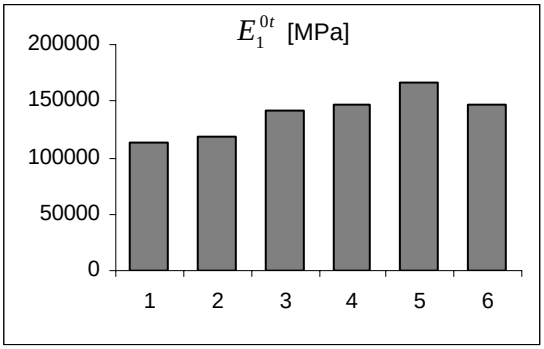

Initial elastic modulus

b

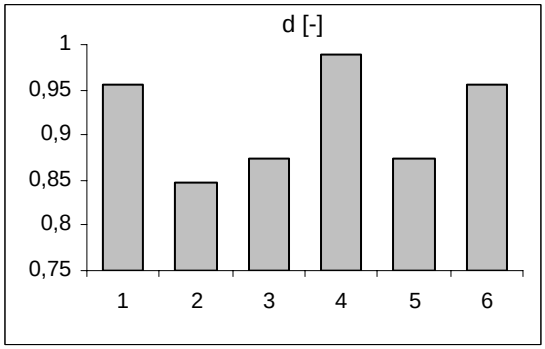

Ultimate value of damage

Figure 10.16: Comparison of the specimens: from P1-1 through P1-6

a: Comparison of initial elastic modulus, E_1^{0t} [MPa]

b: Comparison of ultimate value of damage at tension in fibre direction, d_u^{ft}

The calculated results of the simple tension test on $[0]_8$- laminate are quite constant, with a small standard deviation.

10.4.2. Simple cyclic tension test on $[\pm 45]_{2S}$ laminates

The LAP displacement in figure 10.17 shows the change in shape after testing in red colour.

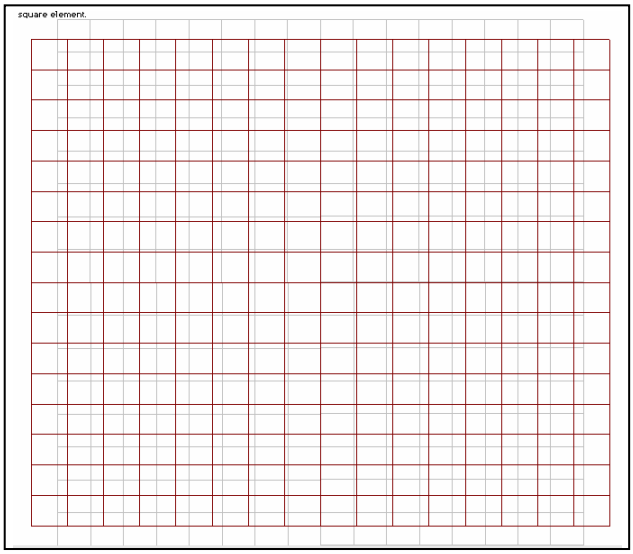

Figure 10.17: LAP displacement shape at simple cyclic tension test $[\pm 45°]_{2S}$

Due to the fibre direction in ±45 °, the filaments are oriented in longitudinal direction at tensile load. This alignment results in a strong longitudinal strain and a large decrease in transverse direction. Therefore, the values of the strains are bigger than the ones from testing the 0 °-laminates.

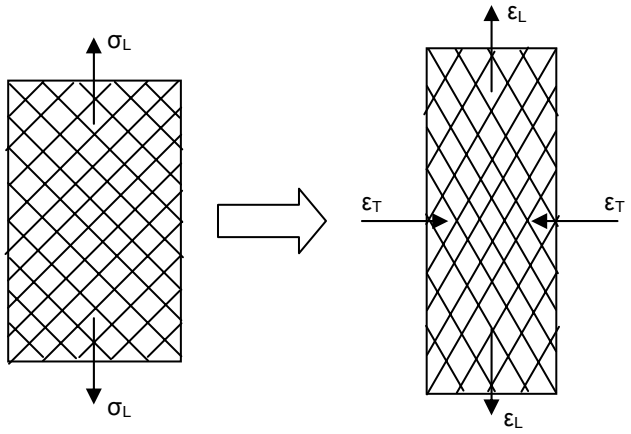

Figure 10.18: Alignment of filaments during tensile loading

For the analysis, the following scheme is used:

- Collection of the raw data from the testing machine
- Reading the raw data into Excel, containing longitudinal and transverse strains in [%], longitudinal stresses in [MPa], applied force in [N] and longitudinal displacement in [mm]
- Calculating stresses and strains of the UD-ply for each measuring point *i* : ε_{12} in [%] and σ_{12} in [MPa] for the determination of the initial shear modulus

- Determining the initial shear modulus G_{12}^0 by defining the Young's modulus of the plotted experimental stress-strain curve $\frac{\sigma_L}{2} = f\left(\varepsilon_L - \varepsilon_T\right)$, i.e. $\sigma_{12} = f\left(2\varepsilon_{12}\right)$, from the first 100 measuring points
- Manually determining maximum and minimum strains of each cycle *i*
- Calculating for each cycle *i* the corresponding stresses and strains of the UD-ply: 2 ε_{12} in [%] and σ_{12} in [MPa]
- Finding the shear modulus for each cycle *i* : $G_{12}^i = \frac{\Delta\sigma_{12}}{\Delta 2\varepsilon_{12}}$
- Calculation of d_i, $Y_{12}(t_i)$ and Y_{12}^R
- Plotting of $Y_{12}(t_i)$ versus d_i , adjusting a linear fitting curve to define Y_{12}^c and Y_{12}^0 from the equation: $Y_{12}\left(t_i\right) = Y_{12}^c d_{12}^i + Y_{12}^0$
- Recalculation of the results from the actual fibre volume fraction of 55.8 % to a standard volume fraction of 60 %

The results of the test analysis according to Ladevèze are summarised in table 10.4.

Table 10.4: Results of cyclic simple tension test on $[\pm 45]_{2S}$- laminate

Test	No. of cyles	G_{12}^0 [MPa]	$Y_{12}^0\ \sqrt{MPa}$	$Y_{12}^R\ \sqrt{MPa}$	$Y_{12}^c\ \sqrt{MPa}$	d [-]
P2-1	12	4140.8	-0.006	1.219	3.314	0.347
P2-3	7 (8)	8161.8	-0.201	0.980	2.804	0.411
P2-4	7	4372.3	-0.020	1.061	3.185	0.330
P2-5	7	7019.4	-0.047	1.000	2.214	0.433
P2-6	7	7958.6	-0.083	0.942	2.482	0.385
Average	**-**	**6330.6**	**-0.071**	**1.041**	**2.800**	**0.381**
Stand. dev.	-	1943.5	0.078	0.109	0.463	0.043
Max	-	8161.8	-0.006	1.219	3.314	0.043
Min	-	4140.8	-0.201	0.942	2.214	0.330
CV	-	30.7	109.2	10.4	16.5	11.3

For P2-3, the cycle number until breakage is 8, however only 7 cycles are used as the strain gauges detached during testing at the 8th cycle.

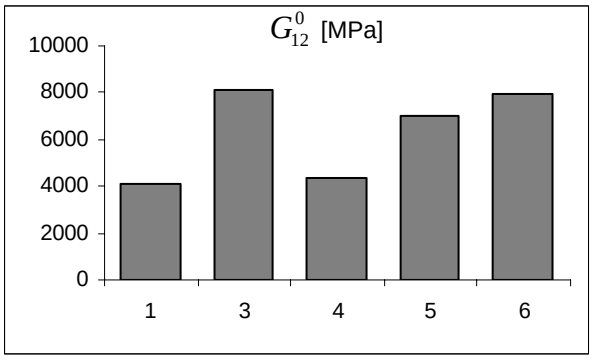

Figure 10.19: Comparison of initial shear modulus of the UD-ply in ply plane direction

The value of G_{12}^0 of the specimens P2-1 and P2-4 is quite low in comparison to the other specimens; additionally, the values for Y_{12}^0 deviate strongly. The C-scans do not indicate any problems with voids or inclusions.

The problem during the strain measurement with the strain gauges can be the small size of the strain gauge. The strain gauge is only 10 mm in length and a roving under a 45 °- direction has a length of 12.44 mm (see figure 10.20). It is advised to use strain gauges larger than one unit cell for future measurements.

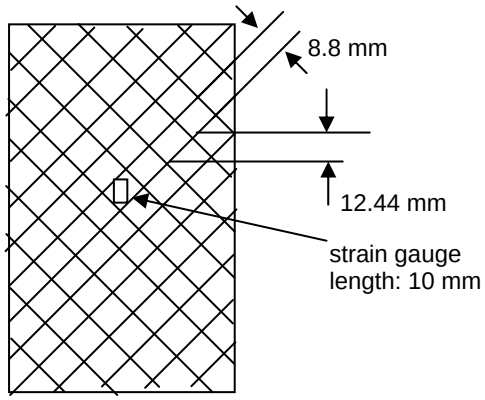

Figure 10.20: Dimension comparison of size of strain gauge and roving

A validation of this assumption is given by the measurements with the Aramis system in section 10.5.2.

10.4.3. Simple cyclic tension test on $[+45]_8$ laminates

In figure 10.21 deformation of the $[+45]_8$ –laminate is shown caused by a tensile load.

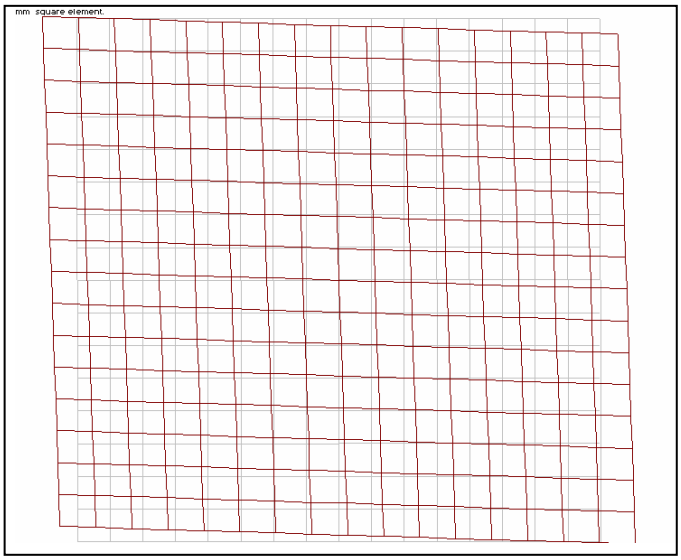

Figure 10.21: LAP displacement shape at simple cyclic tension test $[+ 45°]_8$

In this test, the behaviour of the laminate due under transverse load is investigated. The load bearing capacity of such a stacking sequence is very low and should be avoided in practical use. The laminate shows low damage until the ultimate failure of the laminate. This can be derived from the graph in figure 10.22.

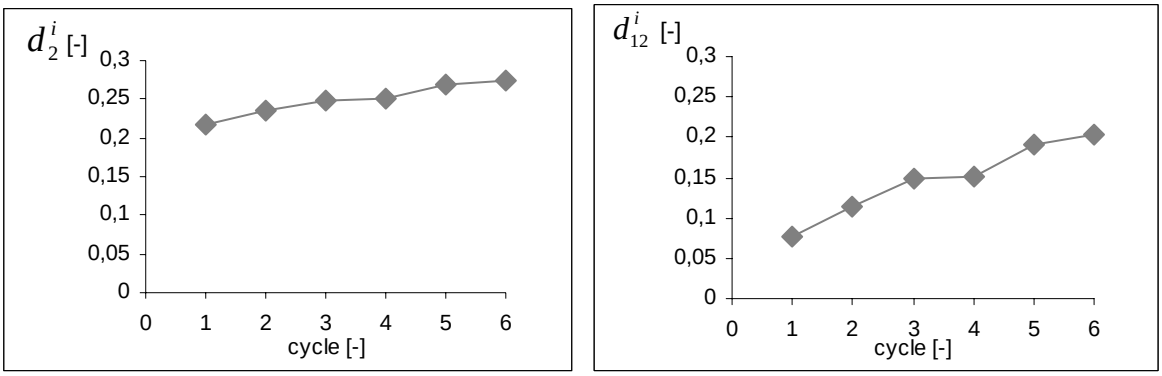

Figure 10.22: Damage factor uncoupled, test on P3-4

i.e. for transverse (plane 2; d_2^i) and plane 1,2- direction (d_{12}^i)

for each cycle

The damage factor in plane 1,2 is calculated dependent upon of the initial shear modulus G_{12}^0 obtained in the tests on the ±45 °- laminate.

The procedure for the analysis of the experimental data from the testing machine and the strain gauges is like the following:

- Collection of the raw data from the testing machine
- Reading the raw data into Excel, containing longitudinal and transverse strains in [%], longitudinal stresses in [MPa], applied force in [N] and longitudinal displacement in [mm]
- Calculating stresses and strains of the UD-ply for each measuring point *i* : ε_{12} in [%] and ε_{22} in [%], $\sigma_{12} = \sigma_{22}$ in [MPa]
- Determination of the initial transverse elastic modulus E_2^0 from the Young's modulus of the plotted experimental stress-strain curve $\frac{\sigma_L}{2} = f\left(\varepsilon_L - \varepsilon_T\right)$, i.e. $\sigma_{12} = f\left(2\varepsilon_{12}\right)$, from the first 100 measuring points
- Determining manually maximum and minimum strains of each cycle *i*
- Calculating for each cycle *i* the corresponding stresses and strains of the UD-ply: 2 ε_{12} in [%], ε_{22} in [%] and $\sigma_{12} = \sigma_{22}$ in [MPa]
- Finding the shear modulus for each cycle *i* : $G_{12}^i = \frac{\Delta\sigma_{12}}{\Delta 2\varepsilon_{12}}$ and $E_2^i = \frac{\Delta\sigma_{22}}{\Delta\varepsilon_{22}}$
- Calculating d_{12}^i and d_2^i
- Calculation of *A*
- Recalculation of the results from the actual fibre volume fraction of 55.4 % to a standard volume fraction of 60 %

In the test on +45 °- laminate, the plastic forces are not necessary to evaluate for the FEM calculation. However, the cyclic tests are performed to get a database for other modulations. For the FEM simulation only the transverse elastic modulus E_2^0 is interesting. The results are summarised in table 10.5.

Table 10.5: Results of cyclic simple tension test on $[+45]_8$- laminate

Test	No. of cycles	E_2^0 [MPa]
P3-1	7	11364.3
P3-4	6	12593.5
P3-5	5	12236.1
P3-6	7	12856.7
Average	**-**	**12262.6**
Stand. dev.	-	650.7
Max	-	12856.7
Min	-	11364.3
CV	-	5.3

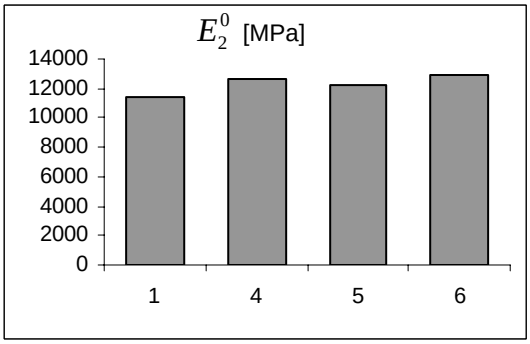

Figure 10.23: Comparison of the initial transverse elastic modulus E_2^0 for each specimen

The initial transverse elastic modulus E_2^0 shows strong variations when considering also the specimens P3-2 and P3-3. The values of the longitudinal elongation measured by the strain gauges are for both specimens quite low; they are only 1/3 of the other values obtained from the tests on P3-1, P3-4, P3-5 and P3-6. The problem during the strain measurement with the strain gauges is again the small size of the strain gauge.
Therefore, the values obtained from testing P3-2 and P3-3 are not considered in calculating the average.

10.4.4. Simple cyclic tension on [±67.5]$_{2S}$ laminates

The fibre orientation in ±67.5 ° is an unusual stacking for a laminate and is not used in practice. The load, which the laminate can take up till breakage, is even lower than the one of the +45 °-laminate.
With the LAP, not only the displacement of the laminate is predicted, but also the stresses and strains for the whole laminate and each lamina, considering the exact angle of each ply and the thickness, analysed from the cross-section in section 8.1 and 8.4.

a b

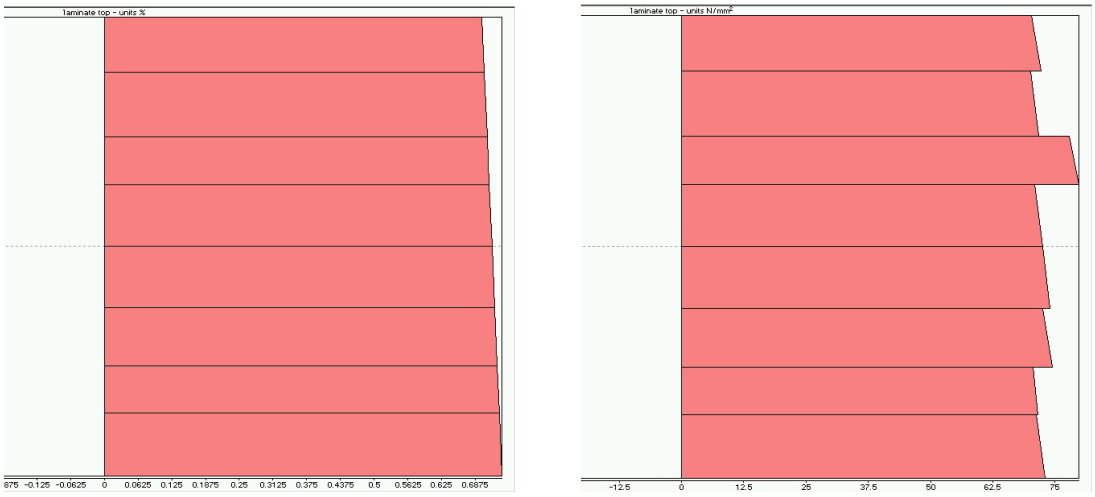

Figure 10.24: LAP of stresses and strains at simple cyclic tension test [± 67.5°]$_{2S}$
a: strains in longitudinal direction
b: stresses in longitudinal direction

The LAP analysis shows that the different thicknesses of the plies have a minor influence on the stresses and strains acting on each individual ply. The deviation from the expected angle of the third ply increases the stress acting on the ply more significant, see table 8.8.

The experimental results, on the basis of the test series interpreted above, are analysed according to the following scheme:

- Collection of the experimental test data from the testing machine and the strain gauges
- Reading the data into Excel
- Calculation of ε_{11}, ε_{22} and ε_{12}, σ_{11}, σ_{22}, σ_{12} and $\upsilon_{12}^{0}\varepsilon_{11}+\varepsilon_{22}$ for each cycle *i*
- Determination of maximum and minimum of σ_{12} and $2\varepsilon_{12}$ for each cycle *i* to calculate the initial shear modulus: $G_{12}^{i}=\dfrac{\Delta\sigma_{12}^{i}}{\Delta\varepsilon_{12}^{i}}$
- Calculation of d_{12}^{i}, d_{2}^{i}, Z_{12}^{i}, Z_{2}^{i}, Y_{2}^{i} and b_i
- Determination of Y_{2}^{c} and Y_{2}^{0} from the linear fitting curve: $Y_{12}(t_i)=Y_{2}^{c}d_{2}^{i}+Y_{2}^{0}$, see figure 10.25
- Defining the parameter Y_{2}^{S}
- Recalculation of the results from the actual fibre volume fraction of 58.3 % to a standard volume fraction of 60 %

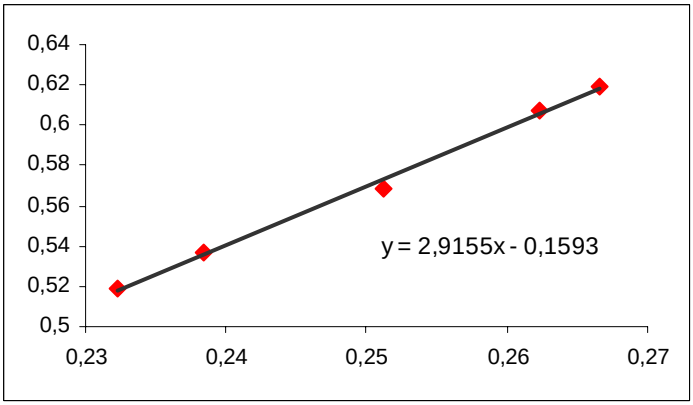

Figure 10.25: Y_2 versus d_{2}^{i}, with fitting curve $Y_{12}(t_i)=Y_{2}^{c}d_{2}^{i}+Y_{2}^{0}$

In figure 10.25, each point corresponds to one cycle, calculated from the maximum and minimum stresses and strains.

To evaluate the experimental test results, the following material parameters obtained from the tests on the $[0]_8$, $[+45]_{2S}$ and $[\pm45]_8$- laminate are used:

Table 10.6: Material data used for test evaluation of the [±67.5]- laminate

Material data	Value	Source of data
E_1^0	138579.6 MPa	$[0]_8$- laminate
E_2^0	12262.6 MPa	$[+45]_{2S}$- laminate
G_{12}^0	6330.6 MPa	$[\pm45]_8$- laminate
υ_{12}^0	0.287	$[0]_8$- laminate
Y_{12}^c	2.102 $\sqrt{MPa}$	$[\pm45]_8$- laminate
Y_{12}^0	0.371 $\sqrt{MPa}$	$[\pm45]_8$- laminate

Table 10.7: Results of cyclic simple tension test on $[\pm67.5]_{2S}$- laminate

Test	No. of cycles	Y_2^c $\sqrt{MPa}$	Y_2^0 $\sqrt{MPa}$	Y_2^S $\sqrt{MPa}$	*b* [-]
P4-1	3	3.136	-0.284	0.450	1.334
P4-2	5	2.916	-0.159	0.211	3.126
P4-4	6	2.928	-0.185	0.208	1.335
P4-5	6	2.967	-0.234	0.208	1.795
P4-6	6	3.129	-0.277	0.218	1.460
Average	**-**	**3.015**	**-0.228**	**0.259**	**1.810**
Stand. dev.	-	0.109	0.055	0.107	0.760
Max	-	3.136	-0.159	0.450	3.126
Min	-	2.916	-0.284	0.208	1.334
CV	-	3.6	24.2	41.2	42.0

The values show strong variations, as many parameters of former tests have an effect on the calculations. Additionally, Y_2^c and Y_2^0 are derived from a fitting curve. Each small variation of one measuring point causes a notable change in the fitting curve. Therefore, the standard deviation of these values is quite high.

10.4.5. Simple compression test on $[0]_8$ laminates

The LAP program shows the displacement of the specimen. Therefore, the elongation in the transverse direction is positive and in the longitudinal direction negative.

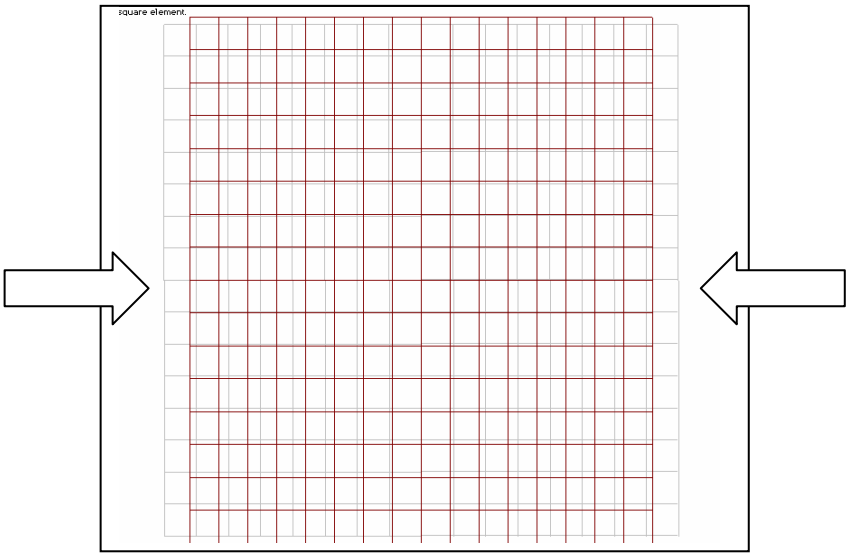

Figure 10.26: LAP displacement shape simple compression test $[0°]_8$

The strain gauge is attached on the front and backsides of the specimen to avoid a wrong measurement due to a possible bending of the specimen.
For the analysis of the experimental data, obtained from the strain gauges, the following routine is applied:

- Collection of the experimental test data from the testing machine and the strain gauges
- Reading the data into Excel
- Calculation of ε_{11} from the average of the two longitudinal elongations ε_L for each measuring point
- Determination of E_1^{0c} from the Young's modulus of the plotted experimental stress-strain curve $\sigma_L = f(\varepsilon_L)$, i.e. $\sigma_{11} = f(\varepsilon_{11})$, from the first 100 measuring points
- Calculation of E_1^c, d_i for each measuring point
- Determination of the corrective factor γ:
    - o Plotting the graph: $E_1 = f(\varepsilon_{11})$
    - o Calculating the sum of the values obtained by: $\left(\frac{E_1^{0c}}{1-E_1^{0c}\gamma'|\varepsilon_{11}|}\right)$, with γ' as an estimated value of γ
    - o Adjusting the value of γ, to approach the plotted curve $\sum\left(\frac{E_1^{0c}}{1-E_1^{0c}\gamma'|\varepsilon_{11}|}\right) = f(\varepsilon_{11})$ to the plotted graph $E_1 = f(\varepsilon_{11})$

- Determination of ε_i^{fc} , ε_u^{fc} and d_u^{fc} according to figure 10.1 and figure 10.27.
- Recalculation of the results from the actual fibre volume fraction of 55.6 % to a standard volume fraction of 60 %

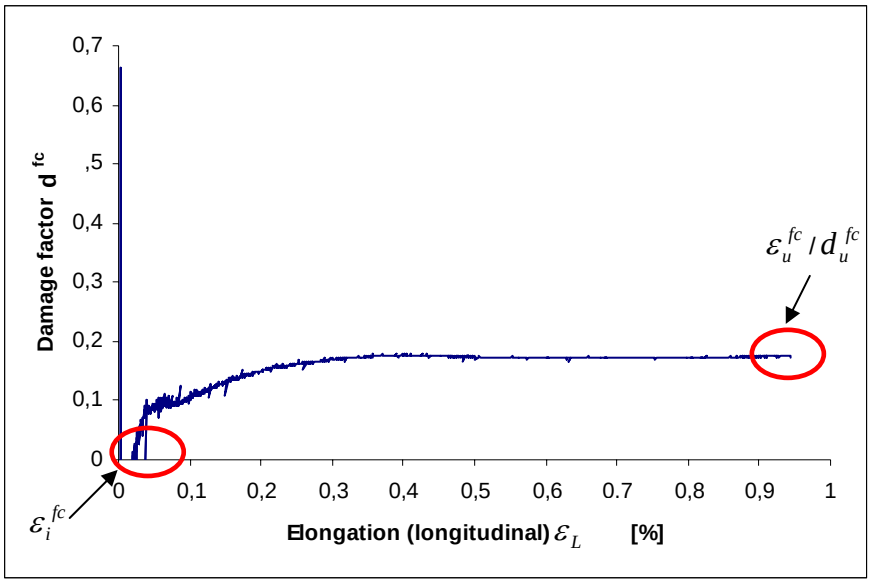

Figure 10.27: Fibre damage function, P1-6c

The results of the experimental values derived from the calculations according to the Ladevèze program are summarised in table 10.8:

Table 10.8: Results of simple compression test on $[0]_8$- laminate

Test	E_1^{0c} [MPa]	ε_i^{fc} [%]	ε_u^{fc} [%]	d_u^{fc} [-]	γ [-]
P1-1c	138366.9	0.003	1.143	0.123	-0.00008
P1-2c	140654.7	0.050	1.292	0.413	-0.00039
P1-3c	137460.4	0.433	0.818	0.076	-0.00002
P1-4c	144474.8	0.063	0.907	0.176	-0.00021
P1-5c	138949.6	0.298	1.000	0.103	-0.00008
P1-6c	151305.8	0.025	0.943	0.174	-0.00026
Average	**141868.7**	**0.146**	**1.017**	**0.177**	**-0.00017**
Stand. dev.	5244.8	0.177	0.173	0.122	-0.00014
Max	151305.8	0.433	1.292	0.413	-0.00002
Min	137460.4	0.003	0.818	0.076	-0.00039
CV	3.7	121.7	17.0	68.7	80.6

As the values for ε_i^{fc} , ε_u^{fc} and d_u^{fc} are look for in a manual way from the experimental curves, illustrated in figure 10.27, and many parameters influence the values, the standard deviation is quite high.

10.5. Test results from ARAMIS

For validation of the data, obtained from the measurements from the strain gauges, the results of the Aramis system are evaluated.
The cameras of the Aramis system record the displacement and strains of the specimen and store the data in form of pictures. figure 10.28 shows one picture (stage) of a specimen during testing.

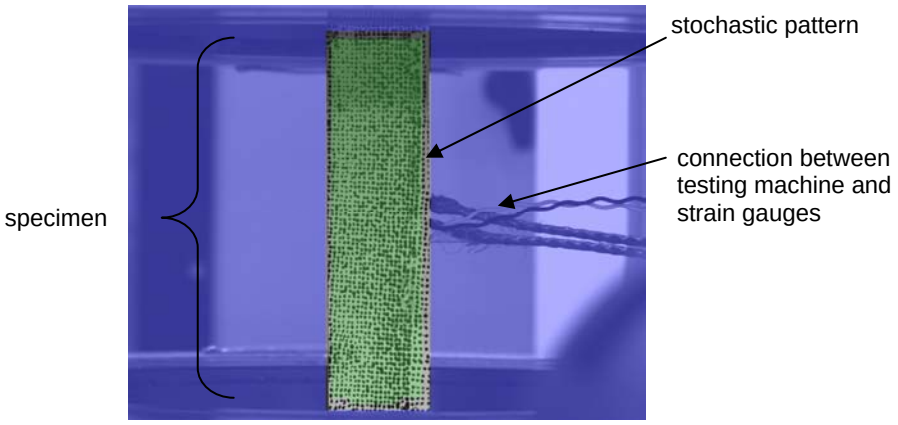

Figure 10.28: Aramis system, picture of one stage

In the software program of the Aramis system, reports of the data received from each stage, which means from each picture recorded, can be created. For the report generation of strain versus time, two points in y-direction for the displacement [mm] in length and two points in x-direction for the displacement in width of the specimen are selected and marked as stage points. The distance between the two points is chosen larger than the length of the strain gauge to avoid the problems described in figure 10.20. The raw files of the report are imported into an Excel file and analysed. From the displacement of the two correlating points, the displacement of the section between the two points on the specimen is calculated. ε_L and ε_T are computed from the correlating displacement in the x- and y- directions.
figure 10.29 shows as example of the evaluation of the last stage of P3-1, before the specimen breaks, recorded by the Aramis system. Four stage points are marked and the distances L_0 and L_{act} are measured. The difference between the original distance L_0 and the actual distance L_{act} is the correlating elongation. The displacement of the whole specimen is colour coded.

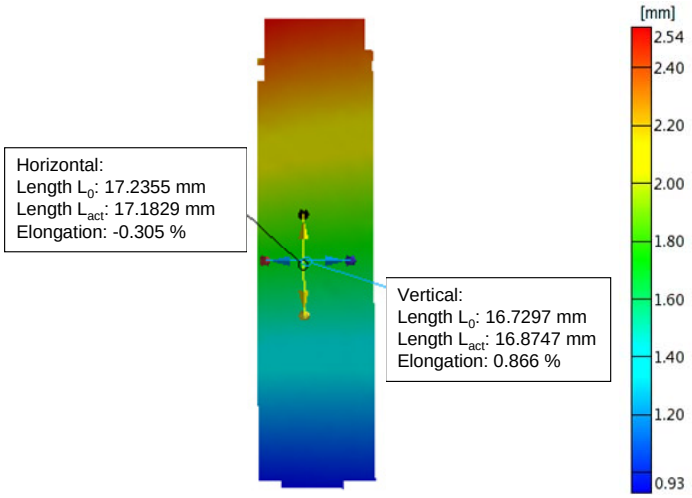

Figure 10.29: Result from Aramis as an example, displacement [mm] in the y-direction

The procedure for the calculation of the Ladevèze parameters is similar for all of the tests. After the calculation of the strains ε_L and ε_T from the displacement of the stage points in Excel, the corresponding parameters for each test are determined according to a similar procedure as with the data from the strain gauges. The stresses σ_L are also taken from the data obtained from the testing machine. For each measuring point, a calibration of the time between the stages (time) of the Aramis and the run-time of the testing machine to obtain the corresponding stress for the measured strain from Aramis has to be made.

10.5.1. Simple tension test on $[0]_8$ laminates

The parameters to find are E_1^0, E_1, d and υ_{12}^0. The calculation for these parameters is according to the calculations described in section 10.4.1. As input ε_L and ε_T from the Aramis measurements are taken and σ_L as measured by the testing machine. The parameters ε_i^{fc}, ε_u^{fc} and d_u^{fc} cannot be determined. The breakage of the specimens happens so suddenly in just a few milliseconds that the CCD cameras do not measure the strains at that specific point of breakage. The results of E_1^0 and υ_{12}^0 are presented in table 10.9.

Table 10.9: Results of simple tension test on $[0]_8$- laminate

Test specimen	E_1^0 [MPa]	υ_{12}^0 [-]
P1-1t	137934.5	0.262
P1-2t	157868.7	0.261
P1-3t	133099.6	0.294
P1-4t	151891.3	0.212
P1-5t	138838.2	0.237
P1-6t	145236.6	0.297
Average	**145811.5**	**0.260**
Stand. dev.	9115.6	0.033
Max	157868.7	0.297
Min	133099.6	0.212
CV	6.3	12.6

In the pictures from the report generation, the displacement in the y-direction is illustrated for each stage. Figure 10.30 shows the last stage before breakage of the specimen, colour-coded according to the displacement in vertical direction.

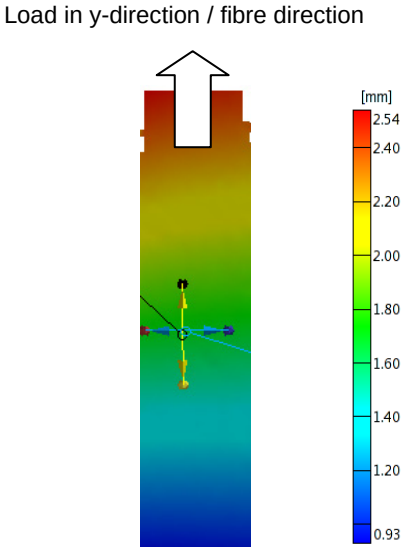

Figure 10.30: Aramis; displacement in the y- direction of specimen P1-1t

In figure 10.31 a picture of the breakage of the laminate is shown. During testing a lot of energy is built up in the specimen, which comes free in the form of an explosion of the specimen during specimen breakage. It is a sudden failure of the laminate.

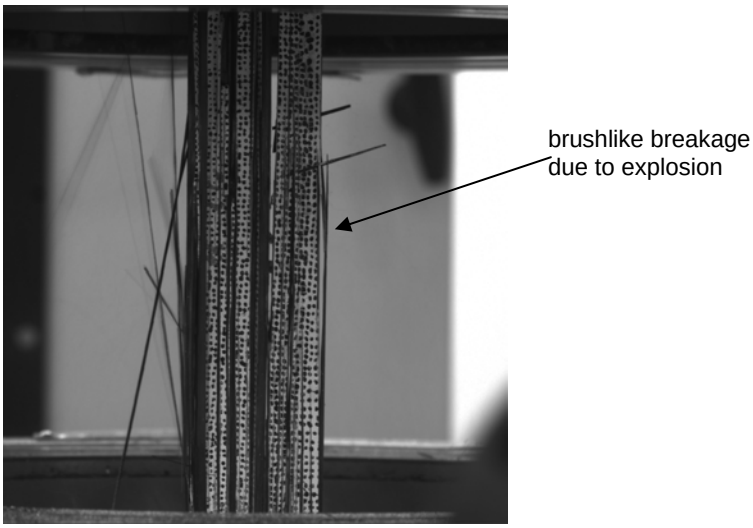

Figure 10.31: Specimen P1-1t during breakage

10.5.2. Simple cyclic tension test on $[\pm 45]_{2S}$ laminates

For the cyclic tension test on the $[\pm 45]_{2S}$ laminates, the analysis of the data obtained from the Aramis system is more complicated. The routine is similar to the calculations in section 10.4.2. However, the calibration of the stresses causes some difficulties, especially when determining the corresponding maximums and minimums of the stresses and strains. The stresses are measured by the testing machine in a much shorter interval than the corresponding strains recorded by Aramis, which is only every 4 seconds. Therefore, a macro is written in Microsoft Visual Basic, to find the stresses to the corresponding time. The value σ has to be recalculated to obtain the correct value. This is illustrated in figure 10.32.

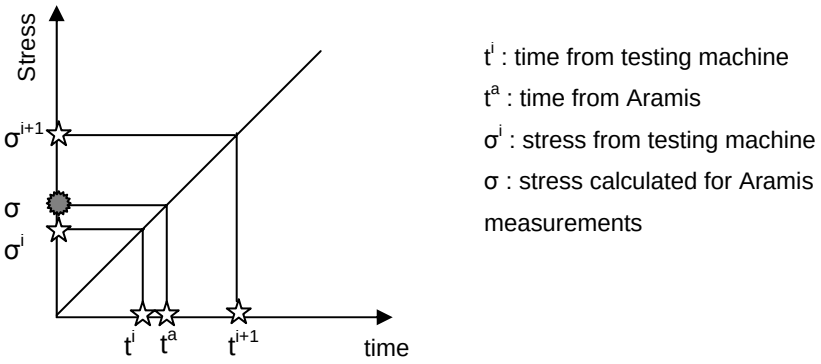

Figure 10.32: Principle for calculation of the stresses corresponding to the time

With:

$$\sigma = \frac{\sigma^{i+1} - \sigma^{i}}{t^{i+1} - t^{i}} \left(t^{a} - t^{i} \right) + \sigma^{i} \qquad (69)$$

G_{12}^0 results from the first cycle:

$$G_{12}^0 = \frac{\Delta\sigma_{12,calc}}{\Delta 2\varepsilon_{12}} \qquad (70)$$

$\Delta\sigma_{12,calc}$ and $\Delta 2\varepsilon_{12}$ are derived from half and 1/10 of the maximum value of the stresses from the first cycle, as described in the standard AITM 1-0007.

The results are presented in table 10.10:

Table 10.10: Results of simple tension test on $[\pm 45]_{2S}$- laminate with v_f = 60%

Test	No. of cyles	G_{12}^0 [MPa]	$Y_{12}^0 \left[\sqrt{MPa}\right]$	$Y_{12}^R \left[\sqrt{MPa}\right]$	$Y_{12}^c \left[\sqrt{MPa}\right]$	d [-]
P2-1	12	4670.0	0.291	0.855	2.015	0.254
P2-3	7	3806.3	0.626	1.379	1.855	0.340
P2-4	7	4226.9	0.336	1.240	2.243	0.366
P2-5	7	4375.5	0.304	1.116	2.201	0.207
P2-6	7	4487.9	0.298	1.152	2.199	0.330
Average	**-**	**4313.3**	**0.371**	**1.148**	**2.102**	**0.391**
Stand. dev.	-	326.4	0.144	0.193	0.164	0.042
Max	-	4670.0	0.626	1.379	2.243	0.366
Min	-	3806.3	0.291	0.855	1.855	0.254
CV	-	7.6	38.8	16.8	7.81	13.3

Y_{12}^c and Y_{12}^0 are derived from the fitting curve d_{12}^i versus Y_{12}^i. The values vary a lot, although the individual values of each cycle are comparable. In figure 10.33 the fitting curves for all specimens are shown, together with the corresponding equations, from which the values for Y_{12}^c and Y_{12}^0 are obtained.

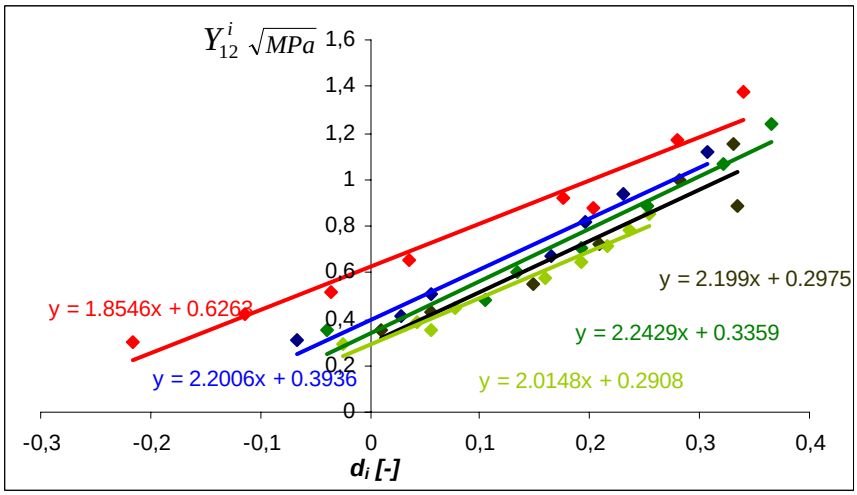

Figure 10.33: Comparison of fitting curves to define Y_{12}^c and Y_{12}^0

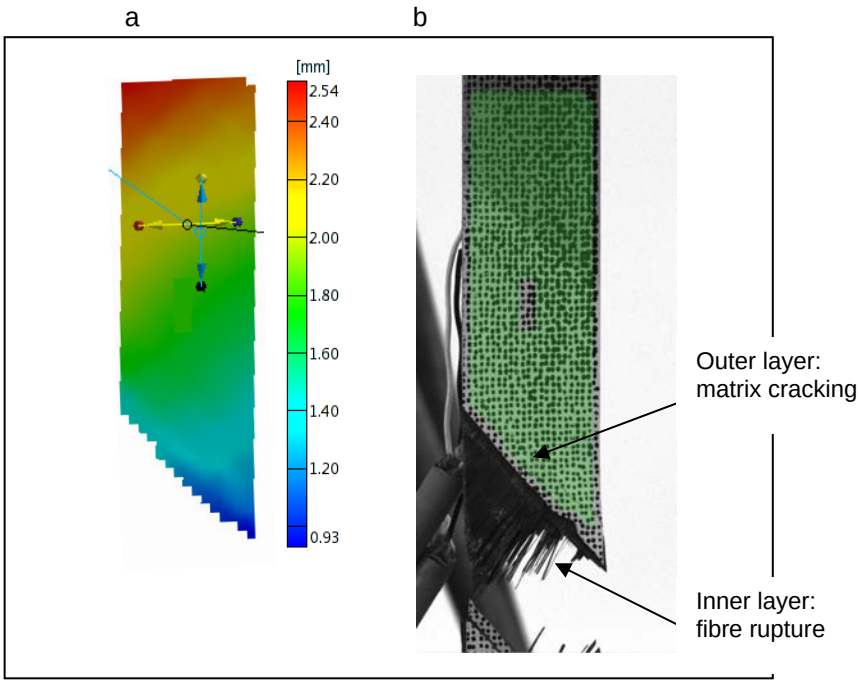

Figure 10.34: P2-1 after breakage

a: Stage picture, result analysis

b: Picture recorded by the CCD camera

Figure 10.34 shows the completely different behaviour of the laminate due to the different stacking sequence in the example of the kind of breakage. First the fibres under an angle of ±45 ° align their position in the direction of the applied load, before matrix cracking and fibre breakage. In the stage picture, the straining of the outer ply with an angle of +45 ° is visible.

10.5.3. Simple cyclic tension test on $[+45]_8$ laminates

After reading in the raw data of the Aramis system the strains from the longitudinal and vertical displacement are calculated. E_2^0 is again determined from the recalculated stresses corresponding to the strains, measured by the Aramis system. The same macro in Visual Basic from section 10.5.2 is used to calculate the corresponding stresses. For the further calculations of the Ladevèze parameters of the cyclic maximums and minimums, the same routine as in section 10.4.3 is applied. The results for a fibre volume fraction of 60 % is summarised in table 10.11.

Table 10.11: Results of simple tension test on $[+45]_8$- laminate with v_f = 60%

Test	No. of cycles	E_2^0 [MPa]
P3-1	7	10169.9
P3-2	6	10008.0
P3-3	5	8052.8
P3-4	6	9971.5
P3-5	5	11006.4
P3-6	7	10118.4
Average	**-**	**9887.8**
Stand. dev.	-	977.0
Max	-	11006.4
Min	-	8052.8
CV	-	9.9

10.5.4. Simple cyclic tension on $[\pm 67.5]_{2S}$ laminates

For the analysis of the data obtained from the Aramis system, the same calculations as for the analysis of the data from the strain gauges are used. The input data for the matrix calculations used to determine ε_{11}, ε_{22} and $2\varepsilon_{12}$, is taken from the results calculated for P 1, P 2 and P 3 on the basis of the Aramis measurements.

As values for G_{12}^0 and E_2^0, the values from G_{12}^i and E_2^i of the first cycle are taken.

Table 10.12: Results of cyclic simple tension test on $[\pm 67.5]_{2S}$- laminate

Test	No. of cycles	$Y_2^c \left[\sqrt{MPa}\right]$	$Y_2^0 \left[\sqrt{MPa}\right]$	$Y_2^S \left[\sqrt{MPa}\right]$	$b\,[-]$
P4-1	3	2.679	0.326	0.368	0.490
P4-2	5	0.621	0.199	0.121	0.593
P4-4	6	0.526	0.383	0.142	3.838
P4-5	6	2.134	0.382	0.115	2.025
P4-6	6	1.727	0.381	0.124	2.419
Average	**-**	**1.537**	**0.334**	**0.174**	**1.873**
Stand. dev.	-	0.943	0.079	0.109	1.391
Max	-	2.679	0.383	0.368	3.838
Min	-	0.526	0.199	0.115	0.490
CV	-	61.4	23.8	62.6	74.2

The point of breakage is illustrated in figure 10.35. The type of breakage is similar to the one of the specimens of the ±45 °- laminate, with matrix cracking of plies 1, 3, 6 and 8 and fibre alignment and fibre rupture of the other plies.

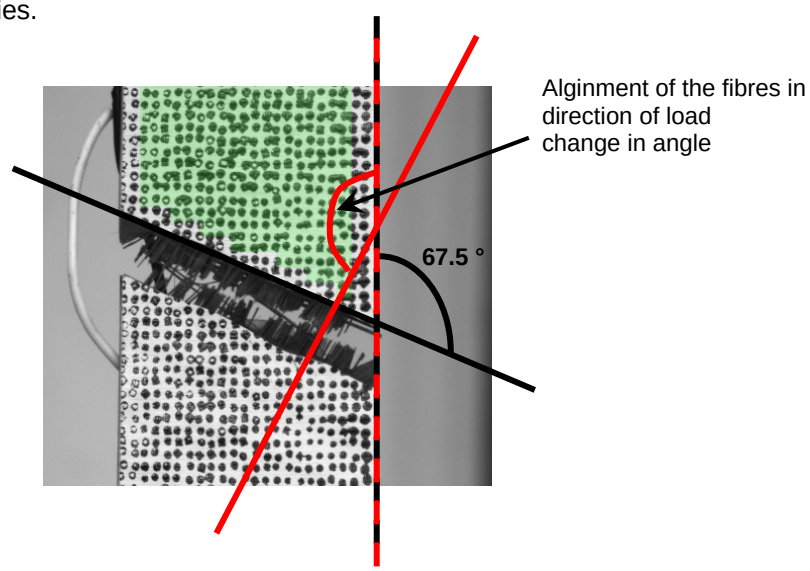

Figure 10.35: Point of breakage of P4-1

10.6. Comparison of strain gauges and Aramis

When comparing the results obtained from the two different measuring methods, it is important first to make a calibration of the vertical and longitudinal strains. Figure 10.36 shows the longitudinal strains for the cyclic test on specimen P3-1 as an example.

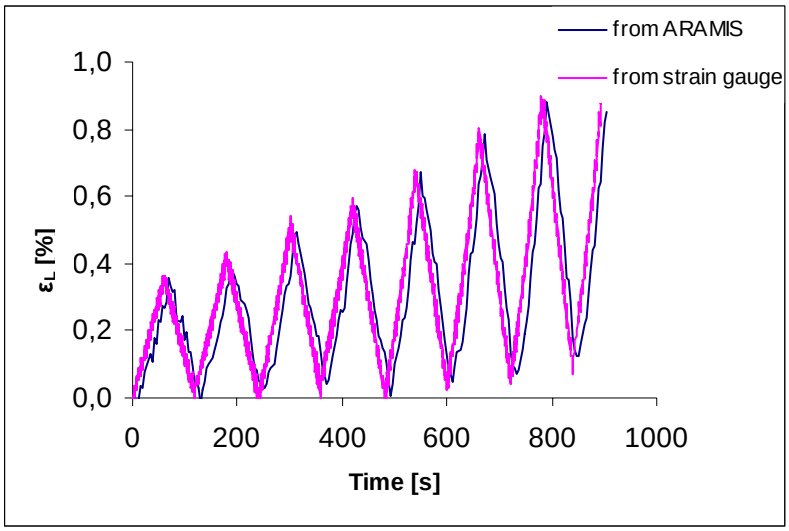

Figure 10.36: Comparison of ε_L obtained from strain gauges and Aramis of P3-1

The strains of all tests are comparable and have almost the same values. However, in the case of the two tests, where the strain gauges did not measure the strains correctly and the values of the elongation are lower than from the other tests, the Aramis system recorded the strains of the

specimen during testing. The difference in measurement for one of the specimens P2-2 and P2-3 as an example is shown in figure 10.37.

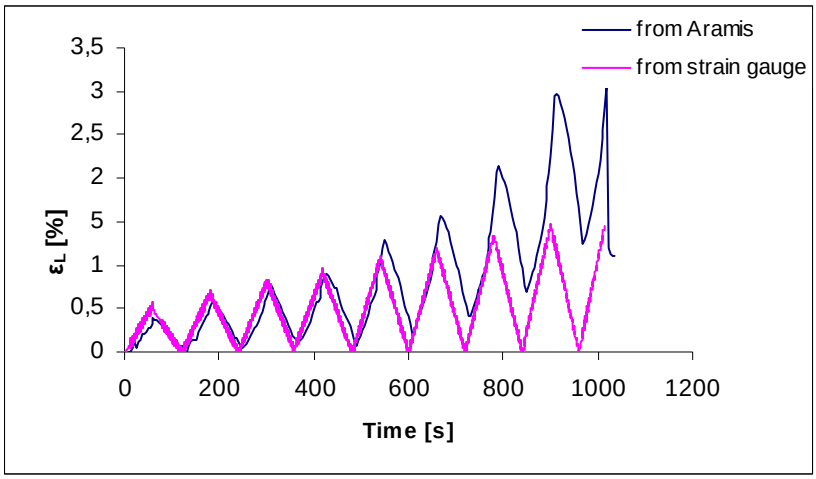

Figure 10.37: Comparison of ε_L obtained from strain gauges and Aramis of P2-3

Another disadvantage of the measurement with the strain gauges in combination with the testing machine is the limit of recording the elongation. It is only possible to determine strains until the limit of 2 %. In comparison, the Aramis system has virtually no limitations. This is especially notable for the ±45 °- laminate, where the alignment of the filaments results in a strong elongation in the vertical direction.

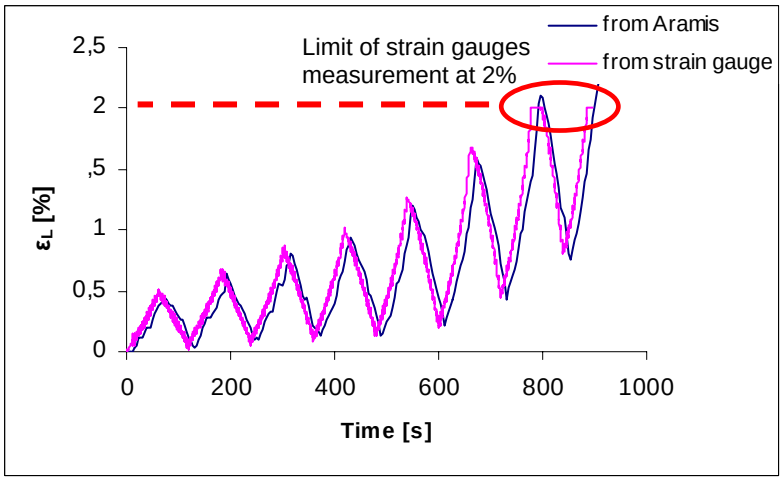

Figure 10.38: Limitation of strain measurement of strain gauges in comparison to Aramis, P2-4

The results of the mechanical characterisation of the 0 °- laminate are very similar. However, the results of G_{12}^0 obtained from the strain gauges show stronger variations. This is illustrated in figure 10.39, with the results of the Aramis system in blue and the values from the strain gauges in pink.

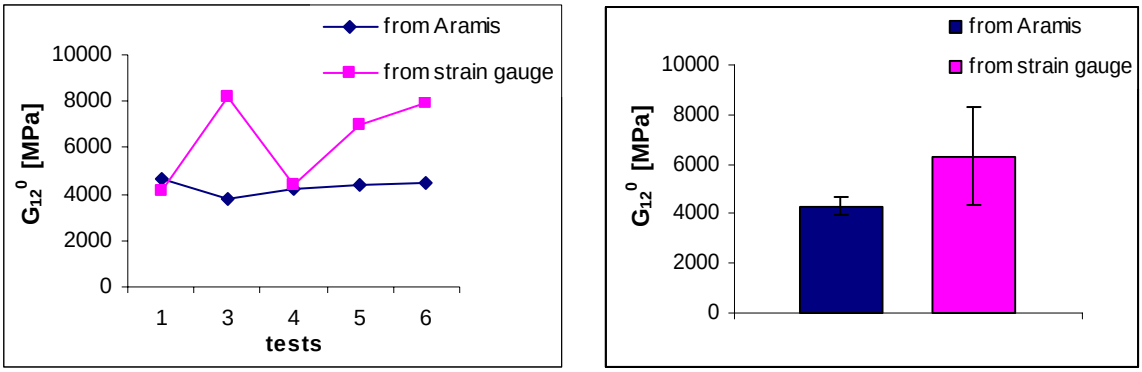

Figure 10.39: Comparison of G_{12}^{0}, obtained from strain gauges and Aramis

The other results of the test on the $[\pm 45]_{2S}$- laminate do not show such a different distribution.
For the $[+45]_{8}$ -laminate the results vary due to the separation of the strain gauges from the specimens.

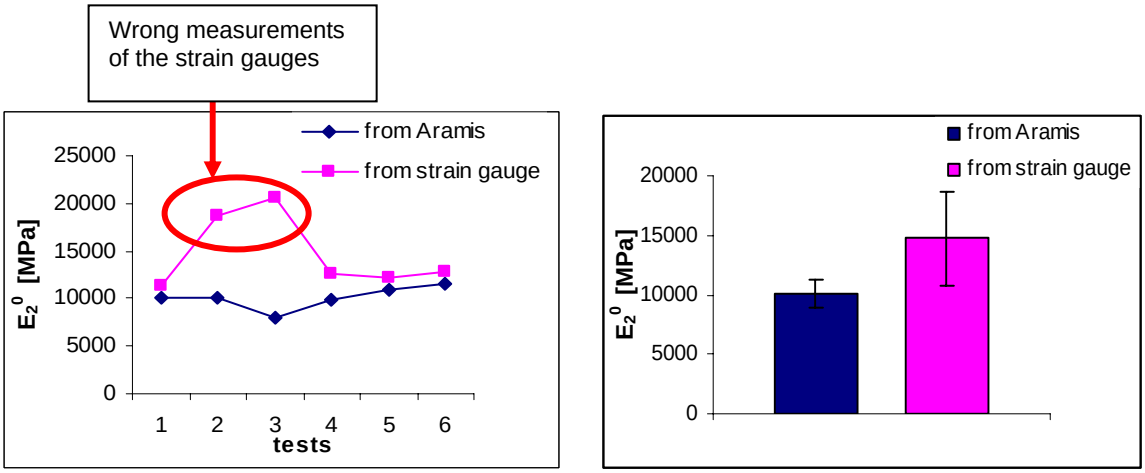

Figure 10.40: Comparison of E_{2}^{0}, obtained from strain gauges and Aramis

Figure 10.40 shows that the result from Aramis lay in the range of the standard deviation of the measurements of the strain gauges, however with a much smaller coefficient of variation.

10.6.1. Final results, used as input for FEM

After the comparison of the results, it is obvious that there is only one series of results from one method which can be used as input for the FEM. The decision is made to use the results obtained from the measurements with Aramis. The standard deviations are much smaller and the results are more realistic. Additionally, there were some problems with the strain gauges, e.g. the disconnection of the gauges from the specimen and wrong measuring. Through the non-contact measuring of the Aramis method the problem of misconnection between the specimen and the strain gauges is eliminated. An exception has to be made for the test on the 0 °- laminate as here

with the Aramis system the strains during breakage could not be measured. Therefore, ε_i^{ft}, ε_u^{ft} and d_u^{ft} are taken from the measurements with the strain gauges.

10.6.2. Comparison of results with other testing material

The results obtained from the experimental tests and the calculations according to Ladevèze are compared with results on other testing material, also tested and analysed according to the Ladevèze method.

Table 10.13: Comparison of Ladevèze parameters with literature values

Parameters	UD-braid (Carbon/Epoxy): by EADS Fibre: HTS5631 Resin: RTM6 *1*	Prepreg (Carbon/Epoxy): by Hexcel [27] Fibre: IM7 (6k) Resin: Narmco 8552 *2*	Prepreg (Carbon/epoxy): [25] Fibre: IM6 Resin: 914 *3*	Prepreg (Carbon/Epoxy): by Hexcel [28] Fibre: T800S Resin: M21 *4*
E_1^0 [MPa]	145812 ±9116	171700	170000	172000
E_2^0 [MPa]	9888 ±977	8983	10800	-
G_{12}^0 [MPa]	4313 ±326	5520	5800	4800
d_u^{ft} [-]	0.26 ±0.03	0.32	0.34	0.37
Y_{12}^c [$\sqrt{MPa}$]	2.102 ±0.164	2.217	2.77	-
Y_{12}^0 [$\sqrt{MPa}$]	0.371 ±0.144	0.181	0.15	-
Y_{12}^R [$\sqrt{MPa}$]	1.148 ±0.193	1.318	-	-
Y_2^c [$\sqrt{MPa}$]	1.537 ±0.943	3.967	3.78	-4.743
Y_2^0 [$\sqrt{MPa}$]	0.334 ±0.079	0.0419	0.24	3.162
Y_2^S [$\sqrt{MPa}$]	0.174 ±0.109	0.459	0.7	0.506
b [-]	1.873 ±1.391	1.577	2.5	1.5

Figure 10.41 gives an overview of the comparison of the different material tested.

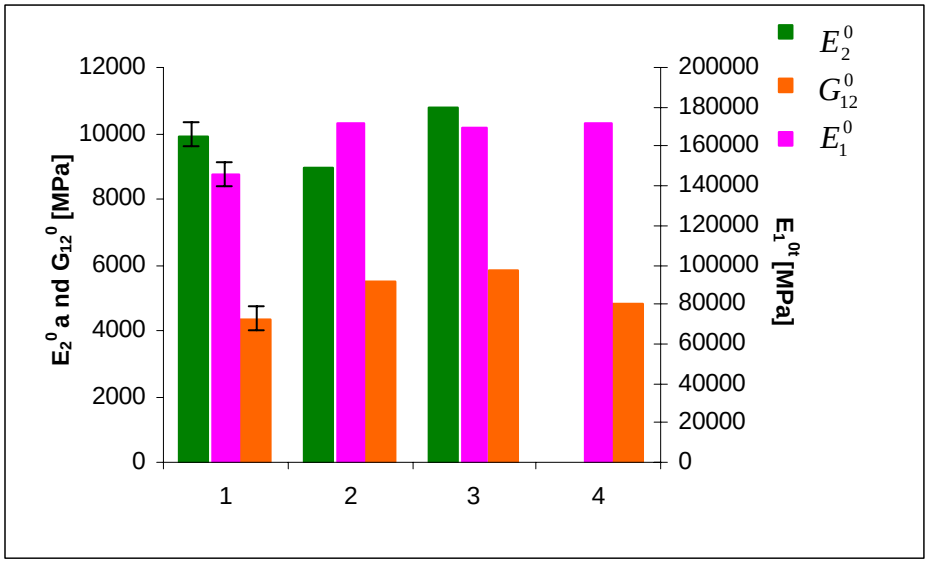

Figure 10.41: Comparison of E_1^{0t}, E_2^0 and G_{12}^0 in [MPa] with literature values

The values of E_2^0 and G_{12}^0 are comparable and correlating. However the tensile Young's modulus E_1^0 is relatively small in comparison to the prepreg material. This is due to the fact that the filaments lie completely straight in the prepreg material. Every degree of misalignment in the filaments results in an extreme decrease in the modulus and tensile strength.
This can be predicted with the LAP program, illustrated in figure 10.42.

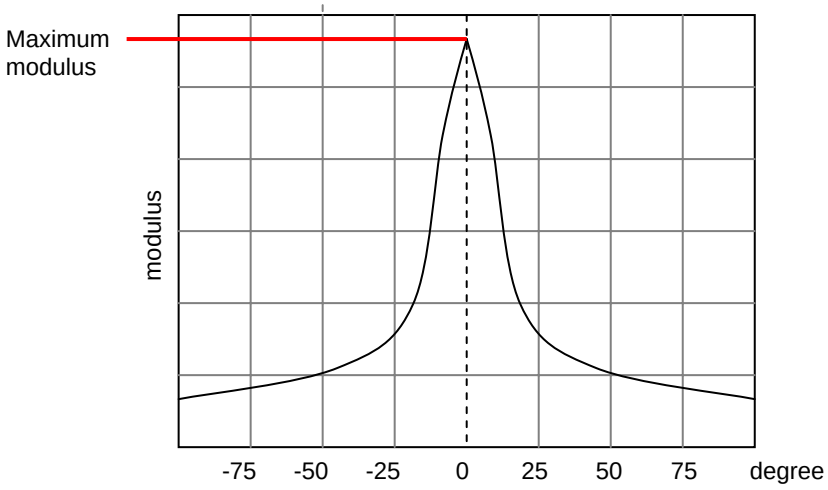

Figure 10.42: Decrease of modulus depending on filament / ply direction

Therefore, the values of modulus and tensile strength are in general lower for a textile structure than a prepreg.
When comparing the Ladevèze parameters of the damage value, a clear trend can be observed. The values of pregreg number 4 are quite small in comparison to the others. The transverse damage values Y_2^0, Y_2^c and Y_2^S lie very close to the ones of the other testing material, indicating a

similar resin system. The shear damage values are lower probably due to a different fibre-matrix adhesion and different auxiliaries used.

10.7. Conclusion of test results

In the chapter 10 the whole mechanical characterisation of the laminate according to the Ladevèze continuum damage model is described. The Ladevèze parameters of the laminate, which is produced out of eight layers with different stacking sequences, give a complete mechanical characterisation on the basis of different methods to determine strains. The values obtained from the measurements with the Aramis system are more realistic and the standard deviation is lower than the values calculated according to the values of the strain gauges. When comparing the experimental results of the UD-braid laminate with material from literature, the values are comparable.

Conclusion and Prospect

The UD-braid, a relatively new patent by EADS, is investigated in this Master's Thesis. A full characterisation of this material is done. Both geometrical and mechanical characterisations, including the Ladevèze damage parameters are obtained.

In the geometrical characterisation as a basis for the WiseTex model no great difficulties arose. The only problem was the investigation of the dimensions of the Grilon yarn, as supporting yarn in the UD-braid, especially in compressed state. However, these parameters are not significant for the simulation, as the Grilon yarn smelts in the matrix.

The mechanical tensile properties, tested on the roving from the bobbin as well as from the braid, were planned to be used as input data for the WiseTex model. Due to problems during these tests, the rovings could only be compared with each other obtaining the result that the braiding process hardly damages the filaments. As input data for the WiseTex model, however, the data given by the producer of the carbon rovings were taken to get realistic values.
With the WiseTex software it was possible to simulate the textile structure of the UD-braid in three different stages: the textile in dry state, in compressed state and the fabric inside the laminate.

The geometrical characterisation of the laminate proved the quality of the laminate, showing nearly no voids, a good compressed state of the carbon rovings, quite balanced distribution of the ply thicknesses, little undulation and a small deviation of the ply angles from the desired state.

As a result of the proven quality of the laminate, the mechanical characteristics of the laminate could be tested according to the Ladevèze testing program.
For the cyclic tests, deciding upon the testing machine to be used was quite difficult. For the validation of the test series and the ability for comparison of the tests, it is recommendable to use the same testing machine for all tests. The problem, emerging before and during testing was the absence of a testing machine with a load cell of maximum 20 kN. Therefore, the machine had to be changed for various tests between a machine with a load cell of maximum 10 kN and 100 kN. Due to such a situation, especially when using the load cell of maximum 100 kN, the control of the machine motor was quite a challenge for the testing machine. The experimental stress-strain curves show big variations due to the vibrations of the machine.
Another problem was the size of the strain gauges. The biggest strain gauge available was smaller than one unit cell of the UD-braid. Therefore, the measurements are in some cases incorrect where the strain gauge was attached directly over one carbon roving and not as preferable over the size of a unit cell of the textile structure.
During some tests, the strain gauges detached from the specimen. In this case the results could not be used.

The strain mapping parallel to strain measurement with strain gauges revealed new conclusions. The testing with the Aramis system, used for the first time at the research centre of EADS, showed substantially better results. However, it has to be noted, that for further testing with the Aramis system, the shutter time of the cameras should be changed during testing. At the beginning, a recording in longer time intervals is necessary due to the limited storage capacity of the computer. However, just before failure of the laminate, the time interval has to be shortened to be able to record the strains directly during breakage. This would be interesting for the test on the $[0]_8$-laminate to determine the critical strain thresholds and the ultimate damage corresponding to fibre rupture, ε_i^{ft}, ε_u^{ft} and d_u^{ft}.

For the results interpretation, only one virtual strain gauge was attached to the specimen. This virtual Strain gauges only gives a punctual evaluation of the specimen. It would be more useful to mark several Strain gauges to get a test interpretation over the whole specimen.

In comparison with reference prepreg material, the Ladevèze parameters calculated from the experimental tests on the UD-braid showed good comparison.

Next to the characterisation of the UD-material this work described in detail a methodology on how to obtain Ladevèze parameters and gives solution of possible problems that occurred during the work.

Appendix

Data Sheets

- Carbon HTS 5631
- HexFlow RTM6
- Grilon MS-matrix soluble
- Grilon MS EP1239

Geometrical characterisation_dry UD-braid

- Orientation, width, spacing
- Textile scan

Geometrical characteriation_laminate

- Cross-section analysis
- Filament height and length
- Polished micrograph section

Infiltration

- Infiltration temperatures

LAP

- UD-braids P1
- UD-braids P2
- UD-braids P3
- UD-braids P4

Mechanical characterisation_dry UD-braid

- Roving out of braid, 6x
- Roving out of braid, 3x
- Roving, 6x
- Roving, 3x
- Roving
- Grilon K-85
- Carbon braid
- Bending stiffness_braid
- Tensile strength_roving

Mechanical characterisation_laminate

- Test results_strain gauges
- Test results_Aramis

Pictures of Specimens

- Specimens before testing
- Specimens after testing

WiseTex model

- UD-braid-dry_tension.b2b
- UD-braid-dry.b2b

References

Books:

[1] Dr. Ko, F., Dr.Pastore, C., Head, A.
Handbook of Industrial Braiding
Atkins&Pearce

[2] Rosenbaum, J.-U.
Flechten: Rationelle Fertigung faserverstärkter Kunststoffbauteile
Ingineurwissen Kunststoffverarbeitung, Verlag TÜV, Köln, 1991

[3] Altenbach, H., Altenbach, J., Rikards, R.
Einführung in die Mechanik der Laminat- und Sandwichtragwerke
Deutscher Verlag für Grundstoffindustrie Stuttgart, 1996

[4] Flemming, M., Ziegmann, G., Roth, S.
Faserverbundbauweisen, Halbzeuge und Bauweisen
Springer-Verlag , Berlin Heidelberg, 1996

[5] Puck, A.
Festigkeitsanalyse von Faser-Matrix-Laminaten, Modelle für die Praxis
Carl Hanser Verlag München, Wien, Immenhausen-Mariendorf, 1996

[6] Eduard Ventsel, Theodor Krauthammer
Thin Plates & Shells: Theory, Analysis, and Applications
Marcel Dekker, Inc., New York, 2001

[7] Ali H. Nayfeh, P. Frank Pai
Linear and Nonlinear Structural Mechanics
Wiley & Sons, 2004

Articles:

[8] Verpoest, I.
TexComp 5, The 5th International Conference on Textile Composites, Leuven, Belgium, 18-20 September, 2000

[9] Roye, A., Stüve, J., Gries, T.
Definition for the differentiation of 2-D and 3-D textiles
Technical Textiles, 4/2005

[10] Schneider, M., Wulfhorst, B.
Importance of the braiding technology for the construction of composite materials
Technical Textiles 40/1997

[11] Schneider, M., Wulfhorst, B.
Modern braiding techniques for braided reinforcements in composites
Band- und Flechtindustrie, 34/1997

[12] Laorine, E., Schneider, M., Wulfhorst, B.
Proc. of The 5th Int. conf. On Textile Composites, Leuven, Belgium, 18-20 September, 2000

[13] Hermann, A.S., Eberth, U.
Textiles for aircraft structures-state of the art of technology and challenges
Konferenz-Einzelbericht: MFG Dornbirn, Internat. Chemiefasertagung, 44

[14] Lomov, S. V., G. Huysmanx, I. Verpoest
Hierarchy of textile structures and architecture of fabric geometric models
Textile Research Journal, vol. 71 (6), p. 534-543, 2001

[15] A. Geßler, Dr. J. Brandt, F. Maidl, Ch. Breu; EADS Deutschland GmbH
Neue Entwicklungen bei der Fertigung von Kohlenstofffaserpreforms mit der Rundflechttechnik
Deutscher Luft- und Raumfahrkongress 2004

[16] Chamis, C. C.
Simplified composite micromechanics equation for hygral, thermal and mechanical properties
Sampe Quarterly, 14:14-23, 1988

Patents:

[17] WO9215740 US
Asymmetric braiding of improved fiber reinforced products

[18] DE102004017311
Method for producing fibre composites semi-finished products by means of a round wickerwork technique

[19] WO0168353 DE
Method and device for producing fibre-reinforced components using an injection method

Manuals:

[20] Dr. Veit, D.
Vorlesung Textiltechnik 1
RWTH Aachen University, 2005/2006

[21] PAM CRASH solver notes manual
ESI group, 2002

[22] S.V. Lomov, E. Bernal, T. Peeters
Integrated Textile Preprocessor, WiseTex, Version 2.4
User's guide, Leuven 2004

[23] Prof. Dr. Kiekens, P., dr. h. c.
High-Performance Fibres, Third edition, revised: 2001
Universiteit Gent, Department of Textiles

[24] Kawabata, S., Niwa, M., Yamashita, Y.
Recent Development in the Evaluation Technology of Fibre and Textiles, Towards the Engineered Design of Textile Performance
100 Year of Modern Fiber Science Conferece, Organized by the U.S. Fiber Society, Asheville, NC, USA, 1998

[25] Ladevèze, P., Le Dantec, E.
Damage Modelling of the Elementary Ply for Laminated Composites
Composites Sciences and Technology, volume 43
Elsevier Science Publishers Ltd., 1992

[26] Aramis manual
by gom (Gesellschaft für Optische Messtechnik)

Diploma thesis:

[27] Ronny Richter
Experimentelle Bestimmung von Materialparametern für das Schädigungsmodell nach Ladevèze
Universität der Bundeswehr München, Fakultät für Luft- und Raumfahrtechnik, Mai 2001

[28] Sébastien Grossir
Mechanical characterization and Simulation of Composite Impacts
Cranfield University, School of Industrial and Manufacturing Sciences, 2004

World Wide Web:

[29] http://:www.msm.cam.ac.uk

[30] http://www.braider.com/braidfaqs.html

[31] http://mathworld.wolfram.com/LeastSquaresFitting.html

[32] http://www.ifb.uni-stuttgart.de/itool/partners/eads-g.htm

[33] http://www.tech.plymouth.ac.uk

[34] http://www.mtm.kuleuven.ac.be/Research/C2/poly/software.html

[35] http://www.netcomposites.com

[36] http://www.wikipedia.org

[37] http://www.machinedesign.com

Figures

Tables

E-TEAM

European Masters in Advanced Textile Engineering

Characterisation of UD-Braids

Charlotte Eisenhauer

Supervisor: **Dipl. Ing. Vera Hanisch**
(RWTH Aachen University)
Dr. Peter Middendorf
(EADS Deutschland GmbH)
Ing. Björn Van Den Broucke
(EADS Deutschland GmbH)

Academic year: 2005-2006